

Alma Mater Studiorum – Università di Bologna

DOTTORATO DI RICERCA

Joint International Ph.D Programme in Cognitive Neuroscience

Ciclo XXX

Settore Concorsuale: 11/E1

Settore Scientifico Disciplinare: M-PSI/02

**Encoding of visual targets during 3D reaching movements
in human and non-human primates**

Presentata da: **Dott.ssa Valentina Piserchia**

Coordinatore Dottorato

Supervisore

Prof.ssa Monica Rubini

Prof.ssa Patrizia Fattori

Esame finale anno 2018

Abstract

Executing a movement towards a sensory target requires a transformation between reference frames. Neuropsychological and neurophysiological studies have provided evidence that the neural correlates of these transformations are reflected in the activity of the posterior parietal cortex (PPC). In addition, the PPC is also crucial for the encoding of reach target position in three dimensional (3D) space. This has been highlighted also by neuropsychological studies on patients with parietal cortex lesion (optic ataxia) which provided evidence of impaired movement control especially in the sagittal plane.

The aim of my thesis was to investigate how reaching for visual targets placed in 3D space, at various depths and directions, influences the coordinate frames and the kinematics in non-human and human primates. To this end, I conducted three studies, which provided new insights in this topic. The first study was conducted on non-human primates to find the predominant reference frame of cells in a specific reach related area of the PPC (area PEc) while reaching towards targets placed at different depths and directions; we tested whether PEc reaching cells displayed hand-centered and/or body-centered coding of reach targets. We found that the majority of PEc neurons encoded targets in a mixed body/hand-centered reference frame. Our findings highlight a role for area PEc as intermediate node between the visually dominated area V6A and the somatosensory dominated area PE. The second study was conducted on healthy human subjects to find the reference frame used while reaching towards targets placed at different depths and directions. Our results revealed reach error patterns based on both eye- and space-centered coordinate systems: in depth more biased towards a space-centered representation and in direction mixed between space- and eye-centered representation. These behavioral results, together with the previous work from my lab where both eye- and space-centered representations were found differently balanced across neurons, can suggest that what we have found here is the outcome, at behavioral level, of the neural discharges investigated in non-human primates. The third study was conducted on a patient with a parietal cortex lesion who showed optic ataxia (OA) symptoms. We wanted to verify which component of visuo-motor control was impaired, given that these patients show deficits in visuo-manual guidance especially when reaching to targets located in the periphery of the visual field. By manipulating gaze position and hand position of visual reaching targets, placed at different depth and directions, we investigated how reaching in peripheral and central viewing conditions

influenced the trajectories and reach errors of the patient and control subjects. Firstly, with our results, we suggest that the reaching inaccuracies observed, in particular in the configurations where the direction of gaze and reach differed, are due to a disruption of the online correction mechanism, which is able to adjust in healthy subjects the predefined motor plan, and secondly, that the PPC is involved in these automatic corrections.

Overall, the studies described in this thesis aim for a deeper understanding of how the brain represents objects in space and how action related regions of the dorso-medial visual stream are involved in higher level cognitive functions related to actions such that of coordinate frame transformations.

Table of Contents

| | |
|---|-----------|
| 1. Introduction | 1 |
| 2. Current state of knowledge and aim | 3 |
| 2.1 The posterior parietal cortex | 3 |
| 2.1.1 <i>General anatomy of the posterior parietal cortex</i> | 4 |
| 2.1.2 <i>Area PEc</i> | 5 |
| 2.2 Reaching and reference frames: the role of posterior parietal areas | 6 |
| 2.3 Coordinate systems for reaching in 3D space: the role of posterior parietal areas | 8 |
| 2.4 Kinematic studies of reference frames and depth and direction contribution to reaching | 10 |
| 2.5 Effects of lesions of the posterior parietal cortex: optic ataxia | 11 |
| 2.5.1 <i>Optic ataxia: deficit in reaching towards targets located at different depths and directions</i> | 14 |
| 2.6 Aim of the projects | 15 |
| 3. Mixed body/hand reference frame for reaching in 3D space in macaque parietal area PEc | 18 |
| 3.1 Abstract | 18 |
| 3.2 Introduction | 18 |
| 3.3 Materials and Methods | 22 |
| 3.3.1 <i>Behavioral Paradigm: reaching in depth task</i> | 23 |
| 3.3.2 <i>Data Analysis</i> | 24 |
| 3.3.3 <i>Population Analysis of Reference Frames</i> | 25 |
| 3.4 Results | 30 |
| 3.4.1 <i>Population Analyses of Reference Frames</i> | 32 |
| 3.4.1.1 <i>Euclidean Distance Analysis</i> | 32 |
| 3.4.1.2 <i>Alternative methods of analyses of reference frames</i> | 34 |

| | | |
|-----------|---|-----------|
| 3.4.1.3 | <i>Convergence of the different analyses</i> | 40 |
| 3.4.1.4 | <i>Correlation Analysis</i> | 43 |
| 3.5 | Discussion | 45 |
| 4. | Multiple coordinate systems and motor strategies for reaching movements when eye and hand are dissociated in depth and direction | 50 |
| 4.1 | Abstract | 50 |
| 4.2 | Introduction | 51 |
| 4.3 | Materials and Methods | 53 |
| 4.3.1 | <i>Participants and Ethics statement</i> | 53 |
| 4.3.2 | <i>Apparatus and Stimuli</i> | 53 |
| 4.3.3 | <i>Behavioral Paradigm</i> | 56 |
| 4.3.4 | <i>Data Analysis</i> | 57 |
| 4.4 | Results | 61 |
| 4.4.1 | <i>Analysis of reach error patterns</i> | 61 |
| 4.4.2 | <i>Analysis of movement variability</i> | 68 |
| 4.5 | Discussion | 72 |
| 4.5.1 | <i>Comparison with other studies of reaching in depth</i> | 76 |
| 4.5.2 | <i>Conclusion</i> | 77 |
| 5. | Reaching in 3D space, effects of brain lesions in the posterior parietal cortex | 79 |
| 5.1 | Abstract | 79 |
| 5.2 | Introduction | 80 |
| 5.3 | Materials and Methods | 82 |
| 5.3.1 | <i>Participants</i> | 82 |
| 5.3.2 | <i>Case history and neuropsychological assessment</i> | 83 |
| 5.3.3 | <i>Apparatus and Stimuli</i> | 84 |
| 5.3.4 | <i>Behavioral Paradigm</i> | 85 |
| 5.3.5 | <i>Data Analysis</i> | 88 |

| | |
|---|------------|
| 5.4 Results | 89 |
| 5.4.1 <i>Analysis of the trajectories</i> | 89 |
| 5.4.2 <i>Analysis of reach errors</i> | 101 |
| 5.5 Discussion..... | 108 |
| 5.5.1 <i>Trajectory impairments</i> | 108 |
| 5.5.2 <i>Reaching errors</i> | 109 |
| 6. General conclusions | 111 |
| 7. References | 115 |

List of figures

| | | |
|-------------------|---|----|
| Figure 2-1 | <i>The two main pathways of visual input into the dorsal and ventral streams..</i> | 4 |
| Figure 2-2 | <i>Dorsal view of left hemisphere and medial view of right hemisphere showing the location and extent of medial PPC areas.....</i> | 5 |
| Figure 2-3 | <i>Posterolateral view of a partially dissected macaque brain illustrating the location of area PEc</i> | 6 |
| Figure 2-4 | <i>Schematic representation of how the brain computes the location of objects in a coordinate system relative to the observer</i> | 8 |
| Figure 2-5 | <i>Reaching for a target in an exemplary patient with optic ataxia</i> | 12 |
| Figure 2-6 | <i>Schematic representation of the experimental setup for movements towards different directions and depths</i> | 15 |
| Figure 3-1 | <i>Brain location of area PEc and experimental setup.....</i> | 21 |
| Figure 3-2 | <i>Examples of neuronal modulation in PLAN and REACH epoch.....</i> | 31 |
| Figure 3-3 | <i>Population analysis of the reference frames of PLAN and REACH activity</i> | 33 |
| Figure 3-4 | <i>Results from separability analysis</i> | 35 |
| Figure 3-5 | <i>Strength of modulation by target and hand signals</i> | 36 |
| Figure 3-6 | <i>Results of the gradient analysis.</i> | 39 |
| Figure 3-7 | <i>Convergence of the results of different analyses</i> | 42 |
| Figure 3-8 | <i>Correlation analysis of the reference frames of PLAN and REACH activity for the population of PEc modulated cells</i> | 44 |
| Figure 3-9 | <i>Functional gradient in medial PPC</i> | 49 |
| Figure 4-1 | <i>Experimental setup.....</i> | 55 |
| Figure 4-2 | <i>Gradient and vector analysis for real reach errors in direction in an exemplary participant.....</i> | 62 |
| Figure 4-3 | <i>Gradient and vector analysis for real reach errors in depth.....</i> | 64 |
| Figure 4-4 | <i>Vector length positions with respect to lower and upper CIs.....</i> | 66 |

| | |
|---|-----|
| Figure 4-5 <i>Correlation analysis</i> | 68 |
| Figure 4-6 <i>Actual trajectories of the movement</i> | 69 |
| Figure 4-7 <i>Spatial variability analysis</i> | 71 |
| Figure 5-1 <i>Site of the lesion of the patient in the right parietal-occipital cortex</i> | 84 |
| Figure 5-2 <i>Experimental setup</i> | 87 |
| Figure 5-3 <i>Examples of hand trajectories</i> | 90 |
| Figure 5-4 <i>Deviation of the first and last half of the trajectories</i> | 92 |
| Figure 5-5 <i>Mean deviations of the first and last half of the trajectories towards targets placed at different depths</i> | 95 |
| Figure 5-6 <i>Mean deviations of the first and last half of the trajectories towards targets placed at different directions</i> | 97 |
| Figure 5-7 <i>Correlation of deviations from the ideal trajectory</i> | 100 |
| Figure 5-8 <i>Reach errors</i> | 104 |
| Figure 5-9 <i>Linear regression of reach errors</i> | 106 |
| Figure 5-10 <i>Representation of the correlation of the reach errors and the deviations of the first and last half of the trajectory</i> | 107 |

1. Introduction

Reaching towards a visual target in space, even though in everyday life is an action that is performed without intense cognitive effort, requires many complex computational processes that integrate visual and proprioceptive information to program and execute reaching movements. The processes between the transduction of the sensory stimulus into biochemical inputs and the muscle contractions that are needed to move the limb include attention, decision-making, response selection, coordinate frame transformations. To execute reaching movements firstly visual information about the object location is mapped within the early stages of the visual cortex in a coordinate system based on eye position (retinocentric frame of reference). Then information about the object location is mapped within the motor cortex in a coordinate system based on hand and body position (hand- and body-centered frame of reference). Executing a movement towards a sensory target requires a transformation between reference frames (for a review see: Soechting and Flanders, 1992; Andersen et al., 1993 and Crawford and Guitton, 1997). Neuropsychological and neurophysiological studies have provided evidence that the neural correlates of these transformations are reflected in the activity of the posterior parietal cortex (PPC) (for a review see: Andersen and Buneo, 2002). In addition, the PPC is also crucial for the encoding of reach target position in three dimensional (3D) space. This has been highlighted by neuropsychological studies on patients with parietal cortex lesion (optic ataxia) which provided evidence of impaired movement control (Holmes, 1919; Brain, 1941; Karnath and Perenin, 2005) especially in the sagittal plane (Danckert et al., 2009).

The present thesis will examine the coordinate frames used during reaching for depth and directional targets and how reach related regions contribute to the planning and control of arm movements towards objects placed at different depths and direction in 3D space.

To this aim we conducted three studies: the first study was conducted on non-human primates to find the reference frame of cells in a specific reach related area of the PPC, area PEc, while reaching towards targets placed at different depths and directions; the second study was conducted on healthy human subjects to find the reference frame used while reaching towards targets placed at different depths and directions; the third study was conducted on a human subject with optic ataxia (OA) to verify which component of visuo-motor control is impaired and to functionally relate the impaired

behavior with the lesioned anatomical substrates. In particular, we studied the involvement of the PPC in eye-hand coordination and tested how depth and direction signals influence arm movements.

The thesis is organized in seven chapters: the first chapter and second chapter report a general introduction and state of knowledge of the topic of encoding of spatial information in the PPC during reaching movements, along with the aim of my research; the third, fourth and fifth chapters include three scientific articles: the first (already published: Piserchia V, Breveglieri R, Hadjidimitrakis K, Bertozzi F, Galletti C, Fattori P. *Mixed body/hand reference frame for reaching in 3D space in macaque parietal area PEc*. Cerebral Cortex, 2017; 27:1976-1990) is based on electrophysiology data from non-human primates, the second (already published: Bosco A, Piserchia V and Fattori P. *Multiple coordinate systems and motor strategies for reaching movements when eye and hand are dissociated in depth and direction*. Frontiers in Human Neuroscience, 2017; 11:323) and the third (in preparation: Piserchia V, Bosco A and Fattori P. *Reaching in 3D space, effects of brain lesions in the posterior parietal cortex*) are based on behavioral data from human subjects. The sixth chapter summarizes the results of my studies and draws a general conclusion. The seventh chapter includes all the references.

2. Current state of knowledge and aim

2.1 The posterior parietal cortex

When we interact with our surroundings, visual information in the brain follows two main pathways: the dorsal and ventral streams (Fig. 2-1). In the classical view, which has been slightly refined in recent years (for a review see: Binofsky and Buxbaum, 2013; Galletti and Fattori, 2017) the ventral stream, which starts from the striate cortex and continues to the temporal cortex, is involved in perception of the incoming visual information (the so called “*what*” pathway) and the dorsal stream, which starts from the striate cortex and continues to the parietal cortex is involved in the guidance of action (the so called “*where/how*” pathway) (Ungerleider and Mishkin, 1982; Goodale and Milner, 1992; Milner and Goodale, 1995). Evidence for this proposal came from findings on neurological patients with lesions of one of the two pathways. Patients with bilateral lesions of the ventral stream showed the inability to identify objects or estimate their shapes and size, whereas they were able to execute correct grasping movements to the same objects (Goodale, Milner, Jakobson and Carey, 1991; Milner et al., 1991); instead it was shown that patients with lesions of the posterior parietal cortex (PPC), located along the dorsal stream, exhibited severe visuo-motor deficits showing large deviations of goal directed movements towards targets whereas they were able to identify correctly shape and size of the targets (Perenin and Vighetto, 1988; Milner et al., 2001).

The PPC, located along the dorsal stream, is a set of regions connected to visual cortices and premotor areas. “It can be considered as an intermediate stage in the process leading from vision to movement” (Battaglia-Mayer et al., 2006). PPC is crucial for the encoding of space and the control of visually guided movements. It includes several reach-sensitive cortical areas: for example area V6A (Galletti et al., 1999; Fattori et al., 2001; 2012; Galletti and Fattori, 2017), area PEc (Breviglieri et al., 2006, 2008; Bakola et al., 2010). Neurophysiological evidence support this division of competence among the ventral and dorsal stream. It has been shown that posterior parietal lesions impair the ability to reach for targets in space (Karnath and Perenin, 2005).

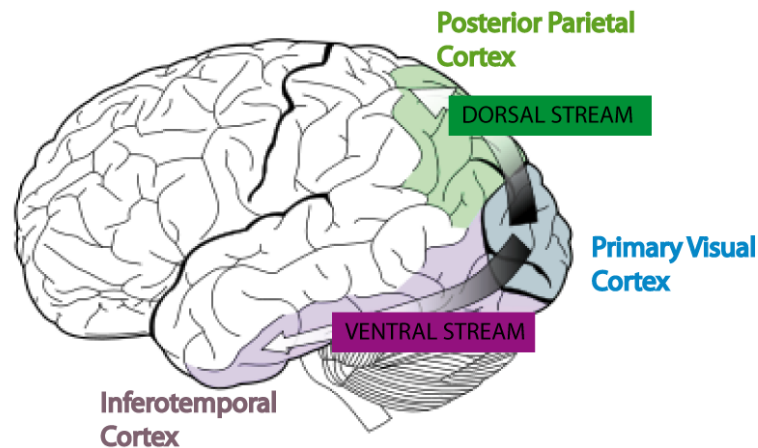


Figure 2-1. (Adapted from Milner and Goodale, 1995). The two main pathways of visual input into the dorsal and ventral streams. The schematic drawing of this human brain illustrates the approximate routes of the cortico-cortical projections from the primary visual cortex to the posterior parietal and the inferotemporal cortex, respectively.

2.1.1 General anatomy of the posterior parietal cortex

The PPC is located between the somatosensory cortex in the postcentral gyrus and the visual cortex in the occipital lobe. Anatomically it is delineated by three sulci: the lateral sulcus (LuS) separates it from the temporal lobe, the central sulcus (CeS) from the frontal lobe, and the parieto-occipital sulcus (POS) from the occipital lobe. The PPC is composed of two lobules: the superior parietal lobule (SPL) and the inferior parietal lobule (IPL) separated by the intraparietal sulcus (IPS). The IPL in humans extends to the angular and supramarginal gyrus, the regions classified as Brodmann area 39 and 40, respectively. The SPL, on the medial part of the PPC, includes several reach selective areas (Fig. 2-2) as demonstrated by recent physiological and neuroanatomical studies in the macaque monkey (Ferraina et al., 1997; Snyder et al., 1997; Battaglia-Mayer et al., 2001; Fattori et al., 2001, 2005, Galletti and Fattori, 2017; McGuire and Sabes, 2011; Hwang et al., 2014; Hadjidimitrakis et al., 2014a, 2015): areas PE and PEc, located nearby on the exposed surface of SPL, area PGm located on the mesial surface of the hemisphere, area V6A, located in the parieto-occipital sulcus, and the functionally defined parietal reach region (PRR) which includes a number of

anatomically defined cortical areas, including MIP (Gail and Andersen, 2006), located in the medial bank of intraparietal sulcus (Andersen et al., 2014; Hwang et al., 2014).

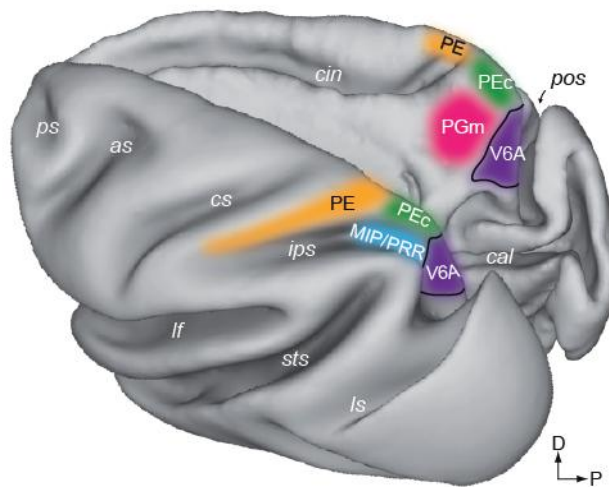


Figure 2-2. (Adapted from Galletti and Fattori, 2017) Dorsal view of left hemisphere (left) and medial view of right hemisphere (right) showing the location and extent of medial PPC areas: purple V6A (Galletti et al., 1991); green: PEc (Pandya and Seltzer, 1982); orange: PE (Pandya and Seltzer, 1982); blue: MIP/PRR, medial intraparietal area/parietal reach region (Colby and Duhamel, 1991; Snyder et al., 1997); magenta: PGm (Pandya and Seltzer, 1982); Sulci are also shown: as, arcuate sulcus; cal, calcarine sulcus; cin, cingulate sulcus; cs, central sulcus; ips, intraparietal sulcus; lf, lateral fissure; ls, lunate sulcus; pos, parieto-occipital sulcus; ps, principal sulcus; sts, superior temporal sulcus. D, dorsal; P, posterior.

2.1.2 Area PEc

PEc is an area of the PPC, located in the posterior part of the SPL, that Brodmann ascribed to area 7 (Brodmann, 1909) and other authors later recognized as a distinct parietal cytoarchitectural pattern (Pandya and Seltzer, 1982; Luppino et al., 2005). It is a small portion of the cortex linking V6A posteriorly with PE anteriorly. It was defined on cytoarchitectural grounds by Pandya and Seltzer (1982). This area belongs to a network of areas in the SPL, the dorsomedial network, that integrate and process visual, somatosensory and motor information to program and control reaching arm movements (Fig. 2-3) (Snyder et al., 1997; Buneo et al., 2002; Galletti et al., 2003; Breveglieri et al., 2006; Bakola et al., 2010; McGuire and Sabes, 2011). Several physiological studies

on non-human primates found that PEc contains cells modulated by passive somatosensory stimuli (Breveglieri et al., 2006), cells sensitive to visual stimuli (Squatrito et al., 2001) as well as neurons sensitive to oculo-motor activity and arm reaching movements (Batista et al., 1999; Battaglia-Mayer et al., 2001; Ferraina et al., 2001). It has been suggested that PEc is a visuomotor area involved in creating and maintaining an internal representation of one's own body (Breveglieri et al., 2006).

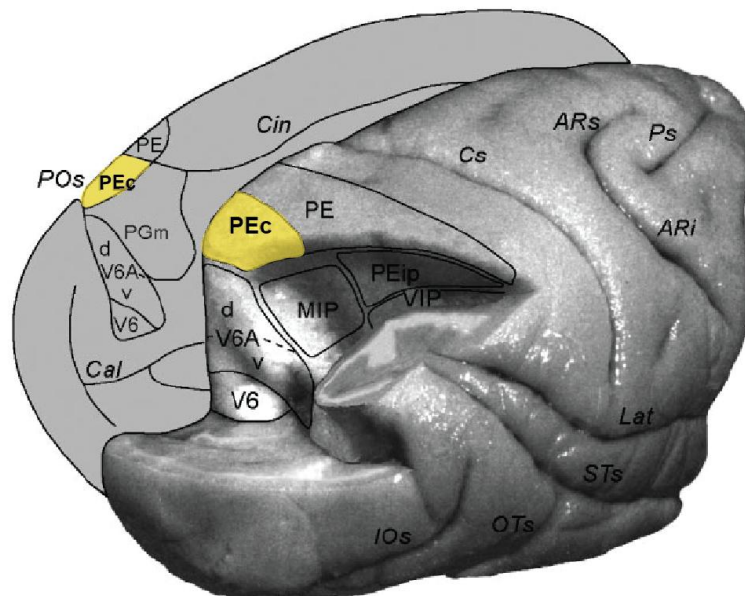


Figure 2-3. Posterolateral view of a partially dissected macaque brain (modified from Galletti et al., 1996; Gamberini et al., 2009) illustrating the location of area PEc and location and extent of all the other areas that form the superior parietal cortex of the macaque brain: V6, V6Ad, V6Av, PE, MIP, PEip, VIP, PGm. PEc is located in the posterior part of the superior parietal lobule of macaque brain. This area belongs to a network of areas in the SPL that integrate and process visual, somatosensory and motor information like areas of the dorsocaudal part of the superior parietal lobule such as area PE and V6A. The main sulci are also shown: POs, parietal occipital sulcus; Cal, calcarine sulcus; Cin, cingulated sulcus; IOs, inferior-occipital sulcus; OTs, occipital-temporal sulcus; STs, superior temporal sulcus; Cs, central sulcus; ARs, superior arcuate sulcus; ARi, inferior arcuate sulcus; Ps, principal sulcus.

2.2 Reaching and reference frames: the role of posterior parietal areas

The PPC has been classically viewed as a sensory and motor structure; it receives visual information from the extra-striate areas and it is connected to the premotor and motor

cortices (for a review see: Battaglia-Mayer et al., 2006). However, recent work indicates that the PPC is involved in higher level cognitive functions related to actions (for a review see: Andersen and Buneo, 2002). Among these cognitive functions there is the planning for action: several and segregated intentions-related areas are involved in multisensory integration and coordinate transformations.

One of the main challenges for the central nervous system (CNS) is how to integrate input signals from different sensory modalities and transform them into motor commands. In order to interact with the world around us, the brain has to construct multiple representations of space. These representations are central for the efficient coordination of behaviors like reaching, walking etc. These maps of space are represented by the brain in a variety of reference frames. The reference frame can be described as a set of axes, reference position and reference orientations, with respect to which the brain represents the location, direction of objects in space. The choice of a particular reference frame impacts on the mathematical operations that the brain undertakes to generate the adequate motor output (Khan et al., 2008). There are two main classes of reference frames: egocentric and allocentric. The egocentric reference frame represents objects and location in a coordinate system relative to the observer (for example eye-centered, head-centered, arm-centered coordinates); allocentric reference frames represent the location in a coordinate system external to the observer: in environmental (world-centered) coordinates, for example room-centered, and in coordinates centered on an object of interest for example object-centered coordinates (for a review see: Colby, 1998; Szczepanski and Saalman, 2013; Filimon, 2015).

As far as the egocentric representations are concerned, to efficiently direct actions to where the target of interest is, firstly visual information about the object location is mapped within the early stages of the visual cortex in a coordinate system based on eye position. We refer to this as coding an object in a retinocentric frame of reference. To code reaching movements in space, information about the object location is mapped within the motor cortex in a coordinate system based on hand and body position. We refer to this as coding an object in a hand- and body-centered frame of reference. For example, when we want to reach for a cup (Fig. 2-4) the brain computes the location of the cup in a coordinate system based on several body parts like eye, head, hand etc. How does the brain translate the position of the cup from the coordinates of the retina into coordinates centered on the hand that executes the reaching? How is eye-hand coordination achieved? Executing a movement towards a sensory target requires a

transformation between reference frames (for a review see: Soechting and Flanders, 1992; Andersen et al., 1993; Crawford and Guitton, 1997). Several studies helped to elucidate the neural correlates of these transformations which are reflected in the activity of the posterior parietal cortex.

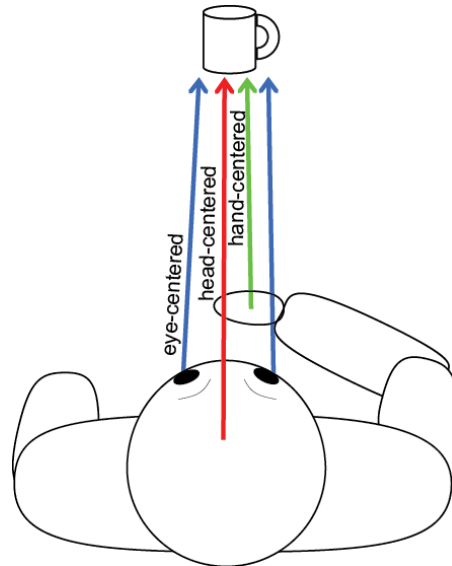


Figure 2-4. Schematic representation of how the brain computes the location of objects in a coordinate system relative to the observer (egocentric representation). Blue vectors represent the location of the cup in an eye-centered frame of reference. The red vector represents the location of the cup in a head-centered frame of reference and the green vector in a hand-centered frame of reference.

2.3 Coordinate systems for reaching in three-dimensional space: the role of posterior parietal areas

The PPC plays an important role in the coding of three-dimensional space, in particular related to the depth and direction dimension.

Several physiological studies showed that the PPC encodes the direction and depth of reaching movements. Several areas of the PPC have been found to be implicated in the processing of distance in peripersonal space. Each area of the PPC of non-human primates studied, encodes the distance in a specific coordinate system: PRR/MIP, located in the medial bank of the intraparietal sulcus, encodes the location of reach targets in an eye-centered reference frame (Batista et al., 1999; Bhattacharyya et al., 2009); area PE, located in the rostral part of the SPL, in hand-centered frame

(Ferraina et al., 2009); area V6A, located in the caudal part of the superior parietal lobule (Galletti et al., 1999) in a body-centered and mixed-centered frame of reference (Hadjidimitrakis et al., 2014a). Hadjidimitrakis and colleagues, tested whether hand-centered coding of reach targets occurs in V6A. Reaching targets were presented at different distances and lateralities from the body and were reached from two initial hand positions located at different depths. The authors found that the majority of neurons encoded targets in a body-centered and mixed body- and hand-centered frame of reference while only a minority of cells encoded targets in a hand-centered frame of reference (Hadjidimitrakis et al., 2014a). Bhattacharayya and colleagues investigated how a reach target is represented in three dimensions in the posterior parietal reach region (PPR) studying the integration of disparity and vergence signals. The authors found that PPR/MIP encoded the location of reach targets in an eye-centered reference frame (Bhattacharyya et al., 2009); Ferraina and colleagues examined how PE integrates information about eye and hand position to encode target distance for reaching in depth. The authors found that PE neurons encoded depth in hand-centered frame of reference (Ferraina et al., 2009); Marzocchi and colleagues (2008), by comparing the neuronal discharges of the same cell during the execution of foveated and non-foveated reaching movements towards the same or different spatial locations, found that in V6A neurons had an eye-centered coding in addition to body- and mix-centered coding. Several of the previous cited works have studied only depth neglecting direction (Bhattacharyya et al., 2009; Ferraina et al., 2009), others have studied direction but not depth (Marzocchi et al., 2008). The first study that showed the neural correlates of both depth and direction in the medial PPC was that by Lacaquaniti and colleagues (1995). The authors tested both the effects of depth and direction on the neurons in area PE during arm reaching movements. The monkeys performed movements starting from one of three possible initial hand positions towards one of eight reach targets located in three-dimensional space. The authors found that the majority of neurons was influenced by the spatial location of the hand within a shoulder-centered reference frame with neurons encoding azimuth, elevation or reach amplitude individually. Lately a study by Hadjidimitrakis and colleagues (2014b) addressed the neural correlates of both depth and direction dimensions; the authors found that in V6A information about distance and direction was jointly encoded in many neurons supporting the existence of a common neural substrate for the encoding of target depth and direction in the PPC.

Recently, Bosco and colleagues (2016) investigated whether eye-centered coding in

depth and direction dimension was present in area V6A during a three-dimensional reaching task with nine target locations where gaze position and target position were decoupled. The authors found a mixed eye- and spatial-centered encoding of target position with the eye-centered encoding and the spatial-centered encoding differently balanced within the same neuron: depth was encoded in an eye-centered reference frame whereas direction was encoded in a spatial-centered reference frames.

In addition, another recent paper showed that a large percentage of neurons in area PEc is involved in encoding both direction and depth during arm reaching movements (Hadjidimitrakis et al., 2015); though the reference frames displayed by PEc neurons during arm reaching movements has not been investigated so far and it is the topic of the present thesis (Chapter 3).

2.4 Kinematic studies of reference frames and depth and direction contribution to reaching

Physiological and behavioral investigations have targeted reaching movements to highlight principles underlying the process of visuomotor transformation. To study how the brain computes locations in space, the role of direction during arm reaching/grasping movements has been investigated in previous psychophysical studies in healthy subjects. Several authors showed that the location of the target is encoded in an eye-centered reference frame (Henriques et al., 1998; Medendorp and Crawford, 2002). The first important study which demonstrated the use of a gaze-centered reference frame in humans was conducted by Henriques and colleagues (1998). Participants had to reach to the location of a remembered, visually presented target (LED). In different conditions, participants had to fixate their gaze on various locations relative to the target when it was presented or had to move their eyes to a certain location between target presentation and movement onset. Results revealed reaching errors that varied systematically with fixation location relative to the target. The authors concluded that the reach targets were encoded in a gaze-dependent frame of references. Of particular interest for our study was the work by Van Pelt and Medendorp (2008) since the authors studied the combined role of depth and direction on healthy subjects (Van Pelt and Medendorp, 2008). Their aim was to study the reference frames used by the subjects to encode reaching movements in depth and direction. Nine LEDs targets were presented in front of the subject on a horizontal plane, slightly below the eyes.

They had either the subject fixating central and touching all the possible nine target locations or the subject changing fixation (intervening saccade) to a second fixation light and touching to where the first fixation target previously appeared. Their results, both in depth and direction, showed that the location of the target was encoded in an eye-centered reference frame. Even though the eye-centered reference frame seems to play an important role, there are also other egocentric reference frames for coding locations of visual and proprioceptive targets (such as eye-centered, hand-centered, body-centered) (Beurze et al., 2006; Tramper and Medendorp, 2015; Mueller and Fiehler, 2016). Khan and colleagues (2007), varying target position and initial hand position in the direction dimension, found that multiple reference frames are used to execute reaching movements: reaching errors of all the subjects revealed an influence of target position in gaze-centered coordinates but also showed a shoulder-centered influence of target position. Gordon et al. (1994), in a task where depth and direction component were studied conjunctly, instead found that the pattern of errors during reaches revealed a hand-centered coding for the reach.

The analyses of kinematics in previous psychophysical experiments suggested that the spatial coordinate system used by the brain to represent target position changes depending on the task requirements (Graziano, 2001a). The topic of the present thesis is to study the effect of both depth and direction signals on the kinematic of movement and to analyze the patterns of errors to define the coordinate system in which the movements are executed: eye-centered, space-centered (Chapter 4).

2.5 Effects of lesions of the posterior parietal cortex: optic ataxia

The role of depth and direction during arm reaching/grasping movements has been investigated both in non-human and human primates. In particular, studies of posterior parietal cortex lesions in human subjects, have been of valuable importance in understanding more in general dorsal stream functions and in discovering the PPC functions. In fact, it has been shown that the accuracy for reaching to targets can be severely affected by lesions of the PPC, like those that are observed in patients with OA.

OA is a high level visuomotor deficit that cannot be attributed to a simple visual or motor deficit since patients can perform accurate reaches under some circumstances and not under others: patients typically misreach when guiding a limb in peripheral

space (Fig. 2-5) towards targets that are not foveated (non foveal OA) (Perenin and Vighetto, 1988; Karnath and Perenin, 2005) and most often make errors in the direction of their gaze (Buxbaum and Coslett, 1997); in a less usual form, called foveal OA, patients misreach targets even when they are directly foveated (Pisella et al., 2000). Performance is generally worse with the hand contralateral to the lesion and in the visual field contralateral to the lesion (Khan et al., 2007; Blangero et al., 2008). Nevertheless it has been found that memorized visual info improve grasping movements when the movement onset is postponed around 5 seconds after target presentation (Milner et al., 2001, 2003; Rossetti et al., 2005; Himmelbach and Karnath, 2005).



Figure 2-5. (Taken from Karnath and Perenin, 2005) Reaching for a target in a patient with optic ataxia. The left brain-damaged patient showed gross and uncorrected misreaching for a target in peripheral vision (when he had to fixate the camera lens in front of him) (left picture) and normal reaching under foveal vision (when he had to orient eyes and head towards the object while reaching for it) (right picture). Ataxic reaches were performed most frequently with the contralesional hand in contralesional space.

Initially OA was described by a Hungarian physician Rezső Balint, and few years later by Holmes, as a component of one of the three visuospatial symptoms of the Balint's syndrome (Balint, 1909; Holmes et al., 1919). The syndrome includes three main spatial deficits including OA; Balint described the other two symptoms as a psychic paralysis of gaze, probably corresponding to simultagnosia (the inability to perceive more than one object at a time), and as lateralized spatial disorder of attention,

probably corresponding to neglect. A few years later Holmes (1918) described a “visual disorientation syndrome” in soldiers who had a bilateral parietal damage, these patients had difficulties in judging the location and distance of an object. The syndrome today is also called Balint-Holmes syndrome, incorporating the reports of Balint and Holmes.

More recent studies showed that OA can also occur as a distinct disorder in isolation, without the other symptoms associated with the Balint’s syndrome (Perenin and Vighetto, 1988). It can occur with unilateral (Perenin and Vighetto, 1988; Karnath and Perenin, 2005) or bilateral PPC lesion (Karnath and Perenin, 2005; Khan et al., 2005; Pisella et al., 2000, 2004). The sites of the lesion typically involve the parietal occipital junction (POJ), the superior parietal lobule (SPL) and areas around the intra parietal sulcus (IPS) (Karnath and Perenin, 2005; Martin, Karnath, Himmelbach, 2015).

Optic ataxia, as originally observed by Balint (1909), is modality specific: patients exhibit misreaching errors towards visual stimuli but not to auditory or tactile stimuli (Rossetti et al., 2003) and this suggests that OA could be the result of a deficit in coupling vision and action. Nevertheless different hypotheses about the causes of the misreachings observed in OA patients have been put forward by several authors according to their results.

The interpretation of OA as a visuomotor deficit came from patients which showed an interaction between reaching deficits in different visual fields (field effect) and reaching deficits with either hand (hand field effect) (Perenin and Vighetto, 1988). Recent studies provided other interpretations of this deficit (Pisella et al., 2000; Khan et al., 2013). Pisella and colleagues proposed that OA is an online control deficit; they found that patients fail to make corrections when the target is unexpectedly displaced (Pisella et al., 2000). In their experiment both healthy subjects and the patient were able to point correctly to a target when it was still, but when the target was unexpectedly displaced the healthy subjects were able to adjust while the patient could not. An alternative hypothesis was provided by other authors who interpreted OA as a coordinate frames transformation deficit (Jax et al, 2009; Khan et al., 2013). Several authors found that reaching errors are caused by the disruption of different reference frames according to the type of task employed: gaze-centered (Khan et al, 2005; Jax et al., 2009), head-centered (Frassinetti et al., 2007; Jax et al., 2009). Khan et al., (2007) proposed that OA is a result in deficit of sensorimotor integration, that is to say that reach errors observed in OA can be explained by deficits which involve sensorimotor

transformation and integration of hand and target position to form the movement vector within the PPC.

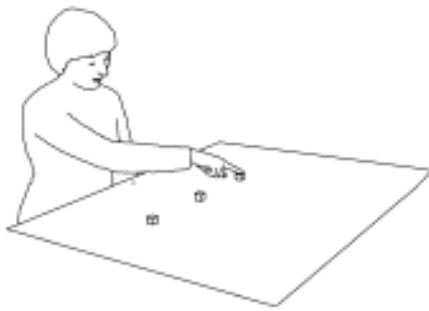
2.5.1 Optic ataxia: deficit in reaching towards targets located at different depths and directions

Several studies showed that patients with OA are able to recognize objects but not their spatial relationships more in depth than in direction (Brain, 1941; Holmes and Horrax, 1919; Perenin and Vighetto, 1988; Baylis and Baylis, 2001; Dankert et al., 2009; Cavina-Pratesi et al., 2010).

Baylis and Baylis (2001) were the first to examine the role of the PPC in depth/direction representation. Their results showed that the OA patient exhibited deficits in visually guided reaching movements towards targets located at different depths more than towards targets located at different directions, underlying that lesions to the SPL produce severe deficits in the depth component of visually guided arm movements.

Consistent with the findings by Baylis and Baylis (2001), also the study by Dankert and colleagues (2009) supported the role of PPC in encoding the location of reach targets. In their experimental set-up (Fig. 2-6), three targets were positioned one after the other in the sagittal plane in one condition and in the frontoparallel plane in another condition. The subjects were required to reach to the foveated targets in sequence. The hand starting position was placed either next to the body or far from it. The eyes were free to move. The authors found that the movements of the controls and the OA patient executed in the sagittal axis were more disordered than movements executed in the frontoparallel plane but the patient showed more deficits compared to the controls, as a consequence of a lesion in the right superior parietal cortex.

Frontoparallel Movements



Sagittal Movements

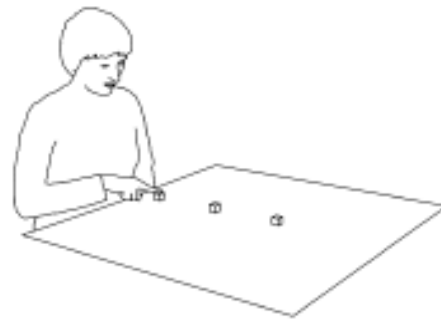


Figure 2-6. (Adapted from Dankert et al., 2009) Schematic representation of the experimental setup for movements towards different directions (frontoparallel movements, left panel) and different depths (sagittal movements, right panel).

In line with the findings by Dankert and colleagues (2009), the study by Cavina-Pratesi and colleagues (2010) explored the role of depth during reaching performance. The authors investigated the performance of an OA patient, manipulating the position of the target either far from the starting hand position or close to it. The subject had to reach or grasp objects of different size placed close or far from the body while always fixating a central fixation cross. The errors in reaching were present only when reaching for objects presented at the far distance.

In this thesis I will examine the mechanism of hand reaching movements towards targets placed at different depth and directions using both a foveal and extrafoveal reaching paradigm in healthy human subjects (Chapter 4) and in a subject with OA symptoms (Chapter 5).

2.6 Aim of the projects

In this thesis, with a series of experiments, I aimed to examine how reaching behavior in depth and direction influences the coordinate frames and the kinematics in non-human and human primates.

The aim of the first experiment (Chapter 3) was to study the coordinate system displayed by cells in area P_{Ec} of non-human primates during arm reaching movements in 3D space.

A very recent paper showed that P_{Ec} is involved in encoding both direction and depth of reaching (Hadjidimitrakis et al., 2015), but the reference frames displayed by P_{Ec} neurons during reaching movements is still unknown. To study the above issues in area P_{Ec}, we used the same experimental paradigm employed by Hadjidimitrakis and colleagues (2014a) in nearby area V6A, where the arm movement started from different positions in depth, and tested whether P_{Ec} reaching cells displayed hand-centered and/or body-centered coding of reach targets. We found that the hand position influences the activity of P_{Ec} cells, but this effect is not strong enough to express a pure hand-centered reference frame. The majority of P_{Ec} neurons encodes targets in a mixed body/hand-centered reference frame. Our findings highlight a role for area P_{Ec} as intermediate node between the visually dominated area V6A and the somatosensory dominated area PE.

In human subjects we have performed two studies (Chapters 4 and 5): one on healthy human subjects and one on a subject with OA symptoms with the primary purpose to investigate the role of depth and direction during arm reaching movements when damage of the parietal lobe is present.

The aim of the second experiment (Chapter 4) was to study how the brain computes locations in space, gaining insight into the underlying reference frames utilized during pointing to targets that vary in depth and direction. The role of depth and the role of direction during arm reaching/grasping movements have been investigated in previous psychophysical studies in healthy subjects, and several authors showed that the location of the target is encoded in an eye-centered reference frame (Henriques et al., 1998; Medendorp and Crawford, 2002; Van Pelt and Medendorp, 2008). In particular, we wanted to elucidate whether the depth and the direction components of a reaching movement were encoded in eye- or space-centered reference frames. To this aim, we employed a memory-guided reaching task with different eye-target configurations in depth and direction. The task design maximizes natural reaching conditions where objects are reached on a horizontal surface and at a comfortable distance. We explored whether different coordinate systems and movement strategies are employed to encode reach direction and depth. Therefore, we compared reach errors patterns and trajectory variabilities for pairs of configurations that shared the same eye/target relative position

and those that shared the same absolute target position. We found a difference between reach errors in direction and depth, with the use of a more mixed reference frame for direction, whereas a stronger tendency towards more space-centered reference frame was found for reaches in depth.

The aim of the third experiment (Chapter 5) was to analyze trajectories and reaching errors to assess the reaching accuracy of a patient with OA in order to study the role of depth and direction on the trajectories of the reaching movement. Several studies, in fact, have shown that the accuracy for reaching to targets can be impaired by lesions of the PPC, like those that have patients who exhibit OA symptoms (Brain, 1941; Holmes and Horrax, 1919; Perenin and Vighetto, 1988; Dankert et al., 2009; Cavina-Pratesi et al., 2010). We employed a reaching tasks with nine target locations at different depth and directions, as already tested in healthy subjects by Bosco and colleagues (Bosco et al., 2017), in which, by manipulating gaze position and hand position (Dankert et al., 2009; Cavina-Pratesi et al., 2010) of visual reach targets we investigate how reaching in peripheral and central viewing conditions influence the trajectories and reach errors of the patient and controls subjects. We employed different configurations of gaze and hand relative position in depth and direction so to test all possible conditions of dissociation of visual target and reaching target, given that OA patients typically show impairments in reaching in peripheral viewing conditions (Buxbaum and Coslett, 1997).

3. Mixed body/hand reference frame for reaching in 3D space in macaque parietal area PEc

A similar version of this manuscript has been published as:

Valentina Piserchia, Rossella Breveglieri, Kostas Hadjidimitrakis, Federica Bertozzi, Claudio Galletti, Patrizia Fattori. *Mixed body/hand reference frame for reaching in 3D space in macaque parietal area PEc*. *Cerebral Cortex*, 2017; 27:1976-1990.

3.1 Abstract

The neural correlates of coordinate transformations from vision to action are expressed in the activity of posterior parietal cortex (PPC). It has been demonstrated that among the medialmost areas of the PPC, reaching targets are represented mainly in hand-centered coordinates in area PE, and in eye-centered, body-centered, and mixed body/hand-centered coordinates in area V6A. Here, we assessed whether neurons of area PEc, located between V6A and PE in the medial PPC, encode targets in body-centered, hand-centered, or mixed frame of reference during planning and execution of reaching. We studied 104 PEc cells in three *Macaca fascicularis*. The animals performed a reaching task towards foveated targets located at different depths and directions in darkness, starting with the hand from two positions located at different depth, one next to the trunk and the other far from it. We show that most PEc neurons encoded targets in a mixed body/hand-centered frame of reference. Although the effect of hand position was often rather strong, it was not as strong as reported previously in area PE. Our results suggest that area PEc represents an intermediate node in the gradual transformation from vision to action that takes place in the reaching network of the dorsomedial PPC.

3.2 Introduction

Reference frames for reaching is one of the most relevant topics of current neuroscience. Defining the reference frame displayed by neurons while a primate is performing, or even just preparing, a reach is of great importance to understand how our

brain encodes object location and processes spatial orientation strategies to interact with objects in the peripersonal space (see for reviews Andersen and Buneo, 2002; Crawford et al., 2011).

Many works performed in the field focused mainly on two portions of the primate cortex: the premotor areas of the frontal cortex and the areas of the posterior parietal cortex (PPC). In the dorsal premotor cortex, neural activity during reach planning is influenced by the location of reach targets relative to the arm and the eyes, either using reference frames centered on hand, eye, or both (Batista et al., 2007), or on the relative position between hand and eye (Pesaran et al., 2006). In the ventral premotor cortex, head- and limb-centered frames of reference are displayed (Graziano and Gross, 1998; Graziano, 1999, 2001a). In the PPC, many distinct subregions were extensively studied at this regard. Among them, there is the parietal reach region (PRR), a functionally defined region located in the medial bank of the intraparietal sulcus. In this region many studies were performed, and gave different contributions: PRR neurons encode object locations in eye-centered coordinates (Batista et al., 1999; Pesaran et al., 2006; Bhattacharyya et al., 2009), in mixed hand-eye reference frames (Chang et al., 2009), or in mixed eye/head reference frames (Mullette-Gillman et al., 2005, 2009). Area V6A, a visuomotor area located in the caudal part of the superior parietal lobule (SPL) (Galletti et al., 1999), has been extensively studied in the last ten years. V6A occupies the most anterior, medial part of Brodmann's area 19 (Brodmann, 1909), but shows a typical parietal cytoarchitectural pattern (Luppino et al., 2005). When reaching targets were arranged in a frontal plane (Marzocchi et al., 2008; Bosco et al., 2014), V6A was reported to encode reach targets in eye-centered and in a combination of eye-centered and spatial reference frames. During reaches in depth, when body-centered versus hand centered coding was compared, V6A neurons showed mostly body-centered or mixed body/hand-centered reference frames, with a few neurons using hand-centered reference frames (Hadjidimitrakis et al., 2014a). Contrary to V6A, area PE (often referred to as area 5 or 5d, Pandya and Seltzer, 1982), located in the rostral part of the SPL, was reported to be strongly influenced by hand position during reaches in depth, and to represent reach targets mainly in a hand-centered frame of reference (Ferraina et al., 2009; Bremner and Andersen, 2012).

In between areas V6A and PE, there is another visuomotor area called PEc (see Fig. 3-1A). PEc occupies a small cortical region in the caudal aspect of SPL, that Brodmann ascribed to area 7 (Brodmann, 1909) and other authors later recognized as a

distinct parietal cytoarchitectural pattern (Pandya and Seltzer, 1982; Luppino et al., 2005). PEc belongs to the dorsomedial network of areas in the PPC that are involved in reaching and integrate visual, somatosensory and motor information to program and control arm movements (Snyder et al., 1997; Buneo et al., 2002; Galletti et al., 2003; Breveglieri et al., 2006; Breveglieri et al., 2008; Bakola et al., 2010; McGuire and Sabes, 2011). It has been also suggested that PEc is an area involved in creating and maintaining an internal representation of one's own body (Breveglieri et al., 2006), and in navigation (Bakola et al., 2010). Finally, a very recent paper showed that PEc is involved in encoding both direction and depth of reaching (Hadjidimitrakis et al., 2015), but the reference frames displayed by PEc neurons during reaching movements is still unknown.

The aim of the present work was to study the coordinate system displayed by cells in area PEc during reaching movements in the 3D peripersonal space. We used the same experimental paradigm employed by Hadjidimitrakis and colleagues (2014a) in nearby area V6A, where the arm movement started from different positions in depth, and tested whether PEc reaching cells displayed hand-centered and/or body-centered coding of reach targets. We found that the hand position influences the activity of PEc cells, but this effect is not strong enough to express a pure hand-centered reference frame. The majority of PEc neurons encodes targets in a mixed body/hand-centered reference frame. Our findings highlight a role for area PEc as intermediate node between the visually dominated area V6A and the somatosensory dominated area PE.

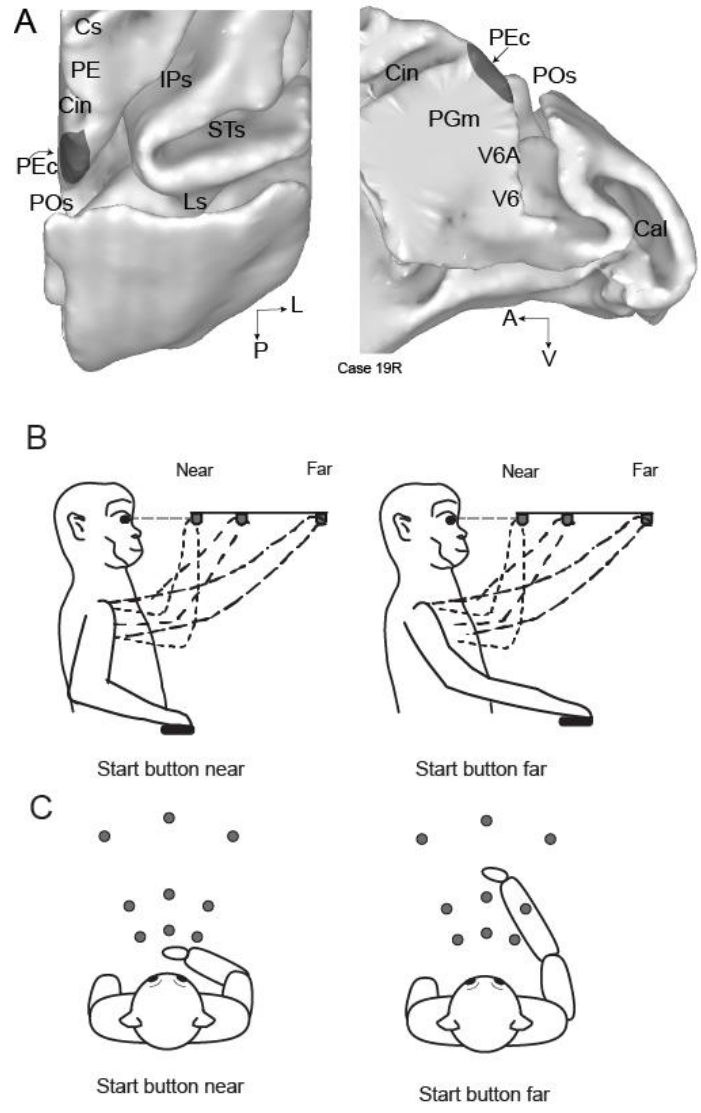


Figure 3-1. Brain location of area PEc and experimental setup. A) dorsal (left) and medial (right) views of the surface-based reconstruction of the caudal half of the right macaque hemisphere. Dark gray areas show the extent and location of area PEc according to the cytoarchitectural pattern (see text). The location of areas PE, V6A, PGm, and V6 is also shown. Cin, Cingulate sulcus; Cal, calcarine fissure; IPs, intraparietal sulcus; Ls, lunate sulcus; POs, parieto-occipital sulcus; STs, superior temporal sulcus; A, anterior; V, ventral; L, lateral; P, posterior. B-C) Setup for the reaching in depth task (B, lateral view, and C, top view). The animals performed reaching movements towards one of the nine LEDs (grey dots) located at different depths and directions starting the movement either from an initial hand position located next to the body (left panel) or from an initial hand position located far from the body (right panel).

3.3 Materials and Methods

Three male macaque monkeys (*Macaca fascicularis*) weighing 3.9-4.4 kg were involved in the study. The animals were first trained to sit in a primate chair and interact with the experimenters. Then, a head restraint system and a recording chamber were surgically implanted under general anesthesia (sodium thiopental, 8 mg/kg*h, i.v.) following the procedures reported by Galletti et al. (1995). A full program of postoperative analgesia (ketorolac tromethamine, 1 mg/kg i.m. immediately after surgery, and 1.6 mg/kg i.m. on the following days) and antibiotic care (Ritardomicina, benzatinic benzylpenicillin + dihydrostreptomycin + streptomycin, 1–1.4 ml/10 kg every 5–6 days) followed surgery. Experiments were performed in accordance with national laws on care and use of laboratory animals and with the European Communities Council Directive of 22 September 2010 (2010/63/EU). All the experimental protocols were approved by the Bioethical Committee of the University of Bologna. During training and recording sessions, particular care was taken to avoid any behavioral and clinical sign of pain or distress.

Extracellular recording techniques and procedures to reconstruct microelectrode penetrations were similar to those described in other papers (Galletti et al., 1996; Breveglieri et al., 2006; Gamberini et al., 2011). Single cell activity was extracellularly recorded from the exposed surface of the posterior part of the superior parietal lobule. We performed multiple electrode penetrations using a 5-channel multi-electrode recording system (Thomas Recording). The electrode signals were amplified (at a gain of 10000) and filtered (bandpass between 0.5 and 5 kHz). Action potentials in each channel were isolated with a waveform discriminator (Multi Spike Detector; Alpha Omega Engineering) and were sampled at 100 kHz.

Histological reconstructions have been performed following the procedures detailed in a recent paper from our laboratory (Gamberini et al., 2011). Electrode tracks and the approximate location of each recording site were reconstructed on histological sections of the brain on the basis of electrolytic lesions and the coordinates of penetrations within recording chamber. The present work include only the neurons assigned to area PEc (Fig. 3-1A) following the cytoarchitectonic criteria according to Luppino et al. (2005) and to Pandya et al. (Pandya and Seltzer, 1982).

3.3.1 Behavioral Paradigm: reaching in depth task

Electrophysiological signals were collected while monkeys were performing a reaching task in darkness with the hand contralateral to the recording site. During the task, the monkeys maintained steady fixation of the reaching targets with their head restrained. The task was performed in two blocks that differed for the starting position of the hand: in both cases, the starting position was on the mid-sagittal plane at waist level, but in one block the hand started from a button placed 4 cm in front of monkey's chest ('near button': left panels in Fig. 3-1B and 3-1C), in the other from a button located 14 cm farther from the near one ('far button': right panels in Fig. 3-1B and 3-1C). In each block, only one of the two buttons was available to press because the other was covered. For each neuron, the block sequence was random. Fixation and reaching targets were 9 Light Emitting Diodes (LEDs) positioned at eye level, at three different distances and directions (Fig. 3-1B and 3-1C). Three LEDs targets were placed at three isovergence angles: the nearest targets were located at 10 cm from the eyes (17.1°); the LEDs located at intermediate and far positions were at a depth of 15 cm (11.4°) and 25 cm (6.9°), respectively. At each isovergence angle, LEDs were positioned in three directions: one central, along the sagittal midline, and two lateral, at iso-version angles of -15° and $+15^\circ$. Target positions were chosen in order to be within the peripersonal space.

The time sequence of the task was identical to the one used in a recent report (Hadjidimitrakis et al., 2014a): a trial began when the monkey pressed the button (far or near). After 1000 ms, 1 of the 9 LEDs lit up green and this cue instructed the monkey to fixate it, while maintaining the button pressed. Then, the monkey had to wait 1000–2000 ms for a change in color of the fixation LED without performing any eye or arm movement. The color change was the go-signal for the animal to release the button and start an arm movement toward the foveated target. Then, the monkey held its hand on the target for 800–1200 ms, keeping the gaze fixed on the same LED. The switching off of the target cued the monkey to release the target and return to the button in order to receive reward. The presentation of stimuli and the animal's performance were monitored using custom software written in Labview (National Instruments), as described previously (Kutz et al., 2005). Eye position signals were sampled with 2 cameras (1 for each eye) of an infrared oculometer system (ISCAN) at 100 Hz and were controlled by an electronic window ($4 \times 4^\circ$) centered on the fixation target. If the

monkey fixated outside this window, the trial was aborted. The task was performed in darkness, in blocks of 90 randomized trials, 10 for each LED target position. The background light was switched on for some minutes between blocks to avoid dark adaptation. At the start of each recording session, monkeys were required to perform a calibration task, following the details reported in Hadjidimitrakis et al. (2014a).

3.3.2 Data Analysis

Data were analyzed with the same approach used in Hadjidimitrakis et al. (2014a) and summarized hereafter. Neural activity was quantified and studied in two epochs: the PLAN epoch that corresponded to the last 500 ms before the go-signal, and the REACH epoch that started 200 ms before the arm movement onset and ended at the pressing of the LED target.

To check the stability of each recorded unit between the 2 blocks, we used the HOLD epoch as a reference. This epoch started with the pressing of LED target and ended with the switching off of the target. The activity in HOLD was assumed to be equal in the 2 blocks because visual, eye position, and arm somatosensory signals were identical. To check for this, we performed a t-test (two sided; Bonferroni's correction, $p = 0.01/9 = 0.001$) for each cell, comparing the nine mean firing rates (1 mean per LED) of the HOLD epoch recorded in one block with the 9 mean firing rates of the HOLD epoch in the other block. Neurons having a significantly different activity in the HOLD epoch between the two blocks were excluded from the analysis. The threshold of statistical difference between the two blocks was in agreement with other criteria of isolation stability (visual inspection of the raster histograms and the distribution of the interspike intervals). A similar procedure has been employed in other studies of reaching activity (Chang et al., 2008; Hadjidimitrakis et al., 2014a). Considering the variability of the neural discharges, only cells tested in at least 7 trials per position and with a mean firing rate higher than 5 spikes/s for at least 1 target position were selected for further analysis (Kutz et al., 2003). Significant modulation of neural activity relative to different positions of the reach targets or to different initial hand positions was studied with a 2-way analysis of variance (ANOVA) performed for PLAN and REACH epochs (factor 1: target position, factor 2: initial hand position). Task-related cells in each epoch were defined as cells where factor 1 and/or factor 2 and/or the interaction factor 1×2 were significant ($p < 0.05$). Only these cells were further analyzed.

3.3.3 Population Analysis of Reference Frames

With the task configuration described above, we could study whether spatial target representation in PEc neurons is organized in body-centered or hand-centered coordinates. It is worth specifying that in the two task conditions the targets were located in the same spatial positions. Therefore, being both tasks foveal reaching, the targets remained in constant eye-centered coordinates, so we cannot assess the eye-centered reference frames in the neurons we studied. It should also be considered that, in our experimental condition, the fact that the monkey fixated the target to be reached may lead to a potential confound between target position coding and eye position gain field. Moreover, given that the head of the animal was fixed, our experiment cannot distinguish body from head- or world-centered frames of reference. We will refer to this frame as “body-centered” coordinates, This terminology has been kept consistent with the one used for area V6A (Hadjidimitrakis et al., 2014a).

All the analyses here proposed have been performed following the approaches used for V6A in a recent paper of our lab (Hadjidimitrakis et al., 2014a), so to allow direct comparisons between the two areas. Several analyses have been used so to avoid that observed differences may be attributed to the different methods of analysis employed (Mullette-Gillman et al., 2009; Bremner and Andersen, 2012).

Euclidean Distance Analysis

At single cell level, to compare the similarity of firing rates in body and in hand-centered reference frames, we calculated in each cell the average activity of all the conditions that were equivalent in each frame of reference. Cells could have significantly different firing rates between condition pairs in both reference frames. To find which reference frame accounted more for the neural responses, we quantified the similarity between the mean firing rates in each frame by computing the normalized Euclidean distance (ED) between them (Batista et al., 2007)

$$ED = \sqrt{\frac{\sum_{i=1}^T (n_i - m_i)^2}{T}}$$

The mean PLAN/REACH activity for targets n and m that were equivalent in a given reference frame were normalized between 0 and 1 and T corresponds to the targets number. The 95% confidence intervals (CIs) on the distance value were estimated using a bootstrap test. Synthetic response profiles were created by drawing N firing rates (with replacement) from the N repetitions of experimentally determined firing rates. Five-hundred iterations were performed, and CIs were estimated as the range that delimited 95% of the computed distances. These confidence intervals indicate the range within which distance metric would have fallen 95% of the time. Neurons falling outside one of these CI are sensitive to one reference frame, whereas neurons falling inside these 2 CIs are influenced by both reference frames. To compare the RFs of single cells in PLAN and REACH, we used their Euclidean distance values in each frame to calculate a single RF index (Fig. 3-3C). To compute the RF index, individual data points from Figure 3-3A, B were projected on the negative diagonal line. The RF index was equal to the distance of the projection point from the upper end of the negative diagonal line that had Euclidean coordinates 0 and 1. As a result, the RF index ranged from 0 to 1.414. Small index values (<0.5) indicate stronger effect of body-centered coordinates, whereas RF index values equal to 1 or higher indicate a prevalence of hand-centered coding.

Separability Analysis

To examine whether in single neurons target location was separable from starting hand position, we applied the singular value decomposition (SVD) analysis (Peña and Konishi, 2001; Pesaran et al., 2006; Bhattacharyya et al., 2009; Blohm and Crawford, 2009; Blohm, 2012; Hadjidimitrakis et al., 2014a). A 2D matrix M was constructed from the mean activity across target and hand conditions. This matrix was subsequently reconstructed to calculate the diagonal matrix S than contained the singular values. Responses were considered to be separable if the first singular value was significantly larger than the singular values obtained when trial conditions were randomized (randomization test, $\alpha = 0.05$). More specifically, we randomly rearranged the data in each matrix 1000 times and subjected each “shuffled” matrix to SVD. The first singular values from each shuffled matrix were accumulated into a vector, which was then sorted in ascending order. This sorted vector ($n = 1000$) formed the reference distribution for determining statistical significance. If the first singular value obtained from the original unshuffled matrix was greater than 95% of the singular values in this distribution, the

responses were considered separable. The fractional energy (FE) of the first singular value was computed from the equation below (Mulliken et al., 2008; Hadjidimitrakis et al., 2014a):

$$FE = 100\% * \frac{s_i^2}{\sum_i s_i^2}$$

Neural responses were classified as separable if the first singular value was significantly larger ($p < 0.05$) compared with the first singular value calculated when conditions were randomized by permuting the rows and the columns of the initial 2D matrix (Randomization test, 1000 permutations) (Mulliken et al., 2008; Bhattacharyya et al., 2009).

Modulation Indexes

To measure the relative strength of neural modulations by target location in body- and hand-centered coordinates, we calculated two indexes in the same way used to quantify modulations in hand or body centered coordinates in area V6A (Hadjidimitrakis et al., 2014a), and to quantify the modulations of reaching activity by disparity and vergence angle in area PRR (Bhattacharyya et al., 2009). Index TB, referring to target in body coordinates, quantified the modulation between pairs of conditions where target position with respect to the body changed while movement vector was constant.

$$TB = \frac{(\max - \min)}{(\max + \min)}$$

As we tested neurons in three lines of LEDs (see Fig. 3-1C and Fig. 3-3B), our experimental configuration allowed us to have three pairs of equal movement vectors for each neuron. The three indexes TB were subsequently averaged for each neuron to obtain a single index.

Index TH, referring to target in hand-centered coordinates, measured the strength of the gain modulation by hand position while target position remained the same.

$$TH = \frac{(\max - \min)}{(\max + \min)}$$

Index TH was obtained by averaging three indexes calculated from the same three pairs of conditions (with the same reaching target and different initial hand positions) used for the ED analysis.

To compare the weight of the two indexes, we subtracted TH from TB for each neuron studied. The value of the difference we obtained determined if the firing rate was more influenced by the body-centered target location (positive values) or the movement vector (negative values).

Vector Correlation Analysis

Vector correlation analysis provides information about the degree of relatedness of two response fields. Each 2D matrix was transformed into a 2D vector field that described the gradient of the response (calculated using the Matlab *gradient* function). To calculate the estimate of vector correlation, we used the method first developed by Hanson et al. (1992) to analyze geographic data and used in recent neurophysiological studies (Buneo and Andersen, 2012; Hadjidimitrakis et al., 2014a). By applying this method, a correlation coefficient ρ that is analogous to the Pearson correlation coefficient was calculated. This coefficient quantified how much the 2D vector fields are related to each other. Apart from the coefficient, the method defines the amount of rotation or reflection and the scaling between the two vector fields. If x and y are the 2 dimensions of one vector field, and u and v the dimensions of the other, using the following equation from Hanson et al. (1992) a correlation coefficient ρ is calculated:

$$\rho = \sqrt{\frac{(\sigma_{xu}^2 + \sigma_{yv}^2 + \sigma_{xv}^2 + \sigma_{yu}^2 + 2s\xi)}{(\sigma_x^2 + \sigma_y^2)(\sigma_u^2 + \sigma_v^2)}}$$

where

$$\xi = \sigma_{xu} * \sigma_{yv} - \sigma_{xv} * \sigma_{yu}$$

$$S = \text{sgn}(\xi) = \frac{\xi}{|\xi|}$$

and σ_x^2 , σ_y^2 , and σ_u^2 , and σ_v^2 are the variances of x , y , u and v and σ_{xu} , σ_{yv} , σ_{xv} , and σ_{yu} are the covariances of the 4 dimensions.

A phase angle (θ) can also be calculated:

$$\theta = a \tan \left(\frac{\sigma_{xv} - s\sigma_{yu}}{\sigma_{xu} - s\sigma_{yv}} \right)$$

The coefficient ρ has a range from -1 to 1 , with 1 characterizing a perfect rotational relationship between the two vector fields and -1 denoting that one vector field can be produced by the reflection of the other along a given axis; 0 represents no relationship. Importantly, the correlation represents the degree of relatedness of the two sets of vector fields after accounting for the rotational (or reflectional) dependence. Thus it is possible to have large phase angles with correlations close to 1 (in the case of rotation) or -1 (in the case of reflection). The phase angle θ has a range from -180° to 180° and quantifies the angle of rotation or reflection that is necessary to align the two vector fields.

Correlation Analysis

To study at the population level the influence of movement vector and of the body coordinates, we compared the mean firing rates of single conditions: 1) where targets that had the same location relative to the body were reached from different hand positions (Fig. 3-8A, left), and 2) where targets having the same location with respect to the hand were reached (Fig. 3-8B, left). At the population level, the similarity of the paired firing rates was evaluated calculating the Pearson correlation coefficient (Zar, 1999). A Z-test ($P < 0.05$) was used to compare the correlation coefficients (Hadjidimitrakakis et al., 2014a).

As REACH epoch includes the last 200 ms before movement onset and the entire movement duration, we performed all the analyses also splitting the REACH epoch in two parts: EarlyMOV (from 200 ms before the movement onset to movement onset) and LateMOV epochs (from movement onset to movement end). We found no statistical difference between the results of the REACH epoch and the results of each of EarlyMOV and LateMOV epochs (Chi Squared test and Kolmogorov-Smirnov test, $p > 0.05$). Thus, in the Results section, only results on the entire REACH epoch will be given.

All methods of analysis gave consistent results in the 3 monkeys, and are therefore presented together. All analyses were performed using custom scripts written in MATLAB (Mathworks, Natick, MA, USA).

3.4 Results

We examined the responses of 104 stable, well isolated neurons recorded in area PEc in three *Macaca fascicularis* during the planning (PLAN, the last 500 ms before the Go signal to reach) and execution (REACH, from 200 ms before the movement onset to movement end) of arm reaching movements. Targets, placed at various depths and directions, were reached from two different hand positions, one next to the trunk and the other 14 cm distant from it (see Fig. 3-1B and 3-1C).

We performed a 2-way ANOVA to find cells whose activity during planning (PLAN) and reaching (REACH) was significantly influenced by target position and/or initial hand position. A total of 82 cells in PLAN and 97 cells in REACH showed a significant effect. As shown in Table 3-1, both the initial hand position and the target position affected reaching activity, as well as the interaction between them. During PLAN the effect of the initial hand position was slightly stronger than that exerted by target position, whereas the reverse was true during REACH.

| Epoch | Target position only | Initial hand position only | Both | Interaction |
|--------------|---------------------------------|---------------------------------------|-------------|--------------------|
| PLAN (n=82) | 18 (21%) | 26 (32%) | 22 (27%) | 16 (20%) |
| REACH (n=97) | 31 (31%) | 13 (14%) | 30 (31%) | 23 (24%) |

Table 3-1. Incidence of the effect of target position and initial hand position in each epoch.

Figure 3-2 illustrates examples of neuronal modulation during the task. The cell depicted in Fig. 3-2A was modulated by target position during both PLAN and REACH epochs, with a stronger discharge during REACH. It discharged maximally during reaches toward far targets regardless of the initial hand position (one-way ANOVA, far vs. others, $p < 0.05$). The cell depicted in Fig. 3-2B was strongly modulated during REACH, with the strongest discharges occurring for the movements that started from the ‘near’ button. In this condition, the discharge was strongest for farthest and for rightmost targets. The cell had main effects of both initial hand position and target position, and also showed an interaction effect between them. The cell depicted in Fig.

3-2C fired mostly during reaching execution. Its spatial tuning depended both on hand position and target location: when the hand started the movement from the ‘near’ button, this cell was slightly but significantly modulated by target position (1-way ANOVA, $p < 0.05$), whereas when the hand started from the ‘far’ button, the spatial tuning became more evident, with the farthest positions evoking the highest discharges (one way ANOVA, farthest positions vs. others, $p < 0.05$).

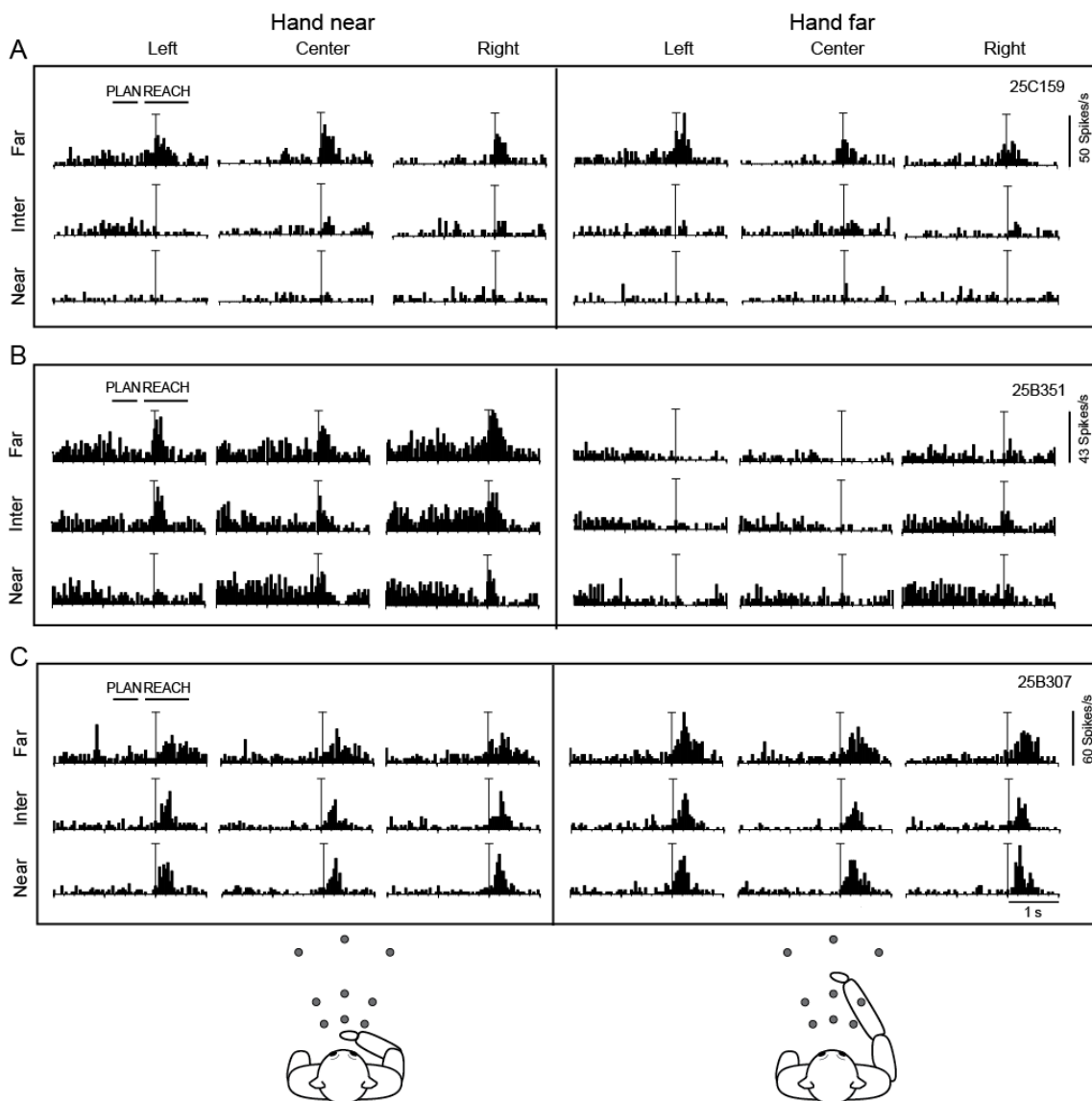


Figure 3-2. Examples of neuronal modulation in PLAN and REACH epoch. Spike histograms for the nine target positions with hand near (left) and hand far (right). The columns represent the directions of the targets, the rows the depths. A) Example of a cell modulated by target position both in PLAN and REACH (ANOVA results: PLAN: main effect of target position ($p=0.00064$); REACH: main effect target position ($p < 0.00001$)). B) Example of a cell modulated by the initial hand position and target position in REACH epoch. (ANOVA results:

PLAN: main effect initial hand position ($p=0.00024$); REACH: main effect of initial hand position ($p<0.00001$), main effect of target position ($p<0.00001$) and interaction effect ($p=0.0004$); C) Cell firing only during reaching execution (REACH) showing a more evident spatial tuning when the reaching movement started from the hand far. Vertical lines indicate the alignment of activity at the start of arm movement. (ANOVA results: PLAN: main effect target position ($p<0.00001$); REACH main effect target position ($p<0.00001$), main effect of initial hand position ($p=0.013$). PLAN epoch starts around 800 ms before this time point and REACH epoch starts 200 ms before this time point, as indicated by the bars on the top left of each inset. The neuron in Fig. 3-2A was classified as a ‘body’, cell in Fig. 3-2B as a ‘hand’, and that of Fig. 3-2C as a ‘mixed’ cell.

3.4.1 Population Analyses of Reference Frames

3.4.1.1 Euclidean Distance Analysis

To compare the relative effect of changing target location and initial hand location at single cell level, we calculated the Euclidean distance metric (Batista et al., 2007; Hadjidimitrakis et al., 2014a). For each neuron and epoch, we calculated the Euclidean distance twice by comparing the pairs of conditions that were equivalent in each reference frame (see “Materials and Methods”). Fig. 3-3A illustrates a plot of the two distances calculated in each cell during reaching preparation (PLAN, left panel) and execution (REACH, right panel). A neuron encoding reach targets in a hand-centered reference frame is expected to have a large Euclidean distance value along the abscissa and a small value along the ordinate; a neuron encoding reach targets in a body-centered reference frame is expected to have a large Euclidean distance value along the ordinate and a small value along the abscissa. Confidence intervals of the Euclidean distance were also calculated with Bootstrap analysis. Neurons with confidence intervals that did not cross the equality line are illustrated with filled circles in Fig. 3-3, neurons with intervals that cross the equality line with empty circles. We used this analysis to divide the neural population into three categories (Fig. 3-3A and B): neurons that encode target position in hand centered coordinates (filled circles below the equality line, ‘hand’ neurons in Fig. 3-3B), that were 5% (4/82) in PLAN and 7% (7/97) in REACH; neurons that encode reach goals in body-centered coordinates (filled circles above the equality line, ‘body’ neurons in Fig. 3-3B), that were 15% (12/82) in PLAN and 28% (27/97) in

REACH; neurons that were sensitive to both hand- and body-centered locations of the target (empty circles, ‘mixed’ cells in Fig. 3-3B), that were 80% (66/82) in PLAN and 65% (63/97) in REACH. The distribution of cells in the three categories was not significantly different in the two epochs (Chi squared test, $p>0.05$). A good proportion of neurons (65%) did not change reference frame going from PLAN to REACH. The consistency of reference frames between PLAN and REACH is evident also in Fig. 3-3C, where we compared the RF indexes of cells tuned in PLAN and REACH and we found that they were significantly correlated ($P<0.001$). This suggests a high consistency of reference frames as the task progressed.

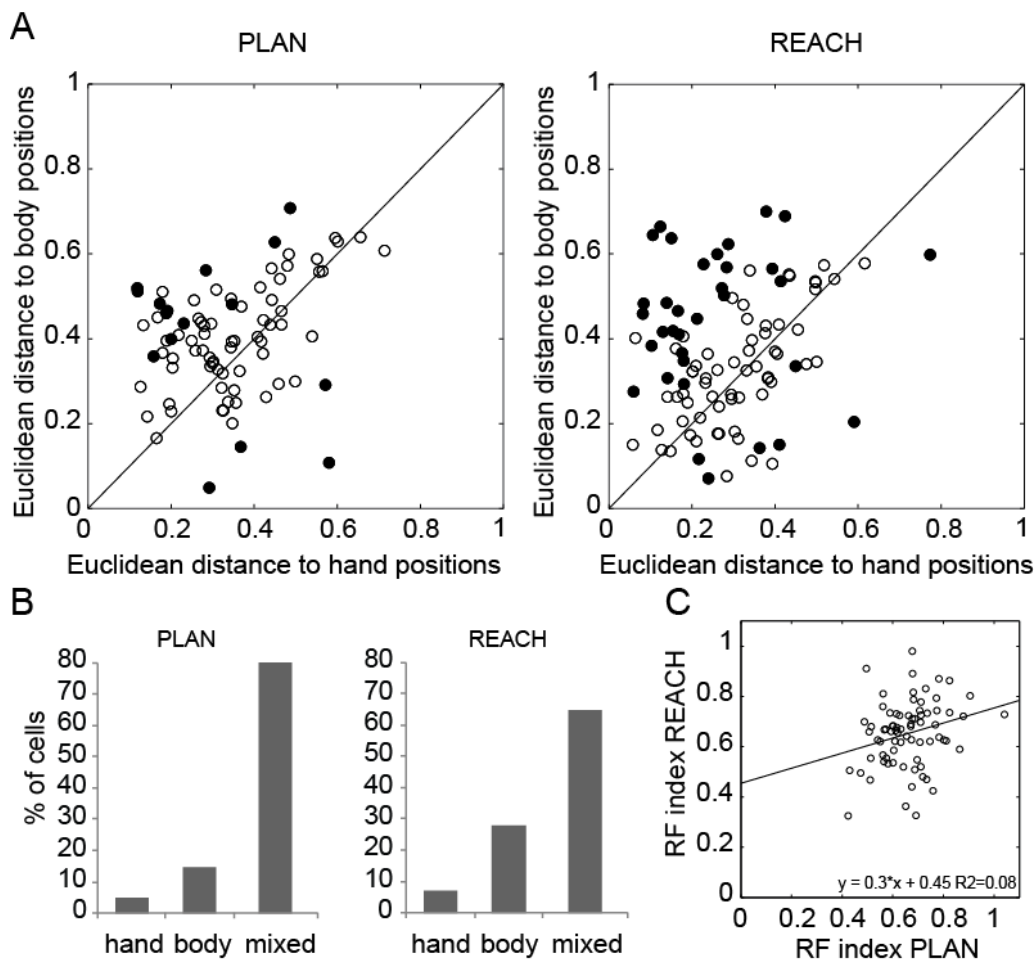


Figure 3-3. Population analysis of the reference frames of PLAN and REACH activity. A) Each data point represents one neuron, showing its sensitivity, calculated as Euclidean distance, in a body-centered and in a hand-centered frame in PLAN (left) and REACH (right) epochs. Filled circles represent neurons with significantly (bootstrap estimated, $n=500$, $p<0.05$) different sensitivities. Empty circles represent neurons with equal sensitivities. The example cell in Fig. 3-2A was classified as ‘body’, cell in Fig. 3-2B as ‘hand’, and that of Fig. 3-2C as ‘mixed’ cell.

B) Frequency distribution of cells classified in A) by the Euclidean distance analysis as having a hand-centered, body-centered or mixed coding behavior. PEc population has very few hand-centered neurons in both epochs considered, a small amount of body-centered and a large amount of mixed hand/body-centered neurons, particularly in PLAN epoch. C) Reference frame consistency across epochs. Scatter plot of the reference frame (RF) index in PLAN versus REACH of the neurons (n=74) tuned in both epochs. The RF indexes were highly significantly ($P < 0.001$) correlated. The equation of the linear regression line is also illustrated.

3.4.1.2 Alternative methods of analyses of reference frames

According to previous works on the same topic (Pesaran et al., 2006; Bhattacharyya et al., 2009; Blohm and Crawford, 2009; Buneo and Andersen, 2012), and in order to help comparisons with the literature, we performed additional analyses of the reference frames on task-related cells. We performed the singular value decomposition (SVD) analysis (Pesaran et al., 2006; Bhattacharyya et al., 2009) to examine whether the initial hand position and the target location were encoded jointly or separately. The neurons were classified separable when their activity encoded target and hand position independently, by a multiplicative coding mechanism, and inseparable when this mechanism could not completely account for the neural responses (Hadjidimitrakis et al., 2014a). We found that only a minority of neurons were “separable” (Fig. 3-4): 15% (12/82) and 22% (21/97) of neurons modulated during PLAN and REACH, respectively, were classified as separable; 85% (70/82) and 78% (76/97) of neurons modulated in PLAN and REACH, respectively, were classified as “inseparable”.

As a further investigation to examine the degree of separability in the two categories of modulated cells, we computed the Fractional Energy (FE) of the first singular value (Mulliken et al., 2008; Hadjidimitrakis et al., 2014a). A cell influenced linearly by two variables should have a high FE; on the contrary a cell coding for a combination of two variables should have a lower FE. In particular, cells using hand-centered reference frame are expected to have low FE values. The distribution of this metric for the population is shown in Fig. 3-4. The mean FE for the separable neuron in PLAN (Fig. 3-4A) was 0.92 ± 0.04 and in REACH (Fig. 3-4B) 0.92 ± 0.06 . For the inseparable neurons in PLAN the mean FE was 0.71 ± 0.08 and in REACH was 0.73 ± 0.08 . In both classes of neurons, the FE of the first singular value was high. The high FE values (>0.6) of most of the inseparable neurons provided another line of evidence

supporting that there is an intermediate encoding i.e. between body- and hand-centered coordinates of reaching targets in area P_{Ec} .

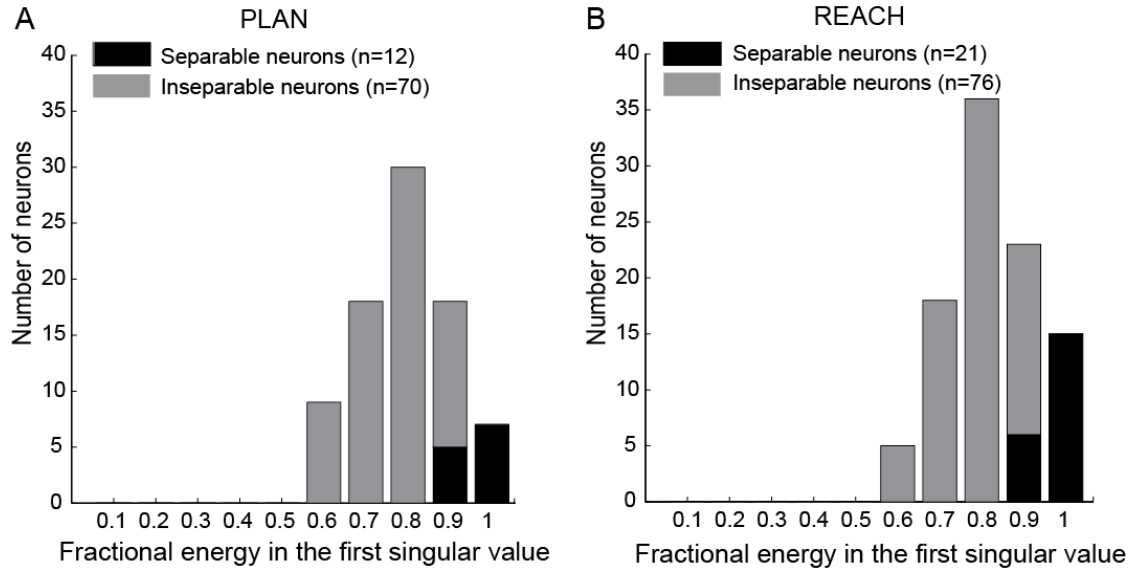


Figure 3-4. Results from separability analysis. Distributions of the fractional energy of the first singular value for all modulated neurons (separable and inseparable) in PLAN (A) and REACH (B). In both A and B, the distributions are shown for significantly ($p < 0.05$) separable ($n = 12$ in A and $n = 21$ in B) neurons and for the rest of the modulated neurons ($n = 70$ in A and $n = 76$ in B) that were found to be inseparable. The fractional energy (FE) of the separable neurons was significantly higher than the inseparable ones (Kruskal–Wallis, $P < 0.05$). In both classes of neurons, the FE of the first singular value was high, thus suggesting an absence of target encoding relative to the hand (movement vector).

We examined the strength of the modulation by target and hand signals by calculating two indexes (TB and TH) used in recent reports on the same topic (Bhattacharyya et al., 2009; Hadjidimitrakis et al., 2014a). The TB index (target in body coordinates index, see Materials and Methods) measures the modulation of cell activity when target position changed with respect to the body and movement vector remained stable. Its distribution is shown in Fig. 3-5, left. Index TH (target in hand coordinates index, see Materials and Methods) quantifies the modulation occurring when location of target changed relative to the hand, but remained the same with respect to the body. Its distribution is shown in Fig. 3-5, middle. For both indexes, a value of zero means that

changing the target or hand position had no effect on the activity, while a value close to 1 indicates a maximum effect. A value of 0.33 means that the change of the target position (TB) and hand position (TH) in space scales activity by a factor of 2 (doubling it or reducing it to its half). To compare the two indexes in individual neurons, we subtracted TH from TB index for each neuron and each epoch. A resulting value of zero indicates that the two modulations had equal strength in a given cell and epoch; positive values indicate that target location with respect to the body had more influence on cell activity than movement vector (target in hand coordinates), and negative values indicate that changes in movement vector had a stronger effect than changes in target location with respect to the body. Results around zero indicate that there is a similar effect of body and hand positions. The distribution of TB-TH values is around zero for both PLAN and REACH epochs (mean values: PLAN 0.07; REACH 0.05) (Fig. 3-5, right). Thus, these results show that, in agreement with the prevalence of mixed reference frames (Fig. 3-3), the effects of body position and hand position were similar.

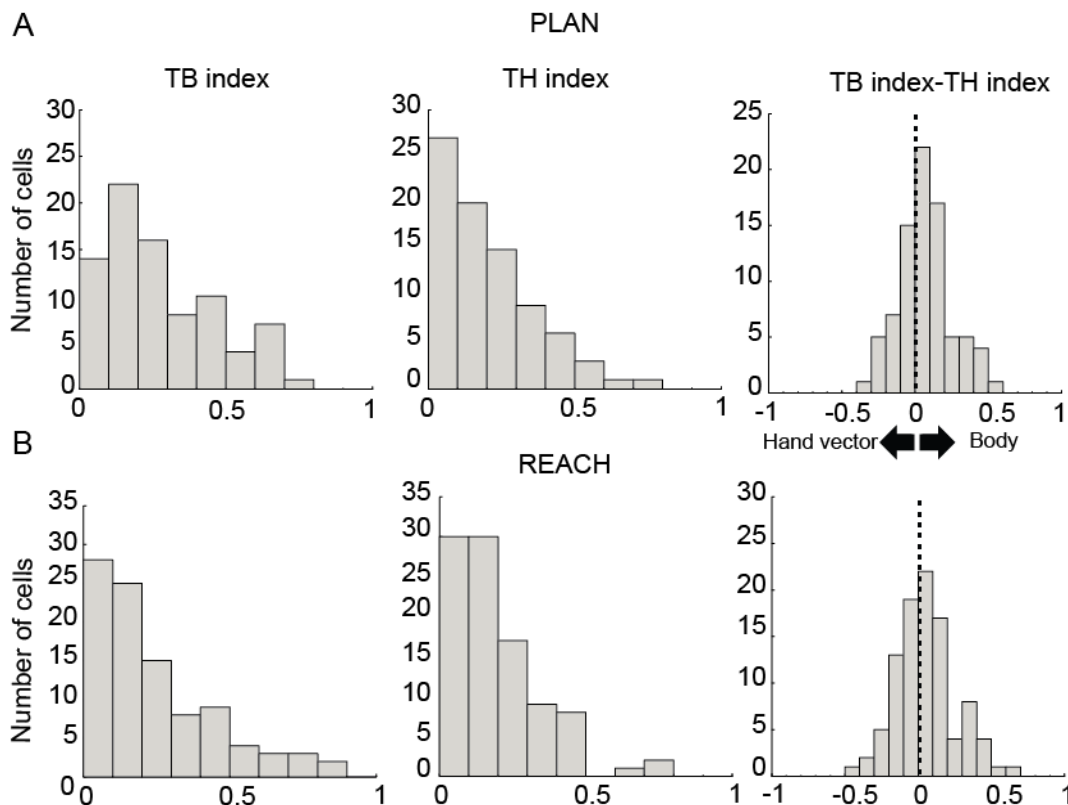


Figure 3-5. Strength of modulation by target and hand signals. The distribution of the modulation indexes TB (left panels), TH (middle panels) quantifying the strength of tuning of the activity in PLAN (A) and REACH (B) by changing the body and hand coordinates,

respectively, of the target. The right panels in A and B illustrate the histogram of difference TB–TH. The distributions of differences between TB and TH indexes are not different ($p>0.05$), with a mean around zero. Both these two distributions are not normal distributions (Kolmogorov-Smirnov test, $p<0.05$) and are skewed to the right, i.e. towards body-centered representation.

All the analyses presented so far do not take into account the overall 2D structure of the arm movement fields of single neurons, i.e. the fact that in our study targets were located at various depths and directions with precise spatial relationships. Thus, to analyze the 2D structure of the arm movement fields of single neurons, we performed the vector correlation analysis (Buneo, 2011; Buneo and Andersen, 2012; Hadjidimitrakis et al., 2014a). This method provides a measure of correlation between 2D response fields. In our case, the response fields were the 2D (depth/vergence - direction/version) matrices of firing rates for movements that started from the near and the far button, respectively (Fig. 3-6A, B). Our hypothesis was that, if neurons encode targets in body-centered coordinates, the response fields should be strongly correlated because targets had the same location with respect to the body. If the two matrices were identical (body-centered reference frame), the vector correlation analysis would give a coefficient ρ of 1 that indicates a perfect rotational relationship between the two response fields and a phase angle θ of 0 that quantifies the angle of rotation or reflection that is necessary to align the two vector fields. In general, body-centered cells would show response matrices that are correlated with high coefficients (ρ) and have a small phase angle (θ) difference between them. In contrast, the correlation distribution for a population of intermediate or hand-centered neurons is not obvious. In general, cells with a strong effect of initial hand position are expected to have much lower positive or negative values of the ρ coefficient that suggests a strong rotation or a reflection, respectively, of one response field with respect to the other.

Figures 3-6A and 3-6B show example vector correlations derived from idealized neural responses. Since we varied the hand position only in depth, the idealized neurons were designed to show only depth tuning (it should be noted that this was not always the case in the population of recorded cells). The field in Fig. 3-6A (right) was designed to be identical as the one shown in Fig. 3-6A (left), and the vector correlation measures reflect this ($\rho=1$ and $\theta=0^\circ$). This is the case of an idealized ‘body’ cell, i.e. a cell whose

spatial tuning is not affected at all by the manipulation of the starting hand position (see Fig. 3-6A). On the contrary, the vector field in Fig. 3-6B (right) was designed to appear as the reflection of the one shown in Fig. 3-6B (left). In fact, in our setup the movement vector for movements from the ‘near’ button to the nearest LEDs is equal to the movement vector for movements from the ‘far’ button to the farthest LEDs. Here, the correlation is best described as a reflectional relationship (negative correlation), rather than a rotational (positive) one. In this case, the idealized cell is strongly influenced by the starting hand position, namely a ‘hand’ cell, and $\rho=-0.98$ with a rotation angle (θ) of -10° . Thus, we can predict that the more neurons show values of ρ far from 1, the more the influence of hand position becomes greater. In addition, the higher is θ , the more influential is hand position.

Figures 3-6C and 3-6D show the distribution of ρ coefficient (top panels) and phase angle θ (bottom panels) of PLAN (Fig. 3-6C) and REACH (Fig. 3-6D) epochs, respectively. The majority of neurons modulated in PLAN and REACH epochs exhibited positive values of ρ coefficient (median value=0.32 for PLAN; 0.48 for REACH). In PLAN epoch, the cells showed phase angles that were widely distributed and not concentrated near 0. Differently, during REACH a peak around values of θ of $\pm 10^\circ$ was evident, and this agrees at population level with the increase of body-centered cells observed in the euclidean distance results (Fig. 3-3A,B). This is also in agreement with the higher correlation between ρ and θ found in REACH (Fig. 3-6E, F).

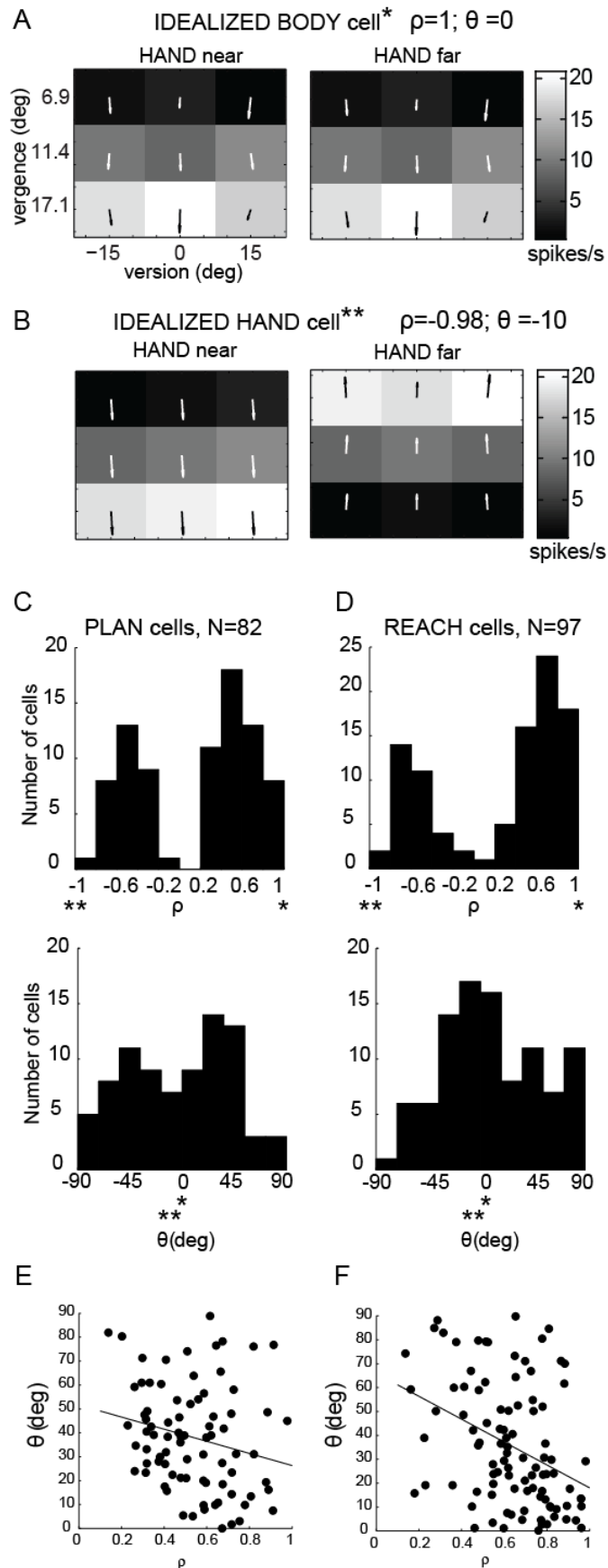


Figure 3-6. Results of the gradient analysis. A-B) Idealized scalar response fields (greyscale maps) with corresponding vector fields superimposed. Data are plotted as a function of version

and vergence (in degrees of visual angle). For the scalar fields, lighter greyscale colors represent higher firing rates. Corresponding vector fields converge toward the highest response. ρ and θ , represent the vector correlation coefficient and phase angle, respectively, obtained by correlating the vector field to the left with those represented to the right. C-D) Distribution of coefficient ρ (top panels) and phase angles θ (bottom panels) for the population of neurons modulated in PLAN (C) and REACH (D). Asterisks indicate the location in the distributions of the ρ and of θ values of idealized ‘body’ (*, A) and ‘hand’ (**, B) cells. The coefficient ρ is analogous to the Pearson linear correlation coefficient and the phase angle θ quantifies the amount of shift needed to align the 2 response fields (see Materials and Methods). The majority of neurons modulated in PLAN and reach epoch exhibits values of ρ coefficient distributed among positive and negative coefficients; the phase angle θ are widely distributed in both epochs (from -90 deg to +90 deg) indicating the prevalence of mixed hand/body-centered representation in PEc. E-F) Correlation of absolute values of ρ and θ values for the population of neurons modulated in PLAN (E) and REACH (F).

Regression line equations: $\theta = -25\rho + 52$; $r^2=0.05$; (E); $\theta = -48\rho + 66$; $r^2=0.14$. (F) Both regressions are significant ($p<0.05$), suggesting that ρ and θ co-vary (the highest is ρ , the smallest is θ).

The distributions of the ρ coefficient and phase angle θ suggest that in the majority of the cases the two response matrices were quite strongly correlated, although often with a considerable degree of rotation/reflection. Thus, the influence of hand position for the majority of PEc cells seems significant, and this agrees with the results shown in Table 3-1. This confirms the prevalence of mixed hand/body-centered representation in PEc, in line with the other methods of analysis described earlier.

3.4.1.3 Convergence of the different analyses

To check whether the results of the different analyses were consistent, we plotted the results of each of the analyses one against the other. SVD and TB-TH indexes analyses gave consistent results. As shown in Figure 3-7A, the majority of separable cells (9/12 in PLAN and 15/21 in REACH) displayed positive values of TB minus TH indexes (TB-TH). This suggests that, in cells where the influence of body-centered coordinates was prevalent (positive TB-TH values), activity encoded target and hand position independently, by a multiplicative coding mechanism. In the same vein, separable cells

contained a major incidence of cells classified as ‘Body’ in the euclidean distance analysis (Fig. 3-7B), since ‘Body’ cells are most likely to be significantly tuned only by target position in the SVD analysis. The euclidean distance results were in good agreement with the modulation indexes analysis (Fig. 3-7C), because almost all the ‘Body’ cells (12/12 in PLAN and 26/27 in REACH) had a positive TB-TH values, whereas all ‘hand’ cells had a negative one (4/4 in PLAN and 7/7 in REACH). Mixed cells displayed both positive and negative values.

We also compared the results from the vector correlation analysis with those from the other analyses, but we did not find as much convergence as in the other comparisons. This is likely because vector correlation correlates 2D matrices (thus considering together all the target positions), so it is also sensitive to the firing rate differences between adjacent positions, both in direction and in depth, whereas the other methods lose this spatial relationship because they compare only pairs of target positions that are located in the same depth in either body-, or hand-centered coordinates. However, it has to be pointed out that, although at a single cell level we found discrepancies between vector correlation and all the other analyses, at a population level all the analyses suggested that mixed body/hand reference frames were prevalent in PEc.

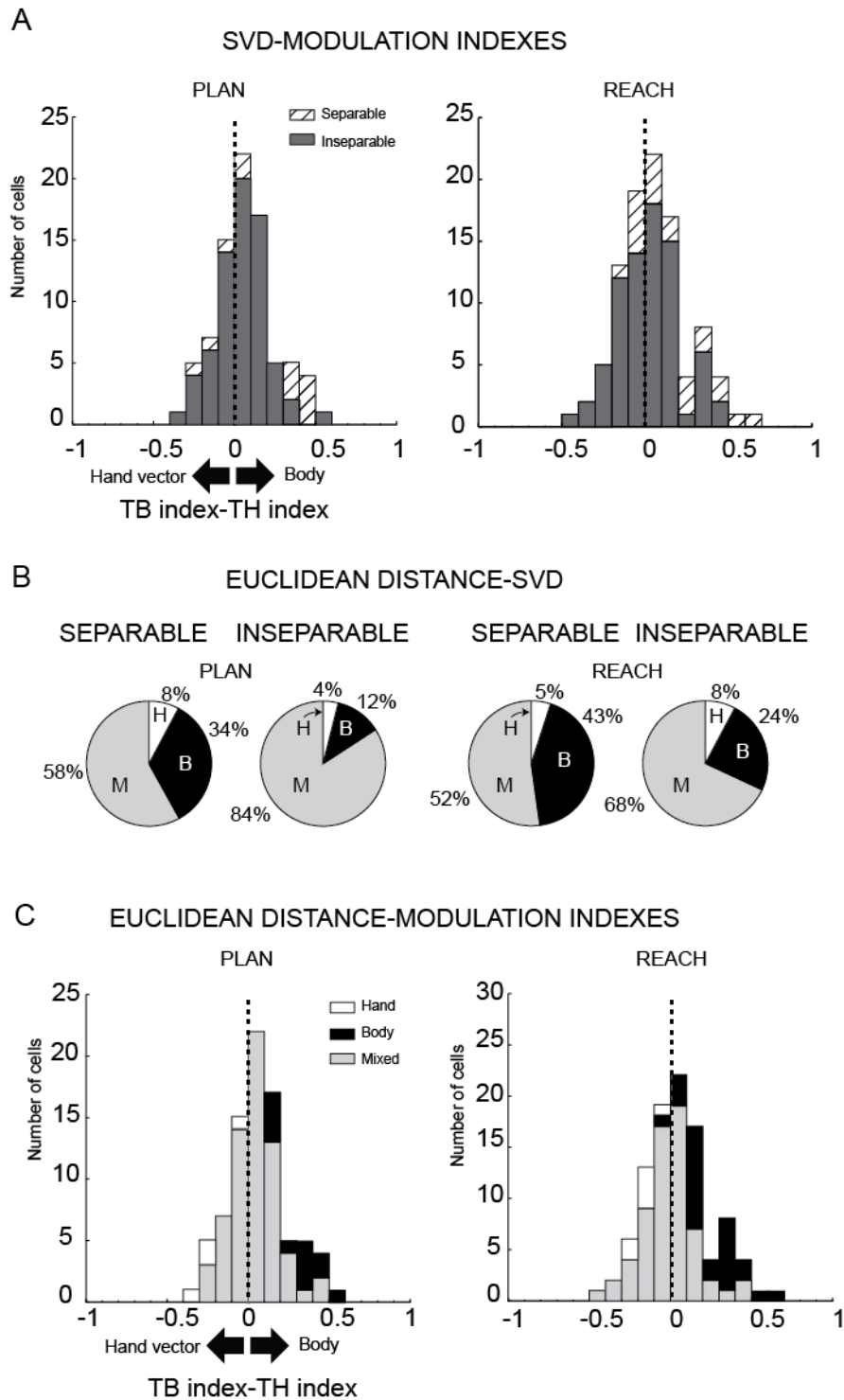


Figure 3-7. Convergence of the results of different analyses. Convergence between the results of: A) SVD and modulation indexes (TB-TH): separable cells are shown in red, inseparable in black; B) SVD and euclidean distance; C) euclidean distance and modulation indexes (TB-TH). In B) and C), ‘Body’ cells are shown in green, ‘Hand’ cells in yellow, ‘Mixed’ cells in grey. There is a good convergence between the results of these analyses at the single-cell level.

3.4.1.4 Correlation Analysis

To check how the cell diversity highlighted by the single cell analyses translates at the population level, we performed a correlation analysis. Our experimental set up allowed us to study whether neurons encode the target in body-centered or hand-centered coordinates by comparing, in the same cell, the neuronal activity of arm movements of different amplitude and direction performed toward the same spatial location (Fig. 3-8A) with the neuronal activity of movements of the same amplitude and direction performed toward different spatial locations (Fig. 3-8B). To study the relative influence of body coordinates and of the movement vector at a population level, we plotted the mean firing rates of single conditions (pair of movements): A) where targets with the same position relative to the body were reached starting from different initial positions (constant target location in body coordinates but different movement vectors, see Fig. 3-8A); each neuron was plotted nine times because there were nine pairs of conditions in the task that matched the above reported features. B) Where targets with the same position with respect to the hand were reached from different initial positions with respect to the body (same movement vector but different position in body coordinates, see Fig. 3-8B); each neuron was plotted 3 times because there were three pairs of conditions in the task that showed the same movement vector. A low scatter (high correlation) indicates that a particular reference frame accounts well for the population activity. Fig. 3-8A, B illustrate that the correlation was quite high for both reference frames. Nevertheless the correlation was significantly higher (z-test, $p < 0.05$) when the target remained in the same position with respect to the body (body-centered frame of reference, $r = 0.76$ in PLAN; $r = 0.89$ in REACH) than when the target remained in the same position with respect to the hand (hand-centered frame of reference, $r = 0.63$ in PLAN; $r = 0.76$ in REACH). In other words, both reference frames accounted for the population activity, but the body-centered frame of reference explained better the neural discharges than the hand-centered one.

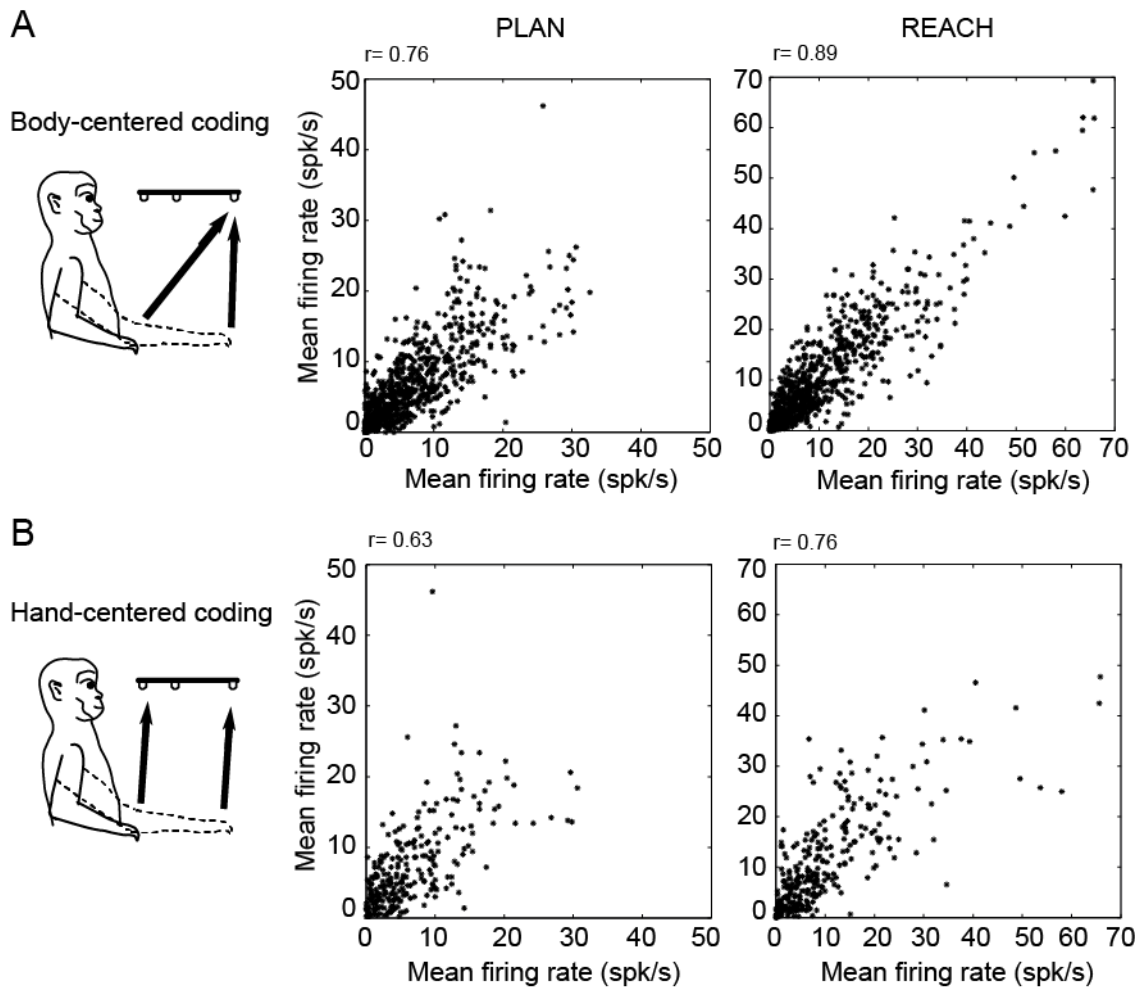


Figure 3-8. Correlation analysis of the reference frames of PLAN and REACH activity for the population of PEc modulated cells. A) Comparison between pairs of movements for targets having the same position in body-centered coordinates. *Left:* sketch of the pairs compared. *Middle:* Scatter plots of neural activity in PLAN epoch of pair of movements identical in body coordinates. *Right:* Scatter plots of neural activity in REACH epoch of pair of movements identical in body coordinates; B) Comparison between pairs of movements for targets having the same position in hand coordinates. *Left:* sketch of the pairs compared. *Middle:* Scatter plots of neural activity in PLAN epoch of pair of movements identical in hand-centered coordinates. *Right:* Scatter plots of neural activity in REACH epoch of pair of movements identical in hand-centered coordinates. It is evident a higher correlation in case of movements identical in body coordinates.

In summary, all the methods employed to ascertain the reference frames of PEc cells indicate a prevalence of mixed body/hand-centered reference frame. In this

scenario, the influence of target position relative to the body was higher than the influence of target position relative to the hand.

3.5 Discussion

In this study, we tested whether neurons of the medial posterior parietal area PEc encode reach targets in hand-centered, or in body-centered reference frame while the animals performed reaches to targets at different depths and directions. To this aim, we recorded preparatory and movement-related activity of PEc cells during a 3D reaching task requiring body-out arm movements starting from two different locations in depth and reaching nine different target positions located at three different depths and in three different directions. We found that most PEc cells encoded targets in a mixed body- and hand-centered frame of reference during both preparation and execution of reaches. We found very little evidence of pure hand-centered representations, although hand position seems to be rather influential in PEc as a main effect, especially before reach (see Table 3-1). However, this influence is not strong enough to be expressed as a clear, pure hand-centered reference frame, so the mixed coding remains the principal representation in PEc during both planning and execution of reaches.

Reference frame transformations

It has been long debated about the existence of distinct reference frames in different brain regions, also because the reference frame may be an emerging computational mean of the neuron rather than an intrinsic feature. Indeed, many cells with mixed reference frames have been described in parietal (Stricanne et al., 1996; Avillac et al., 2005; Mulette-Gillman et al., 2005, 2009; Chang and Snyder, 2010; McGuire and Sabes, 2011) and frontal (Batista et al., 2007) areas, with the frequent interpretation that an orderly progression of coordinate transformations does not exist. However, it was pointed out that the existence of mixed reference frames in the studies involving reaches was caused by the fact that there was not the possibility to distinguish clearly whether changes in firing rate were caused by reference frame shifts or by postural gain fields (Batista et al., 2007; McGuire and Sabes, 2011), a distinction that is critical for determining the appropriate reference frame. In the current study, all neurons (included cells with mixed reference frames) underwent SVD analysis, that is a powerful tool to establish whether there is a gain field in a matrix of responses (see for example Bremner

and Andersen, 2012). Present results (see Fig. 3-4) demonstrate that gain fields are present in a minority of cells, and the majority of “mixed” cells shows a genuine hybrid coding frame without gain fields.

Computational models have proposed that a mixed representation may be explained by considering the PPC as an intermediate layer that uses basis functions to perform multidirectional coordinate transformations (Pouget and Snyder, 2000). Basis function units are thought as an efficient computational step that allows to integrate the sensory signals related to the target with the necessary postural signals (gaze and/or arm position) to define the motor goal. The advantage of the basis functions approach is that it allows single cells to define spatial positions in multiple reference frames simultaneously. Networks with these combinatorial properties also show optimal Bayesian statistical inference, with possible dynamic adjustment of the synaptic weight of each input according to the context (Deneve et al., 2001). Moreover, recent work demonstrated that the use of sigmoid transfer functions, instead of basis functions, can also perform the computations of reference frame transformations and also predicts intermediate reference frames (Blohm et al., 2009; Blohm, 2012). Compared with a basis function, a sigmoid transfer function can be physiologically more realistic (Naka and Rushton, 1966a, b, c). In any case, the presence in PEc of bimodal visuo-somatosensory cells (Breveglieri et al., 2008), together with mixed body/hand-centered reference frames suggest that this area is involved in the coordinate transformation necessary for coding reach targets.

Although mixed reference frames are the most frequent representation in PEc, neurons with body-centered frames increase in number when movement execution occurs with respect to movement preparation. This suggests that the reference frame of sensory signals is likely unconstrained, and a more defined coordinate system only emerges when a specific behavior requiring the computation of target location in that reference frame must be generated. That the reference frame may be dictated by the motor effector and that such coordinate systems may emerge most clearly later in motor pathways has been observed for head movements, reaching movements, and auditory stimuli as well. Visual and auditory signals organized in quite clear eye-, head- and limb-centered coordinates have been observed, for instance, in the superior colliculus and ventral premotor cortex during movement execution (Graziano and Gross, 1998; Graziano, 1999, 2001b; Lee and Groh, 2012). This is in agreement with the “conversion-on-demand” model proposed by Crawford and colleagues: targets are

retained in sensory coordinates and only those relevant to a specific action are made available to motor systems (Henriques et al., 1998; Klier et al., 2001). Thus, the late employment of a reference frame may be a general rule for the brain's strategy of converting signals into a specific reference frame only where and when a command begins to be prepared to direct the effector on a particular location in space. This particularly occurs in PPC that receives sensory signals and sends them to the motor cortex.

Another important point to consider is that the reference frame displayed by a neuron can be influenced by the way the experiments are carried out (Blohm et al., 2009), or be susceptible to plastic changes induced by the training of the monkey (Alemayehu et al., 2015). Thus, we cannot rule out that the presence of mixed and body-centered reference frame in PEc can be an epiphenomenon induced by our experimental conditions.

Functional gradient of reference frames in the superior parietal lobule

Evidence from studies performed independently in different PPC subdivisions suggests that the reference frame used by an individual neuron in reaching depends on that neuron's location within the PPC (Batista et al., 1999; Buneo et al., 2002; Bremner and Andersen, 2012). In a recent study (Hadjidimitrakis et al., 2014a) and in the present one, we studied 2 medial PPC areas (V6A and PEc) with exactly the same experimental paradigm and methods of analysis, that allowed a direct comparisons between the 2 areas. The reference frames investigated were the hand-centred and the body-centred (that is spatial coordinates). We found that both V6A and PEc use mainly "mixed" frames between hand/ and body/centred coordinates, with a difference in the relative contribution of body and hand in spatial encoding. V6A cells encode both the body-centered target position and the hand movement vector, with the former having on average a stronger effect than the latter (Hadjidimitrakis et al., 2014a). The overwhelming majority of PEc cells have a mixed reference frame, with a slightly stronger influence of hand position signals with respect to V6A. Works from other labs showed that area PE, located rostrally to PEc, contains mostly cells representing reach targets in hand-centered coordinates (Ferraina et al., 2009; Bremner and Andersen, 2012), together with body-centered cells (Lacquaniti et al., 1995; Buneo et al., 2002) and 'mixed' cells (McGuire and Sabes, 2011). All the above-mentioned works and present data show that a functional gradient pervades the medial part of the PPC, with

the hand position that gradually becomes more influential going from caudal to rostral regions (see Fig. 3-9). A similar conclusion, though based on different functional grounds, was achieved by a recent paper (Hadjidimitrakis et al., 2015), where the role of depth and direction signals in encoding reaching target was investigated. PEc was shown to be less involved than V6A in encoding the spatial location of reaching target, and to be more functionally similar to area PE and to premotor areas. The existence of this functional gradient is supported by studies on the sensory properties: the caudalmost region, V6A (Galletti et al., 1996) contains about 60% of visual cells and 30% of somatosensory cells (Galletti et al., 1999; Breveglieri et al., 2002). Area PEc (Pandya and Seltzer, 1982), is located anterior to V6A and has less visual and more somatosensory cells than V6A (Breveglieri et al., 2002; Breveglieri et al., 2006). Area PE (Pandya and Seltzer, 1982), located further anteriorly, is poor in visual responses but rich in somatosensory ones (Sakata et al., 1973; Mountcastle et al., 1975), and receives strong somatosensory and sparse visual input (Bakola et al., 2013). Thus, different functional data suggest a caudo-rostral flow of information relative to the targets to be reached between V6A, PEc, and PE, which provides premotor/motor centers with adequate representation of targets with respect to our own body and hands.

Comparison with the human brain

The idea of a rostro-caudal gradient within the parietal cortex has also been suggested in the human brain. For example, a human fMRI study suggested that occipitoparietal regions were more activated by saccade planning than by limb movements, whereas anterior regions of the superior parietal lobule were more activated by limb movements (Heed et al., 2011). Moreover, human posterior parietal and dorsal premotor areas showed gaze-centered integration effects (Serenio et al., 2001; Medendorp et al., 2003; Medendorp et al., 2005b; Medendorp et al., 2005a; Beurze et al., 2010), whereas in regions closer to the primary motor cortex, body-centered hand position effects were found (Beurze et al., 2010).

Recent human studies show that reach-related regions of the human PPC seem to demonstrate a capacity to express different frames of reference depending on the sensory context (Sober and Sabes, 2005; McGuire and Sabes, 2009; Bernier and Grafton, 2010). It has been suggested that flexibility is not achieved by engaging different brain areas, each using a fixed gaze- or body-centered reference frame, but by recruiting areas able to change their mode of representation (Bernier and Grafton,

2010). In our study, we did not vary the sensory modality of the target, thus we are not able to test this hypothesis. However, our finding that most cells show a mixed hand-body reference frames for reaching is in agreement with this view. It could be the case that a differential weighting of sensory modalities in the experimental protocol would switch a mixed reference frame to a purely hand- or body-centered reference frame. Future experiments will be addressed to verify this hypothesis.

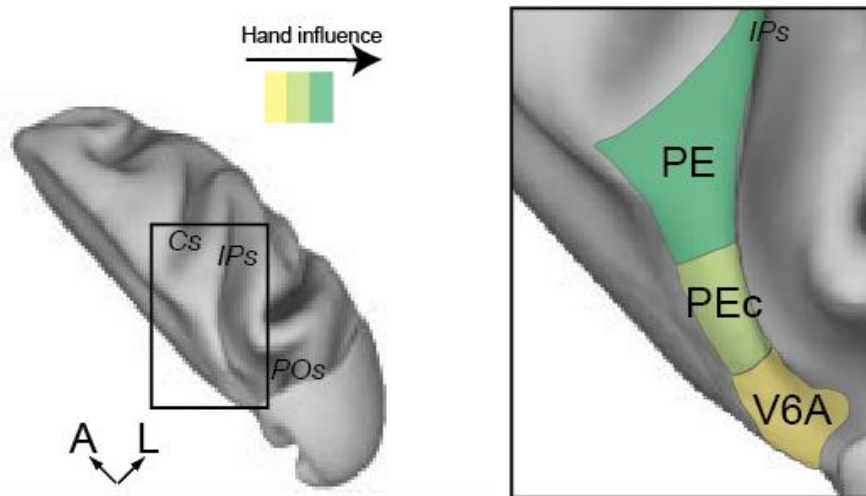


Figure 3-9. Functional gradient in medial PPC. A) Left, dorsocaudal view of the right hemisphere of the macaque brain with the main sulci slightly opened (POs=parieto-occipital sulcus; IPs=intraparietal sulcus; Cs=central sulcus). L=lateral; A= anterior. The area under the rectangle has been enlarged (right) to show the extent of areas V6A (Galletti et al., 1999), PEc and PE (Pandya and Seltzer, 1982). Colored areas represents areas studied for the influence of the hand upon reaching activity (yellow: weak influence of the hand position; green: high influence of hand position).

4. Multiple coordinate systems and motor strategies for reaching movements when eye and hand are dissociated in depth and direction

A similar version of this manuscript has been published as:

Annalisa Bosco, Valentina Piserchia and Patrizia Fattori. *Multiple coordinate systems and motor strategies for reaching movements when eye and hand are dissociated in depth and direction*. *Frontiers in Human Neuroscience*, 2017; 11:323.

4.1 Abstract

Reaching behavior represents one of the basic aspects of human cognitive abilities important for the interaction with the environment. Reaching movements towards visual objects are controlled by mechanisms based on coordinate systems that transform the spatial information of target location into appropriate motor response. Although recent works have extensively studied the encoding of target position for reaching in 3-dimensional space at behavioral level, the combined analysis of reach errors and movement variability has so far been investigated by few studies. Here we did so by testing twelve healthy participants in an experiment where reaching targets were presented at different depths and directions in foveal and peripheral viewing conditions. Each participant executed a memory-guided task in which he/she had to reach the memorized position of the target. A combination of vector and gradient analysis, novel for behavioral data, was applied to analyze patterns of reach errors for different combinations of eye/target positions. The results showed reach error patterns based on both eye- and space-centered coordinate systems: in depth more biased towards a space-centered representation and in direction mixed between space- and eye-centered representation. We calculated movement variability to describe different trajectory strategies adopted by subjects while reaching to the different eye/target configurations tested. In direction, the distribution of variability between configurations that shared the same eye/target relative configuration was different, whereas in configurations that shared the same spatial position of targets, it was similar. In depth, the variability showed more similar distributions in both pairs of eye/target configurations tested. These results suggest that reaching movements executed in geometries that require hand

and eye dissociations in direction and depth showed multiple coordinate systems and different trajectory strategies according to eye/target configurations and the two dimensions of space.

4.2 Introduction

When we want to reach for an object in space, visual information about the object location is mapped within the early stages of the visual cortex in a coordinate system based on eye position (eye-centered coordinate system). Within parietal and premotor regions, information about the object location is transformed in extrinsic coordinates, taking into account hand and body position (hand- and body-centered coordinate system). Thus, executing a movement towards a sensory target requires transformations between coordinate systems (Andersen and Buneo, 2002; Andersen et al., 1993; Soechting and Flanders, 1992).

Neurophysiological and behavioral investigations have targeted reaching movements to highlight principles underlying the process of coordinate transformations. In the neurophysiological field, many studies in monkeys have demonstrated the presence of parietal neurons encoding reaching actions in coordinate systems based on eye position (eye-centered) (Batista et al., 1999; Snyder et al., 1997) as well as based on hand, body or target position (space-centered) (Buneo et al., 2002, 2008; Marzocchi et al., 2008). Recently, a mixed coordinate system model, intermediate between eye- and space-centered coordinate systems, has been described in parietal areas of the monkey as representing a successful brain strategy that goes beyond the noise and variability generated by sensorimotor transformation (Deneve et al., 2001; Avillac et al., 2005; McGuire and Sabes, 2009, 2011; Mullette-Gillman et al., 2009; Chang and Snyder, 2010; Bosco et al., 2014, 2016). This variety of coordinate systems used in parietal areas was found both for reaching targets located on a 2-dimensional plane where targets varied the position only in direction dimension (Marzocchi et al., 2008; Bosco et al., 2015a;) and also for reaching targets that varied the positions in depth (Hadjidimitrakis et al., 2014b; Bosco et al., 2016; Piserchia et al., 2017). Specifically, Bosco et al. (Bosco et al., 2016) demonstrated that a prevalent mixed encoding of target position exists within a population of neurons recorded in the posterior parietal area V6A of macaque, using a task where reaching targets were decoupled from eye position in direction and depth.

In the behavioral field in humans, multiple coordinate systems (e.g., eye-, hand- and body-centered) were found for reaching towards both visual and proprioceptive targets (Beurze et al., 2006; Tramper and Medendorp, 2015; Mueller and Fiehler, 2016). Other human behavioral studies that investigated reaching executed to targets located in different depths and directions identified that the most suitable model able to maintain the spatial constancy, was an eye-centered representation (Henriques et al., 1998; Medendorp and Crawford, 2002; Van Pelt and Medendorp, 2008).

All these behavioral works defined the coordinate system by measuring the reach error patterns for combination of eye, target, hand or body positions. However, the trajectories during the movement in configurations of eye and target positions that varied in direction and depth can be generated by common or different mechanisms adopted by the participants. Movement strategies were extensively investigated to define the role of sensory information on movement control and execution (e.g., Pelisson et al., 1986; Carlton, 1992), but little is known about the comparison of trajectory strategies for reaches that share the same eye/target relative positions or the same spatial position of the target. The trajectory strategies towards static targets can be defined as modification of trajectory paths across trial repetitions. This can be evaluated by the analysis of motor variability at various stages throughout the movement (i.e., peak acceleration (PA), peak velocity (PV) and peak deceleration (PD)) (Khan et al., 2002, 2003). The rationale of this method was that if reaching movements are programmed and not altered, movement variability should increase as the movement progresses (Khan et al., 2002, 2003). If corrections in the movement trajectory were made on the subsequent trial, the variability profiles would deviate from the programmed movement trajectory and differ between different stages of movement and across eye/target configurations.

Here, we tested different configurations of eye and target relative positions in depth and direction, using a task design that maximizes natural reaching conditions where objects are reached on a horizontal surface and at a comfortable distance. We explored whether different coordinate systems and trajectory strategies are employed to encode reach direction and depth. We compared reach errors patterns and trajectory variabilities for pairs of configurations that shared the same eye/target relative position and those that shared the same spatial target position. First, we identified multiple coordinate systems adopted to guide reaches directed at different directions and depths. Then, the comparison of variability distribution in pairs of eye/target configurations

allowed us to quantify differences and similarities in the trajectory strategies across trials that were not evident from the simple comparison of the trajectory profiles.

4.3 Materials and Methods

4.3.1 Participants and Ethics statement

Twelve right-handed subjects (average laterality quotients: 0.90 [range 0.70-1.00]; (Oldfield, 1971) with normal, or corrected to normal, vision (3 males and 9 females, age range: 23-42 years; mean age: $29,5 \pm 6,92$ years) completed this study. The participants had no history of musculoskeletal or neurological disorders. This study was carried out in accordance with the recommendations of the Bioethical Committee of the University of Bologna. All participants gave written informed consent in accordance with the Declaration of Helsinki.

4.3.2 Apparatus and Stimuli

In all trials, the starting position of the hand (dominant right hand) was on a board placed adjacent to the touchscreen within a square marked with a tape and detectable by touch (size 12x12 cm) in front of the participant's chest, as sketched in Fig. 4-1A and B.

Reaching movements were performed in a dimly illuminated room. The head of the participants was supported on a chin rest in order to reduce movements. The stimuli were green (diameter 0.3 cm) and red dots (diameter 1.2 cm) presented at different depths and in different directions with respect to subject's midline. The stimuli presented a luminance of ~ 17 cd/m². Stimuli were presented on 19-in touchscreen (ELO IntelliTouch 1939L) laid horizontally on a desk located at waist level with a visible display size of 37.5 x 30 cm and 15.500 touch points/cm². The display had a resolution of 1152 x 864 pixels and a frame rate of 60 Hz.

Reaching movements were recorded using a motion tracking system (VICON motion capture system[®]) by sampling the position of two markers at a frequency of 100 Hz; markers were attached to the wrist (on the scaphoid bone) and on the nail of the index finger (reaching finger). The marker on the wrist was used to detect the onset and offset of reaching movements and was used to characterize the reaching component, as commonly done in kinematic studies of reaching (e.g., Roy et al., 2000; Gentilucci et

al., 2001); the marker on the tip of the index finger was used for the kinematic analysis, as it was the hand portion that made contact with the target (e.g., Carey et al., 1996). Participants were asked to move at a fast but comfortable speed, and as accurately as possible.

Eye position was recorded using a Pan/Tilt optic eye-tracker (Eye-Track ASL-6000) recording real-time gaze position at 60 Hz. The participant's dominant eye was illuminated by invisible infrared light, and the reflections were recorded by a video camera positioned 64 cm from the eye. The elevation distance between the eyes of the participants and the touchscreen was 27 cm. During the task, fixation was additionally monitored on-line by the experimenter on all trials. Before collecting data from each participant, the equipment was calibrated using a nine-point grid. Participants were asked to fixate successively on each of a series of small dots arranged on three lines in the form of a square (23x23 cm).

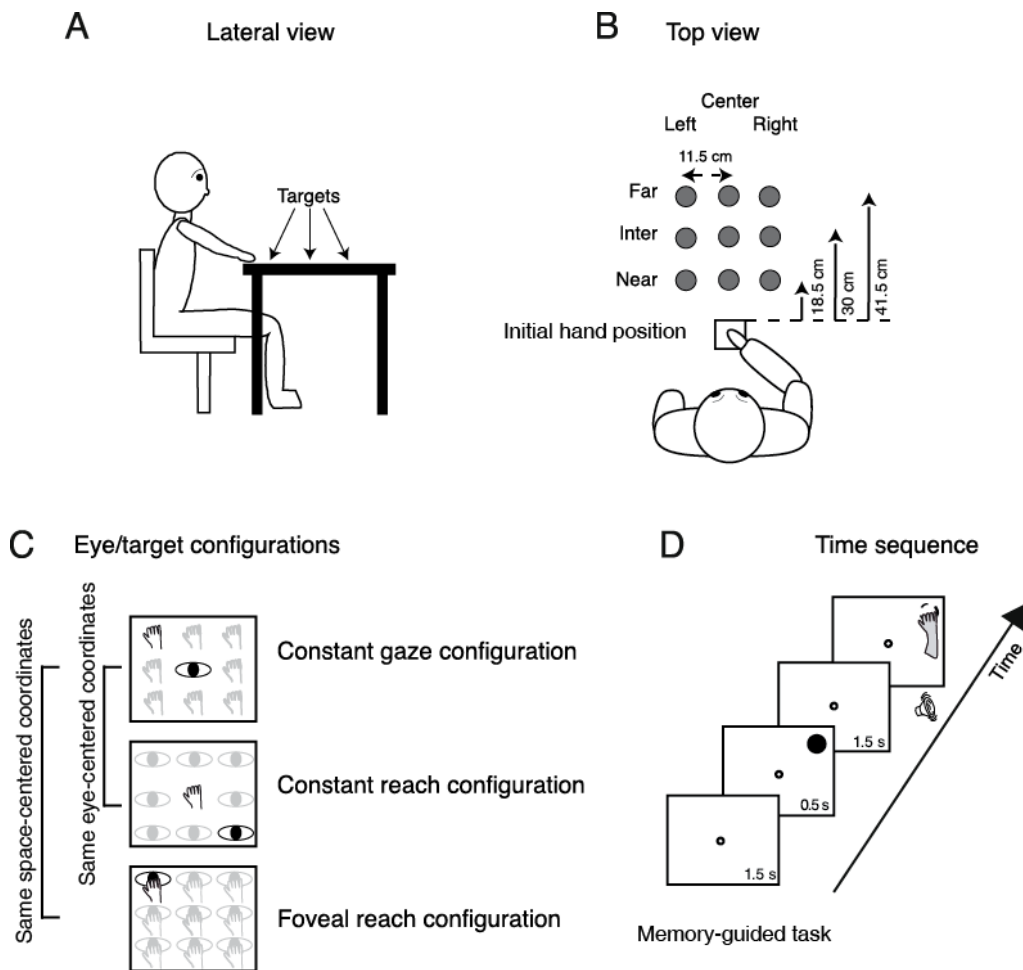


Figure 4-1 Experimental setup. A) Lateral view of the target arrangement with respect to the subject's body. B) Top view of the target arrangement in the peripersonal space. The subjects performed reaching movements with their right hand towards one of the nine LEDs targets located at different depths (far, intermediate and near) and in different directions (left, center and right), grey dots. Reaching movements were performed in a dimly lighted room from the initial hand position located next to the body and marked by a squared perimeter, as indicated in the bottom. C) Top view of the three task configurations. Top panel, Constant gaze configuration: reaching movements were performed towards 1 of the 9 targets (hands). The spatial position of the target changed trial to trial, but gaze was kept constant at the central position. Central panel, Constant reach configuration: reaching movements were performed always toward the target located in the central position. During the execution of the task, subject had to fixate 1 of the 9 different positions (eyes). Bottom panel, Foveal reach configuration: reaching movements were performed toward 1 of the 9 targets. During the task, the subject had to fixate and reach the same target (eye and hand on the panel). The Constant gaze and the Constant reach configuration shared the same eye/target relative position (eye-centered representation); the Constant gaze and the Foveal reach shared the same spatial target position

(space-centered representation). The two brackets on the left join parts of exemplary positions that share a common eye-centered coordinate system (first two panels) or a common space-centered coordinate system (first and last panels). D) Time sequence of memory-guided reaching in the Constant gaze configuration. The small white dot represents the fixation target; the filled black dot represents the reaching target and the dashed dot represents the memorized location of the reaching target. The fixation target (a green LED) stayed on for 1.5 sec and then the reaching target (a red LED) was turned on for 0.5 sec in one of the nine locations. After 1.5 sec from target offset, a sound indicated to the subject to reach with his/her right hand the memorized position of the target while maintaining fixation on the fixation target. The fixation target lasted until the subject completed the movement.

4.3.3 Behavioral Paradigm

Participants performed reaching movements on a desk where the touchscreen was positioned using their right hand. Fig. 4-1A shows the target positions at different depths with respect to participant's body. As depicted in Fig. 4-1B, there were 9 possible locations in which targets could appear: three placed at near distance (18.5 cm from the initial hand position), three at intermediate distance (30 cm from the initial hand position), and three at far distance (41.5 cm from the initial hand position). The targets were arranged in a square of 23x23 cm, and were located 11.5 cm apart each, either on the left or the right side, the central targets were placed along the sagittal midline. All targets were located within a comfortable reaching distance.

The task was composed of different eye/target configurations (see Fig. 4-1C): the *Constant gaze configuration*, in which the eye fixated a central fixation target and the hand reached to one of the peripheral reaching targets (thus the reaching target was on the fovea only when presented at the same central location of the fixating target and in the periphery of the retina for the other eight possible locations); the *Constant reach configuration* in which the eyes fixated one of the peripheral targets and the hand always reached the central target; and *Foveal reach configuration* in which the fixation target and the reaching target were coincident. The Constant gaze and the Constant reach configurations were extrafoveal configurations in which the position of the fixation point was dissociated from the position of the reaching targets. These two configurations (eye-centered configurations) shared the same eye/target relative position and were used to study the eye-centered coordinate system (see the black exemplary

positions in the first 2 panels in Fig. 4-1C). The Foveal reach configuration instead was a configuration in which the position of the fixation point coincided with the position of the reaching target and shared the same spatial positions with the Constant gaze configuration. The pairs of targets in the same spatial position (space-centered configurations) allowed us to describe the space-centered coordinate system as it is indicated on the left of Fig. 4-1C. On the left of Fig. 4-1C the pairs of comparisons used to assess the two types of coordinate systems is indicated by grouping a pair of exemplary positions in the same eye-centered coordinates and a pair in the same space-centered coordinates. The combinations of the configurations as described above enabled us to define the coordinate systems as was done in neurophysiological experiments (Bosco et al., 2016).

We tested the participants in a memory guided reaching task as shown in Fig. 4-1D. The sequence of the memory guided reaching consisted in the presentation of a fixation target (a green LED, diameter 0.3 cm) that stayed on for 1.5 s. Then, the reaching target (a red LED, diameter 1.2 cm) was flashed for 0.5 s. After 1.5 s from target offset, an acoustic signal indicated to the subject that they should reach the remembered position while maintaining fixation on the green-fixation target. The fixation point remained illuminated until the subject completed the movement.

The task was composed of 5 blocks of 27 trials. Within each block, trials of the three configurations were randomized. For stimuli presentation and data analysis, we used Matlab with the Psychophysics toolbox extension (Brainard, 1997).

4.3.4 Data Analysis

After recordings, data positions were interpolated at 1000 Hz and were run through a fifth-order Butterworth low-pass filter (cutoff frequency, 30 Hz (Bosco et al., 2015b)). For data processing and analysis, we wrote custom software in Matlab (Mathworks) to compute the velocity profiles of all markers. Onset of movement was detected when wrist velocity remained above 5 mm/s for 200 ms; the following offset was detected when wrist velocity remained below 5 mm/s for 200 ms. Reach endpoints were extracted from touchscreen recordings; movement trajectory and variability from motion capture system recordings (Vicon[®]).

We measured two-dimensional reach endpoints and analyzed the horizontal (direction) and vertical (depth) dimensions of reach errors calculated by subtracting the

respective horizontal and vertical coordinates of physical target location from the reach endpoint in that trial. We performed a gradient analysis (Peña and Konishi, 2001; Andersen and Buneo, 2002; Pesaran et al., 2006, 2010; Bremner and Andersen, 2014; Bosco et al., 2016) that has been applied previously to neural data to determine which combination of eye/target configurations (eye-centered and space-centered configurations) had the most influence on the pattern of reach errors or whether the configurations had equivalent influence. This technique allowed us to capture the complex geometry of task and extract the relevant features. 9/12 participants (7 females and 2 males, age range from 23 to 42 years) were included in this analysis, three participants were excluded because some target positions were discarded for missed detection of some endpoints by the touchscreen. The gradient of reach error matrices (X-reach error matrices for direction dimension and Y-reach error matrices for depth dimension) was estimated with the Matlab gradient function and plotted as white arrows on the matrix elements. The directions and lengths of the set of white arrows indicate the relative importance of each variable on the reach error patterns of the participants. Specifically, the direction of the arrows indicates whether reach errors in X or Y dimension were influenced by the near-far and/or the left-right target positions and the length of arrows is proportional to the magnitude of reach errors for each position. We performed separated gradient analysis for Constant gaze and Constant reach configurations to extract relevant spatial features for configurations that shared the same eye/target relative positions (eye-centered configuration) and for Constant gaze and Foveal reach configurations to extract spatial features for configurations that shared the same spatial target positions (space-centered configuration), as also simplified by the left part of Fig. 4-1C. The x and y component of the 2 vector fields corresponding to the pair of the eye-centered and space-centered configuration, respectively, were summed together in order to obtain two resultant vectors (eye-centered and space-centered resultant vector) defined by the length. The two resultant vectors therefore indicate the overall contribution of the eye- and space-centered coordinate systems on the reach error pattern of each subject. For example, in Fig. 4-2A, (shown in the “Result” section), the Constant gaze and Constant reach matrices, the arrows reflect a reach error pattern that changes according to the eye position (eye-centered representation). As they point predominantly to left and right, respectively, they subtract one from the other so their sum is near zero (little arrow in the circle on the right of Fig. 4-2A). In Fig. 4-2B (shown in the “Result” section), the Constant gaze and Foveal reach matrices, the

arrows indicate a reach error pattern that changes according to the spatial position of targets. As all the arrows point to the left, their sum is high (right of Fig. 4-2B). This indicates an example of space-centered encoding of reaching for this participants.

The prevalent coordinate system employed by each participant was ascertained by randomization of the matrix elements (randomization test, 1000 iterations). The randomization allowed us to extract confidence intervals (CIs) that included the 99% of values for each pair of configurations analyzed (first pair: eye-centered configuration; second pair: space-centered configurations). As the eye-centered representation tends to have opposite directions of vector fields in Constant gaze and Constant reach configurations and consequently the resultant vector length is close to zero, we defined participants as encoding in eye-centered coordinates when the resultant vector was smaller than the lower CI for this pair of configurations (see Fig. 4-4A, shown in the “Result” section). The space-centered representation assumes that the vector fields in Constant gaze and Foveal reach configurations have the same direction and consequently the vectors add together. We defined that there was a space-centered representation when the resultant vector was larger than the upper CI extracted from the sum of vector fields of Constant gaze and Foveal reach (see Fig. 4-4B, shown in the “Result” section). The participants that showed resultant vectors not responding to previous criteria were defined as those encoding in mixed coordinate systems.

It is worthwhile noting that the term “space-centered” includes head-centered and world-centered coordinate systems, since the position of the target was kept constant with respect to the space, the head of the participant and the external world.

To assess the correspondence of results of the gradient analysis with more standard techniques to study reference frames at behavioral level, we performed a correlation analysis. The correlation analysis of reach errors has been previously applied in human and monkey behavioral studies (Scherberger et al., 2003; Beurze et al., 2006; Dessing et al., 2011). We reasoned that if the participants coded the movement in an eye-centered coordinate system, the reaching accuracy should be more similar in the configurations that share the same eye/target relative position compared to the configurations that share the same spatial target position. If the movement was encoded in space-centered coordinates, the reaching accuracy should be more similar in the configurations sharing the same spatial position of targets. We first calculated correlation coefficients for reach errors in depth and direction and then we extracted correlation coefficients for each participant, separately (Beurze et al., 2006; Dessing et

al., 2011). This analysis estimates if the correlation coefficients are higher in eye-centered or space-centered coordinate systems in each subject when pointing to targets placed at different locations relative to the body and with gaze fixed at different directions. Specifically, we compared the similarity of reach errors among configurations presenting the same eye/target relative position (Constant gaze and Constant reach configuration) and configurations presenting the same spatial positions of targets (Constant gaze and Foveal reach configuration) as described for gradient analysis. To evaluate whether correlation coefficients were more deviated towards an eye-centered or a space-centered coordinate system with respect to diagonal, we calculated the average correlation coefficients across participants in depth and direction separately, and corresponding CIs were estimated by the standard deviations of the data.

As a measure of movement corrections along the motor execution, we performed an analysis of the variability of trajectories across trials. For each participants (N=12) we calculated standard deviations across trials in both Y (depth) and X (direction) dimensions at four relevant points of movement for trajectories described by the marker located on the index finger and that corresponded to: peak acceleration (point of maximum acceleration, PA), peak velocity (point of maximum velocity, PV), peak deceleration (point of maximum negative acceleration, PD) and the end of movement (END); then we averaged across the subjects (Khan et al., 2002, 2003; Kasuga et al., 2015). We compared the distribution of spatial variability for eye-centered configurations (Constant gaze and Constant reach configurations) and for space-centered configurations (Constant gaze and Foveal reach configurations) in depth and direction by a two-way ANOVA (2 eye/target configurations \times 4 points on the trajectory) and by a Bonferroni post hoc test when the interaction was significant.

We carried out the three-way ANOVA on the trajectory variabilities separated for eye-centered and space-centered configurations with reach dimension as factor 1 (2 levels, depth and direction), eye/target configuration as factor 2 (2 levels, Constant gaze and Constant reach in eye-centered configuration and Constant gaze and Constant reach in eye-centered configuration, respectively) and points on the trajectory as factor 3 (4 levels, PA, PV, PD and END) to assess the interaction of these three factors on movement variability.

We included the central positions of the two constant configurations only in the qualitative data of gradient analysis (Figs. 4-2 and 4-3, shown in the “Result” section). We excluded them from the calculation of resultant vectors and trajectory variabilities.

4.4 Results

We used a three-dimensional memory-guided reaching tasks with nine target locations that participants had to reach with different combinations of eye and target position, for a total of 27 types of trials. Reaching targets were located on a table arranged at a comfortable distance from the subjects' body that allowed a natural interaction with targets, as shown in Fig. 4-1.

4.4.1 Analysis of reach error patterns

To define the predominant coordinate system employed by each subject and characterize the pattern of reach errors in depth and direction dimension, we used a combination of gradient and vector analysis which has been used by other authors to describe the influence of more than one variable simultaneously (Pesaran et al., 2006, 2010; Bremner and Andersen, 2014; Bosco et al., 2016). Fig. 4-2 shows example vector correlations derived from one exemplar subject. Three 3 x 3 gradient fields represent the reach errors along the X dimension (direction) for every configuration of eye and reaching target position in each of the three tasks tested. Each element within the matrices therefore represents the gradient plotted as two-dimensional vector fields. We calculated the length of resultant vector as the sum of the x and y component of each arrow forming the vector field pair (Constant gaze/Constant reach configurations; Constant gaze/Foveal reach configurations). The fields in Fig. 4-2A depict the two configurations sharing the same eye/target relative position. The two vector fields show opposite direction mainly distributed on the X dimension. In particular, the participant exhibits higher positive X-reach errors for targets located to the left of eye position in both configurations. This suggests that the reach error pattern changed according to the eye position (eye-centered coordinates). The sum of the vector fields tends to give a small resultant vector in length (Fig. 4-2A, polar plot on the right; eye-centered resultant vector = 0.91 cm) since the two fields are characterized by arrows pointing into opposite direction and subtract each other. In Fig. 4-2B, the combination of Constant gaze and Foveal reach, that shared the same spatial position, showed a similar alignment of vector fields that pointed towards left targets. In this specific case, the alignment of vector fields suggests a reach error pattern based on the spatial position of the target not dependent on the eye (space-centered coordinates). For this combination, the sum of

vector fields generates a larger resultant vector because the vector fields are characterized by similar directions of the arrows and add together (space-centered resultant vector = 8.71 cm, Fig. 4-2B, polar plot on the right). This example suggests the presence of two coordinate systems according to the combination of eye/target configurations.

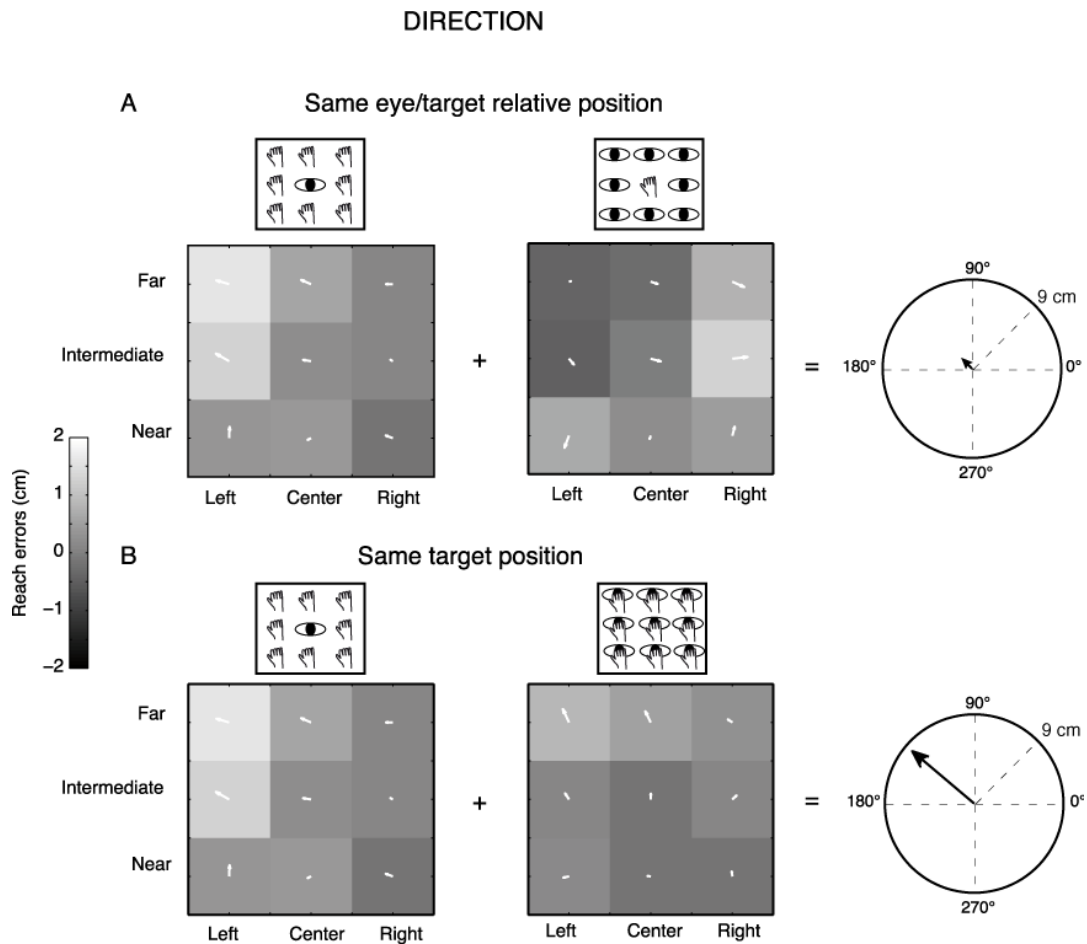


Figure 4-2. Gradient and vector analysis for real reach errors in direction in an exemplary participant. A) The vector fields show the convergence for higher positive reach errors for targets to the left of the eye position in the Constant gaze and Constant reach mainly distributed along the direction dimension. The resultant vector on the right have a length of 0.91 cm. B) The vector fields corresponding to Constant gaze and Foveal reach configurations show higher positive reach errors for left targets along the direction dimension. The resultant vector on the right presents length of 8.71 cm. See text for more details.

Fig. 4-3 shows the same type of analysis but for a different participant and in contrast to the previous example we considered the depth dimension (Y-reach errors) rather than the direction. This participant showed a different pattern of vector fields of reach errors when we considered the Y reach errors (depth). In this case, the vector field combination of the configurations sharing the same eye/target relative position (Constant gaze and Constant reach configuration, Fig. 4-3A) did not show a specific alignment suggesting a reach error distribution not consistent with the eye-centered pattern (eye-centered resultant vector = 7.93 cm). The vector fields in the same target configuration (Constant gaze and Foveal reach, Fig. 4-3B) showed the same alignment with arrows that mainly pointed towards the near positions with the space-centered resultant vector equal to 7 cm (Fig. 4-3B, polar plot on the right). In this case, the analysis of vector fields suggests a reach error pattern more based on the target position (space-centered coordinates) rather than on the eye/target relative position (eye-centered coordinates).

DEPTH

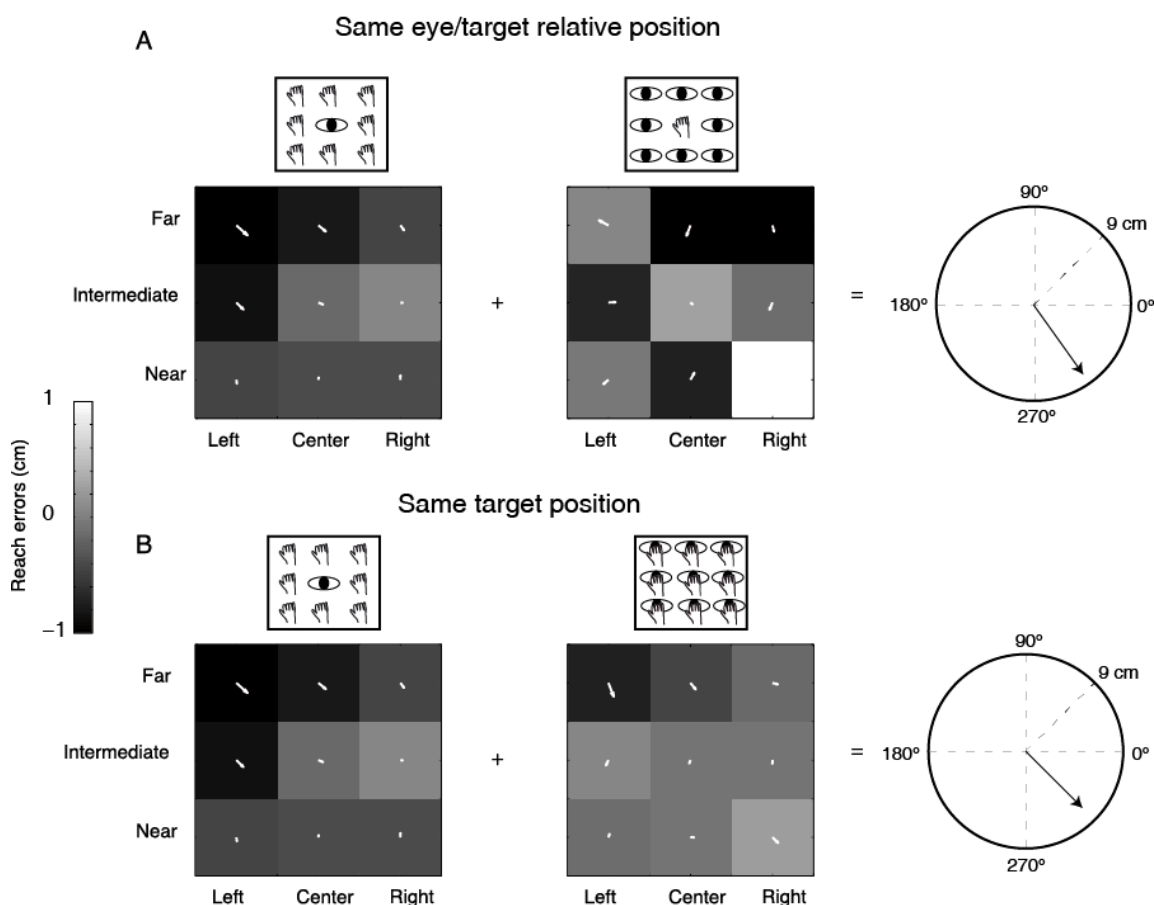


Figure 4-3. Gradient and vector analysis for real reach errors in depth. A) The vector fields show higher positive reach errors for targets nearer than the fixation point in Constant gaze and not homogeneous distribution of reach errors in Constant reach configuration (arrows directed towards the bottom). The resultant vector on the right polar plot measures 7.93 cm. B) Vector fields and resultant vector when reaching movements were made in the constant space-centered coordinates (the combination of Constant gaze and Foveal reach configurations). The pair of vector fields shows convergence for reach errors evoked by targets located near to the subject in both cases. The resultant vector length is 7 cm.

In order to statistically determine the prevalent coordinate system employed by each participant, we resampled the resultant vector lengths to obtain lower and upper CIs that included 99% of values for each pair of configurations analyzed (Fig. 4-4). The eye-centered resultant vector was derived from the sum of vector fields of Constant gaze and Constant reach configurations (Fig. 4-4A), whereas the space-centered resultant vector resulted from the sum of vector fields of Constant gaze and Foveal

reach configurations (Fig. 4-4B). The eye-centered representation tends to have opposite directions of vector fields corresponding to reach errors varying according to the eye position. We defined the eye-centered coordinate system when the resultant vector of Constant gaze and Constant reach combination was shorter than the lower CI for this pair of configurations. We then defined the space-centered coordinate system when the resultant vector of Constant gaze and Foveal reach combination was larger than the upper CI. In this way, the lower and the upper CIs were extracted from two different distributions corresponding to the two combinations used. The positions of eye-centered resultant vectors (Constant gaze + Constant reach configurations), for direction and depth dimensions, are represented in Fig. 4-4A as white dots. In our hypothesis, significant eye-centered representation included eye-centered resultant vector smaller than the lower CI. From Fig. 4-4A it is evident that this never happened in our study as all participants showed eye-centered resultant vectors larger than the lower CI in both direction and depth. Fig. 4-4B shows the positions of space-centered resultant vectors (white dots) with respect to the upper CI. In direction, one out of nine participants presented the resultant vector larger than the upper CI and six out of nine participants in depth; so 11% of the participants used space-centered coordinates to encode the direction of reaching target and 89% used mixed coordinates. We found that the majority of tested participants (67% of participants) encoded the depth of target position using space-centered coordinates and 33% of the participants using mixed system coordinates.

An interesting aspect is represented by the number of participants that changed or maintained the same type of coordinate system across depth and direction dimension. The majority of the participants (77%) used different coordinate system in depth and direction and 23% used the same coordinate system. Among the participants that changed the coordinate system, 14% of the subjects switched from space-centered representation in direction to mixed in depth; 86% of the subjects switched from the mixed coordinates in direction to space-centered coordinates in depth.

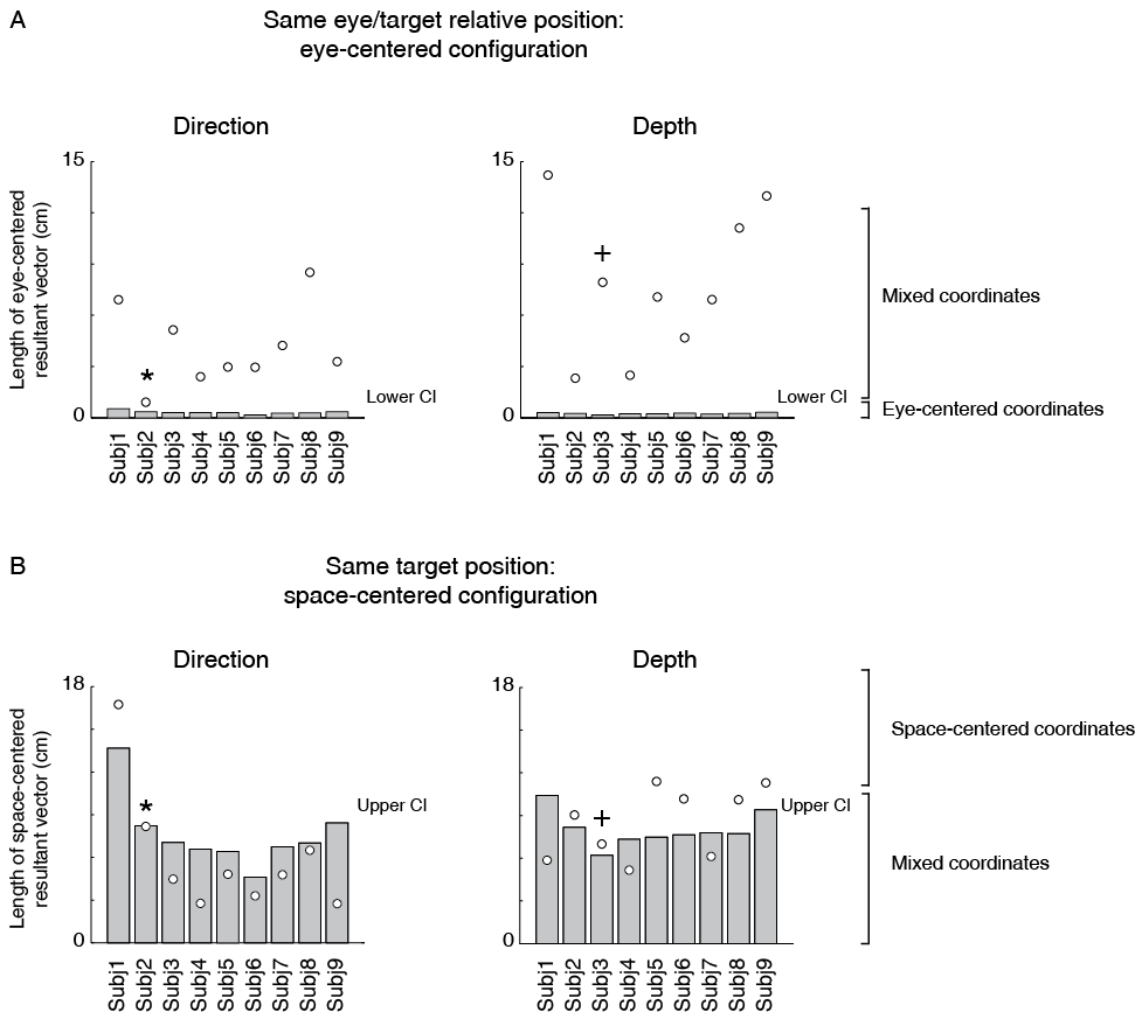


Figure 4-4. Vector length positions with respect to lower and upper CIs. A) Position of resultant vector lengths from the gradient and vector analysis extracted by the combination of Constant gaze and Constant reach configurations (eye-centered combination) of each subject (white dots) with respect to the lower CI (grey bar) for direction and depth, respectively. All values are above the lower CI. B) Position of resultant vector lengths extracted by the combination of Constant gaze and Foveal reach configurations (space-centered combination) of each subject (white dots) with respect to the upper CI (grey bar) for direction and depth, respectively. Asterisks and crosses correspond to individual examples in Fig. 4-2 and 4-3, respectively. For direction, the majority of values fall below the upper CI; for depth, the majority falls outside the upper CI. For attribution criteria of eye-centered, space-centered and mixed coordinate systems see the text.

The vector fields in the study of coordinate systems adopted by the brain have been mostly used for the analysis of neural data and, to our knowledge, have never been

applied to behavioral variables (e.g., reach errors). However, to assess the reliability of the vector field analysis in a way more standardized for behavioral studies, we calculated correlation coefficients on reach errors in order to compare the similarity of reach errors among configurations presenting the same eye/target relative position (Constant gaze and Constant reach configurations) and configurations presenting the same spatial positions of the targets (Constant gaze and Foveal reach configuration). In Fig. 4-5, we plotted the correlation coefficients for each subject in eye-centered versus space-centered coordinate systems for reach errors in depth (white circles) and direction (black circles). The majority of points were located on the upper side of diagonal suggesting higher correlation for reach errors in space-centered coordinates. Additionally, we calculated the averaged correlation coefficient with the corresponding CIs (represented as crosses in Fig. 4-5). In depth, the correlation coefficient averaged across participants and relative to the eye-centered coordinate system was 0.02 ± 0.28 ($P < 0.05$ in 5/12 subjects). For the space-centered coordinate system, the averaged correlation coefficient was 0.33 ± 0.16 ($P < 0.05$ in 3/12 subjects). In direction, the averaged correlation coefficients were -0.27 ± 0.16 for the eye-centered coordinate system ($P < 0.05$ in 3/12 subjects) and -0.07 ± 0.29 for the space-centered coordinate system ($P < 0.05$ in 3/12 subjects), respectively. In general, CIs of averaged correlation coefficients in depth did not touch the diagonal indicating a preponderance of the space-centered representation while, in direction, the CIs crossed the diagonal indicating a mixed representation.

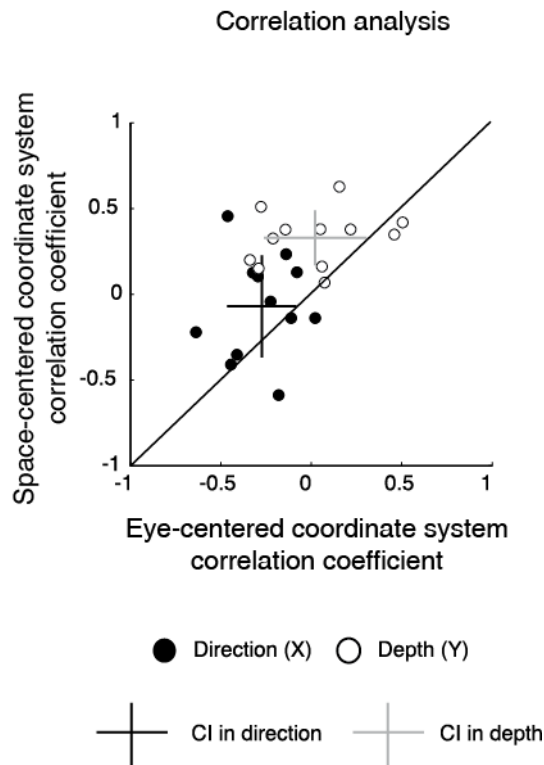


Figure 4-5. Correlation analysis. Correlation coefficients for eye-centered coordinates vs. space-centered coordinates for all the participants. Each data point represents the value of the correlation coefficient of each participant in direction (black) and depth (white). Black cross represents the average correlation coefficient in direction with the corresponding confidence intervals; grey cross represents the average correlation coefficient in depth with the corresponding confidence intervals. For depth, the confidence intervals do not cross the diagonal, indicating a significant representation in space-centered reference frame, whereas for direction, intervals cross the diagonal, indicating a mixed representation.

The results from the correlation analysis confirm the previous results of vector analysis by showing a preponderant space-centered representation for depth and a mixed representation for direction.

4.4.2 Analysis of movement variability

Participants performed smooth trajectories to acquire target positions in each of the three different eye/target configurations, as reported in the individual example of Fig. 4-6.

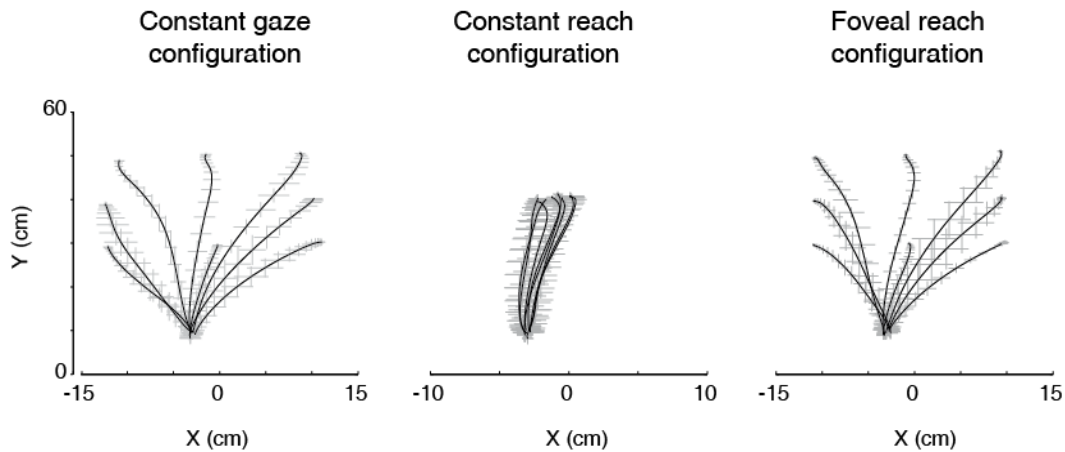


Figure 4-6. Actual trajectories of the movement. The trajectories of the index finger during movement in the three eye/target configurations in one participant. Solid lines indicate the averaged trajectory and grey crosses the X and Y variabilities along the movement. Note that, although the square of the initial hand position was on the midsagittal line (see Fig. 4-1B), as all participants held the hand horizontally rotated with respect the midline of the screen, the marker of the index resulted more deviated to the left with respect to the origin of the axes defined, by system calibration, on the center of initial hand position square.

Our hypothesis was that the distribution of variability, as a measure of modifications of trajectory paths across trials, could be different across the three eye/target configurations and space dimensions (direction and depth). For this reason, we analyzed the variability in the trajectories of each participant ($N = 12$) at relevant points during the movement (peak acceleration, PA; peak velocity, PV; peak deceleration, PD) and at the end of the movement (END) (Khan et al., 2002, 2003). Fig. 4-7 shows the average of variability distributions in black and individual participant variability distribution in grey. We then performed a two-way ANOVA on trajectory variabilities separately for pair of configurations sharing the same eye/target relative position (eye-centered configurations; Fig 4-7, left) and for the two that shared the same spatial target position (space-centered configuration; Fig. 4-7, right) and for direction and depth (Figs. 4-7A and B, respectively). This statistical analysis allowed to assess whether the distributions of variabilities differed between the pair of configurations sharing the same coordinate system. In direction, we carried out the two-way ANOVA on the trajectory variabilities with the eye-centered configuration as factor 1 (Constant gaze and Constant reach, 2 levels) and the points on the trajectory as factor 2 (PA, PV, PD and END, 4 levels). We found main effects of the eye-centered configuration ($F_{1,3} = 716.53$, $P <$

0.05) and of the points on the trajectory ($F_{1,3} = 49.80$, $P < 0.05$). In addition, we found significant two-way interactions between eye-centered configurations and points on the trajectory ($F_{1,3} = 56.25$, $P < 0.05$). The distribution of variabilities in Constant gaze and Constant reach significantly differed in all the four points on the trajectory (Fig. 4-7A-left, Bonferroni post hoc test, $P < 0.006$). For direction, we compared the trajectory variabilities by the two-way ANOVA with the space-centered configuration as factor 1 (Constant gaze and Foveal reach, 2 levels) and the points on the trajectory as factor 2 (PA, PV, PD and END, 4 levels). We found main effects of space-centered configuration ($F_{1,3} = 6.04$, $P < 0.05$) and of the points on the trajectory ($F_{1,3} = 173.02$, $P < 0.05$). The analysis showed a significant interaction between space-centered configurations and points on the trajectory ($F_{1,3} = 7.15$, $P < 0.05$). The multiple comparison analysis revealed a significant difference only at the PA between Constant gaze and Foveal reach configurations (Fig. 4-7A-right, Bonferroni post hoc test, $P < 0.006$).

In depth, for eye-centered configuration, the two-way ANOVA analysis showed significant main effects of eye-centered configuration (Constant gaze vs Constant reach; $F_{1,3} = 77.35$, $P < 0.05$) and of points on the trajectory (PA, PV, PD and END; $F_{1,3} = 47.17$, $P < 0.05$) and significant interaction was found between these two factors ($F_{1,3} = 18.09$, $P < 0.05$). The multiple comparison analysis revealed that the variabilities at the PD and at the END of movement were significantly different between Constant gaze and Constant reach configuration (Fig. 4-7B-left, Bonferroni post hoc test, $P < 0.006$). When we considered the space-centered configuration, we found significant main effects of space-centered configuration (Constant gaze vs Foveal reach; $F_{1,3} = 4.60$, $P < 0.05$) and of points on the trajectory (PA, PV, PD and END; $F_{1,3} = 61.38$, $P < 0.05$). A significant interaction was found between the two factors ($F_{1,3} = 2.77$, $P < 0.05$) and the multiple comparison analysis showed significant difference in variabilities only at the PA between Constant gaze and Foveal reach configurations (Fig. 4-7B-right, Bonferroni post hoc test, $P < 0.006$).

The distributions in Fig. 4-7A-B illustrate how different or similar the movement variabilities were within each pair of eye/target configurations in direction (Fig. 4-7A) and depth (Fig. 4-7B). In direction, the movement variability showed that in space-centered coordinates the distribution of variabilities was similar from the peak velocity to the end of movement (Fig. 4-7A, right). The variability in eye-centered coordinates was completely different for the entire duration of the movement, meaning that the

participants used two different strategies in approaching the targets (Fig. 4-7A, left). On the contrary, in depth, the distribution of variabilities in eye-centered coordinates was similar for the first part of the movement (Fig. 4-7B, left) and in space coordinates overlapped from the peak velocity to the end of movement (Fig. 4-7B, right). All comparisons show a consistent variability distribution across subjects (Fig. 4-7, grey lines).

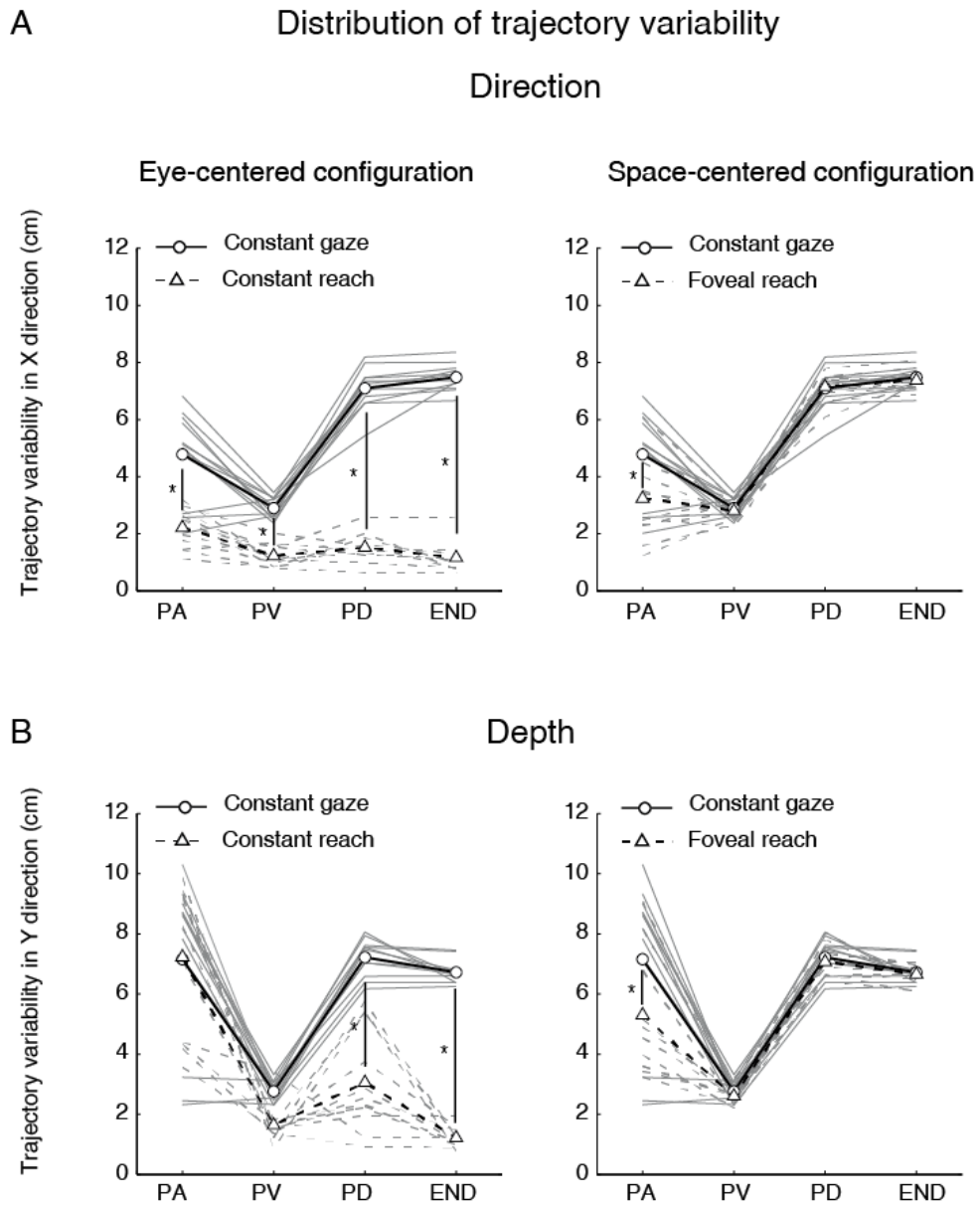


Fig. 4-7. Spatial variability analysis. A) Distribution of variability (cm) in the X dimension (Direction) for pairs of movements that were identical in eye-centered coordinates (left) and of pairs of movements towards targets having the same position in space-centered coordinates (right). Circles connected by solid lines correspond, on the left and on the right, to Constant

gaze averaged variabilities. Triangles connected by dotted lines correspond, on the left, to Constant reach averaged variabilities and, on the right, to Foveal reach averaged variabilities. Grey solid and dotted lines indicate, on the left, individual variabilities of each subject for Constant gaze and Constant reach configurations, respectively and, on the right, Constant gaze and Foveal reach configurations, respectively. PA, peak acceleration; PV, peak velocity; PD, peak deceleration; END, end of movement. B) Distribution of variability (cm) in the Y dimension (Depth) for pairs of movements that were identical in eye-centered coordinates (left) and of pairs of movements towards targets having the same position in space-centered coordinates (right) as in Fig. 4-7A. All conventions are as in Fig. 4-7A. Asterisks indicate significant Bonferroni Post hoc test when two-way ANOVA interaction was significant, $P < 0.05$.

We then performed the three-way ANOVA to assess whether the trajectory variabilities were influenced by the interaction between the dimensions of reach (direction and depth), the eye/target configurations and the points on the trajectory (see “Materials and Methods” Section). In eye-centered configuration, we found significant interactions between dimensions of reach (direction and depth) and eye-centered configurations ($F_{1,3} = 15.82$, $P < 0.05$) as well as between dimensions of reach and points on the trajectory ($F_{1,3} = 28.33$, $P < 0.05$). In space-centered configuration, we found significant interaction between dimensions of reach and points on the trajectory ($F_{1,3} = 17.32$, $P < 0.05$). All these results suggest that movements along direction and depth dimensions depend on different trajectory strategies in eye- and space-centered coordinates. In general, the motor strategies across trials adopted by each participant were influenced by the eye/target relative configurations and by the reach dimension (direction and depth).

4.5 Discussion

In the present study, we examined different aspects of the encoding of memory-guided reaching movements to targets placed at different depths and different directions. The specific set of experimental configurations, dissociating or consistent, in eye and target positions, allowed us to analyze the predominant coordinate system used in a reaching setup very similar to natural conditions that maximized an easy interaction with the targets.

Our results reveal a predominant use of mixed coordinate system when different directions are considered, whereas space-centered coordinate system predominates for changes in depth. To assess this, we applied a combination of vector and gradient analysis that is typically used for neural data (Pesaran et al., 2006; Bremner and Andersen, 2014; Bosco et al., 2016) but, to our knowledge, it is the first time that these analyses have been used for behavioral data. The analysis of the combination of vector fields across the different eye/target configurations (Figs. 4-2, 4-3 and 4-4) highlighted that both eye-centered and space-centered representations were present, but space-centered was predominant in depth and the two coordinate systems showed the same influence in direction (mixed coordinate system, see Fig. 4-2 for an example). Our laboratory (Bosco et al., 2016) investigated the encoding of reaching target located at different depths and directions in a parietal area of the macaque and we found both eye- and space-centered representations differently balanced across neurons, similar to present behavioral results.

As mixed coordinate systems have been found in the complex network of parietal regions (Stricanne et al., 1996; Buneo et al., 2002; Cohen and Andersen, 2002; Battaglia-Mayer et al., 2003; Avillac et al., 2005; Mullette-Gillman et al., 2005, 2009; Chang and Snyder, 2010; McGuire and Sabes, 2011; Hadjidimitrakis et al., 2014a; Bosco et al., 2015a, 2016; Piserchia et al., 2017) and this parallels the present behavioral data, it can be suggested that what we have found here is the outcome, at behavioral level, of the neural discharges investigated in those works. The impact of mixed representations show several advantages, as described in several modeling and human studies. In fact, some authors described that, if the system can simultaneously represent different coordinate systems, the noise associated with coordinate conversion is strongly reduced (Deneve et al., 2001; Avillac et al., 2005; McGuire and Sabes, 2009, 2011; Bernier and Grafton, 2010; Beurze et al., 2010; Blohm, 2012; Buchholz et al., 2013). In addition to noise reduction, a further advantage of flexible coordinate systems derives from evidence that the computation of the motor response is complicated due to the necessity to integrate signals in retinal, proprioceptive, and motor coordinate systems (Buneo et al., 2002) and the brain requires some time to converge on a correct movement vector calculation. The adoption of a coordinate system that simultaneously takes into account different landmarks allows successfully fast movement corrections. Here, the prevalent use of mixed coordinate systems in direction is interesting because we have compared two configurations that shared the same eye/target relative position

but that required different organization of movement trajectories: in one configuration subjects reached the peripheral positions and in the other always the central position. This suggests that, in direction, the relative position of eye and target strongly contributes to spatial coordinates rather than the dynamical requirements of movement trajectories. Overall, our results support the view that spatial locations are represented in multiple coordinate systems with their individual contributions depending on the target modality (Bernier and Grafton, 2010), task demands (Badde et al., 2014, 2015) and sensory experience (Reuschel et al., 2012).

In depth, we found a preponderant space-centered representation that is commonly considered a more stable encoding mechanism (Medendorp and Crawford, 2002). In this case, the reach error patterns were more driven by the two eye/target configurations that shared the same spatial target position independently from the eye position. These two eye/target configurations presented the same reaching geometry because, in both cases, the subjects reached peripheral targets that can be foveated or not, but, in general, the same trajectory dynamics were used (see Fig. 4-6, first and last panels). This could indicate that the encoding of target depth is more influenced by the organization of trajectories and must rely on constant coordinates of the space that does not change with eye movements for example.

Many studies investigated coordinate systems used to encode the targets for memory-guided movements (Diedrichsen et al., 2004; Obhi and Goodale, 2005; Byrne and Crawford, 2010; Fiehler et al., 2011). For example, Fiehler et al. (2011) found that reach targets were updated relative to the position of the eyes when the movements were executed after different delays when no other external cues were available. However, other studies suggested the use of allocentric coordinate systems when movements were delayed (Diedrichsen et al., 2004; Obhi and Goodale, 2005). In particular, the presence of landmarks serves to improve the stability of the estimation of target position especially when the target of reaching is memorized (Obhi and Goodale, 2005). Furthermore, more recent work suggests that egocentric and allocentric information are integrated for memory-guided reaching movements by weighting each single input with respect to their reliability (Byrne and Crawford, 2010). In line with all these evidences, in our memory-guided reaching task, we found both space-centered and eye-centered representations differently distributed along the depth and direction dimensions.

By analyzing the kinematics of reaching configurations (see Figs. 4- 6 and 4-7), we found that movement variability was different in depth and direction and in different

eye/target configurations. We used the movement variability as a measure of trajectory strategies used by the subjects across trial repetitions. Typically, this analysis has been applied to study the role of visual information on the reaching execution (Khan et al., 2002, 2003); here we have used it to identify common or different motor strategies for reaching in different eye/target configurations. In direction, we found that the variability distributions in eye-centered coordinates were completely different in the two configurations for the total duration of movement whereas in space-centered coordinates the variability distributions were similar. In depth, the variability distribution in eye-centered coordinates was similar for the first half of the movement (until the peak velocity) while in space-centered coordinate it was comparable for the entire movement. We found trajectory modifications also in the first part of movement: as several studies suggested that online processes do not influence movement at least to peak velocity (Elliott et al., 1999; Krakauer et al., 2000; Proteau and Isabelle, 2002), we can attribute these modifications to offline control processes (correction across trials) that are applied on subsequent trials (Khan et al., 2003).

All the differences in movement variability support two possible views. First, different strategies of movement are used in depth and direction when multiple eye/target configurations are used. This is evident by the distribution of variability for Constant gaze and Constant reach configurations, that was dramatically different in direction but partially similar in depth. Second, we cannot exclude the possibility that the differences between the two configurations were due to different shoulder/elbow postures during the movement. However, in general, a different mechanism in the organization of movement is evident in depth and direction. Previous behavioral studies showed that the encoding of depth and direction does not rely on shared networks in the brain during the execution of movement, but it is processed separately (Flanders et al., 1992; Gordon et al., 1994; Sainburg et al., 2003; Vindras et al., 2005; Bagesteiro et al., 2006; Van Pelt and Medendorp, 2008). However, other evidence suggested that movement amplitude (or depth) is processed later than the direction information during reaching preparation (Fu et al., 1995; Messier and Kalaska, 2000; Hadjidimitrakis et al., 2014a; Davare et al., 2015). The different findings identified here in depth and direction at two levels of behavioral investigation (reach errors and movement variability) are in agreement with both of these views. In particular, the majority of the participants changed coordinate system from mixed in direction to space-centered in depth. As the mixed encoding represents not a final stage of coordinate transformations,

but is important to support non linear computations required by these (Pouget and Snyder, 2000; Blohm, 2012), our data support the idea of a later processing of depth information with respect to the direction.

The differences found in the variability distribution and the consistency of these results across participants also suggest that, despite the presence of the same sensory and motor information in our reaching task, the eye/target configurations and the space dimensions strongly influence the control of movement. That indicates common trajectory strategies that go beyond the individual reaching behavior.

Studies of coordinate systems based on hand and target position demonstrated a correlation between the movement control and the coordinate system used. They have described that the brain extracts estimates of target and hand positions from a visual scene, calculates a difference vector between them, and uses this signal to compute the required motor commands (Cisek et al., 1998). Given that online motor corrections respond to changing visual information at time lags in the range of 100-120 ms (Day and Lyon, 2000; Franklin and Wolpert, 2008; Reichenbach et al., 2014), these computations have to be executed very quickly. In the present study, we can argue that to compensate the differences in movement variability, a mixed encoding was suitable to allow for fast non linear computations that are required for direction processing in order to quickly update the spatial coordinates of the upcoming movement. In depth, we found a space-centered representation and a more homogeneous distribution of variability along movement execution in eye-centered and space-centered coordinates. What we found may suggest that the reaching plans did not require modifications across eye/target configurations and a space-centered coordinate system provided a more stable encoding mechanism (Medendorp and Crawford, 2002). However, future studies must be addressed to clarify these aspects and to study directly the relationship between coordinate system and motor control.

4.5.1 Comparison with other studies of reaching in depth

In several studies, it was found that subjects did not use a stable non-retinal spatial mechanism to guide the arm movement but an eye-centered spatial mechanism, which is updated across eye movements for near and far space (Bock, 1986; Enright, 1995; Henriques et al., 1998; Lewald and Ehrenstein, 2000; Medendorp and Crawford, 2002). Medendorp et al. (Medendorp and Crawford, 2002) investigated only reaching towards

targets located on a central straight line with respect to subjects' body and at eye level. The investigation of reaching target representation located at different depth and directions with respect to the body's midline was introduced by Van Pelt et al. (Van Pelt and Medendorp, 2008). They found that depth and direction are coded in a pure eye-centered coordinate system. In this study, the targets were presented in a horizontal plane at eye level, hence the reaching movements were from bottom to top (anti-gravity movements). In the present study, we found results that differ from those described above. These differences might originate from the different task conditions. In fact, we demonstrated that reach errors in direction mainly followed both eye-centered and space-centered representations and reach errors in depth were mainly characterized by representation shifted towards space-centered encoding. In our experiment, reaching movements were parallel to the touchscreen placed horizontally on the desk and the reaching movements were tested for targets located in the lower part of working space. This region of space is where most of the primate motor behavior takes place (Previc, 1998). Our setup was similar to natural conditions but more complex because the encoding of reaching targets not only requires an update of vergence signal but also an integration of vergence, elevation signals of the eyes and egocentric distance representation of the target. The discrepancy between the present work and the previous one may be caused by all these reasons.

4.5.2 Conclusion

This study shows that when eye and hand are dissociated in depth and direction, the behavioral encoding of target positions is based on both eye-centered and space-centered representations. Interestingly, when we consider changes along depth dimension, the influence of space-centered representation becomes higher than the influence of changes in direction. This different balance of space encoding mechanisms represents a suitable method used by the brain to adapt to the possible perturbations that can occur during the movement and provides the motor system with necessary information to accurately correct the movement. The variability distribution along the movement execution was influenced by the eye/target configurations as well as by depth and direction suggesting that subjects adopted different strategies accordingly to movement geometries and task demands. Finally, our behavioral results support the hypothesis that the brain needs the conjunct contribution of multiple coordinate systems

to efficiently compensate the variety of corrections required by the complex metrics of reaching movements executed to targets located at different depths and directions.

5. Reaching in 3D space, effects of brain lesions in the posterior parietal cortex

A similar version of this manuscript is currently in preparation for submission:

Valentina Piserchia, Annalisa Bosco and Patrizia Fattori. *Reaching in 3D space, effects of brain lesions in the posterior parietal cortex.*

5.1 Abstract

The accuracy of reaching movements towards visual targets can be affected by lesions of the posterior parietal cortex (PPC), like those that are observed in optic ataxia (OA). Here we report the case of a patient (C.O.) with right posterior parietal lobe damage caused by a surgery due to a tumor, who after the lesion showed impairments in reaching a target that was not foveated, typical of an optic ataxia behavior. The aim of this work was to analyze trajectories and reaching errors to assess the reaching accuracy of the patient with respect to the controls. By manipulating gaze position and hand position of visual reaching targets we investigated how reaching in peripheral and central viewing conditions influenced the trajectories and the reach errors of the patient and controls subjects. The results showed that the initial part of the trajectories of the patient followed the same path of that of the controls, this suggests that they both have a similar planning of the movement; in the last part instead, the patient failed to make adjustments of the trajectory contrary to the controls, indicating an on-line control deficit of the action (especially in the peripheral viewing conditions, where eye and hand are dissociated). When we evaluated the reach errors in depth and in direction, the results showed that the performance of the patient was significantly different from that of the controls both when reaching targets were placed at different depths and both when reaching targets were placed at different directions: the patient undershooting them especially in the peripheral viewing conditions, where eye and hand are dissociated. In the light of our knowledge about OA, we suggest that also the reaching inaccuracies observed in particular in the configurations where the gaze and reach direction differ can be explained by the lack of the “automatic pilot” which is able to adjust in healthy subjects the predefined motor plan.

The analysis of the reaching responses of the patient firstly can contribute to find the strategy in which the movements are executed and targets are approached. Secondly, OA patients are an ideal sample to study the role the dorsal stream has in eye-hand coordination during reaching in 3D, when gaze and hand direction are dissociated.

5.2 Introduction

The accuracy of reaching movements towards visual targets can be affected by lesions of the posterior parietal cortex (PPC), like those that are observed in optic ataxia (OA). OA, initially described as a component of Balint's syndrome (Balint, 1909), is a high-order disorder that occurs with unilateral (Perenin and Vighetto, 1988; Karnath and Perenin, 2005) or bilateral PPC lesion (Pisella et al., 2000, 2004; Karnath and Perenin, 2005; Khan et al., 2005); the typical sites of the lesion involve the parietal occipital junction (POJ), the superior parietal lobule (SPL) and areas around the intra parietal sulcus (IPS) (Karnath and Perenin, 2005; Martin, Karnath, Himmelbach, 2015).

Impairments in reaching have been observed both in humans (Balint 1909; Holmes, 1914; Perenin and Vighetto, 1988) and in primates model of OA (Battaglia-Mayer et al., 2012; Hwang et al., 2012).

Patients exhibit misreaching errors when directing a limb in peripheral space towards targets that are not foveated (non foveal OA) and most often make errors in the direction of their gaze (Buxbaum and Coslett, 1997); in a less usual form of the deficit (foveal OA) patients misreach targets even when they are directly foveated (Pisella et al., 2000). Performance is typically worse with the hand contralateral to the lesion and in the visual field contralateral to the lesion (Khan et al, 2007; Blangero et al., 2008). Nevertheless, it has been found that memorized visual information improves pointing and grasping movements when the movement onset is postponed around 5 seconds after target presentation (Milner et al., 2001, 2003; Rossetti et al., 2005; Himmelbach and Karnath, 2005). These results are explained with the fact that OA patients have the dorsal stream damaged but the ventral stream is intact and the ventral stream is slower than the dorsal so a delay is necessary to switch to this mode and the result is that the performance of the patients is better when the ventral stream takes control (Milner et al., 1999; Rossetti and Pisella, 2002).

Optic ataxia, as originally observed by Balint (1909) is modality specific: patients exhibit misreaching errors towards visual stimuli but not to auditory or tactile stimuli

(Rossetti et al., 2003) and this suggests that OA could be the result of a deficit in coupling vision and action. Patients are able to recognize objects but not their spatial relationships more in depth than in direction (Holmes and Horrax, 1919; Brain, 1941; Perenin and Vighetto, 1988; Dankert et al., 2009; Cavina-Pratesi et al., 2010). In the experiment by Dankert and colleagues (2009), three targets were positioned one after the other in the sagittal plane in one condition and in the frontoparallel plane in another condition. The subjects were required to reach to the foveated targets in sequence. The hand starting position was placed either next to the body or far from it. The eyes were free to move. The authors found that the movements executed in the sagittal axis were more disordered than movements executed in the frontoparallel plane. The study by Cavina-Pratesi and colleagues (2010) explored the role of depth during reaching performance. The authors investigated the performance of an OA patient, manipulating the position of the target either far from the starting hand position or close to it. The patient had to reach or grasp objects of different size placed close or far from the body while always fixating a central fixation cross. The errors in reaching were present only when reaching for objects presented at the far distance.

The evidence that suggested impaired movement control in the sagittal plane favored the interpretation of OA as a visuomotor deficit (Perenin and Vighetto, 1988). Recent studies provided other interpretations of this deficit (Pisella et al., 2000; Khan et al., 2013). Pisella and colleagues proposed that OA is an online control deficit; they found that patients fail to make corrections when the target is unexpectedly displaced (Pisella et al., 2000). In their experiment both healthy participants and the patient were able to point correctly to a target when it was still, but when the target was unexpectedly displaced the healthy participants were able to adjust while the patient could not. An alternative hypothesis was provided by other authors who interpreted OA as a coordinate frames transformation deficit (Jax et al., 2009; Khan et al., 2013). Several authors found that reaching errors are caused by the disruption of different reference frames accordingly to the type of task employed: gaze-centered (Khan et al., 2005; Jax et al., 2009), head-centered (Frassinetti et al., 2007; Jax et al., 2009).

Here we report the case of a patient (C.O.) with right posterior parietal lobe damage caused by a surgery due to a tumor, who after the lesion showed impairments in reaching a target that was not foveated, typical of an optic ataxia behavior.

The aim of this work is to analyze trajectories and reaching errors to assess the reaching accuracy of the patient with respect to the controls and to study the effect of depth and

direction signals on the trajectories of the reaching movement. By manipulating gaze position and hand position (Dankert et al., 2009; Cavina-Pratesi et al., 2010) of visual reaching targets we investigated how reaching in peripheral and central viewing conditions influence the trajectories and reach errors of the patient and controls subjects. We used a visually guided reaching task and employed different configurations of gaze and hand relative position in depth and direction so to test all possible conditions of dissociation of visual target and reaching target, given that OA patient show impairments in reaching in peripheral viewing conditions. In addition, the task design maximizes natural reaching conditions where objects are reached on a horizontal surface and at a comfortable distance.

The analysis of the reaching responses of the patient firstly can contribute to find the strategy in which the movements are executed and targets are approached; secondly, OA patients are an ideal sample to study the role the dorsal stream has in eye-hand coordination during reaching in 3D, when gaze and hand direction are dissociated.

5.3 Materials and Methods

5.3.1 Participants

We tested one patient, C.O., with right unilateral OA. C.O. is a left-handed 61 years old woman (Laterality Quotient: -30), as assessed by the Edinburgh Handedness Inventory (Oldfield, 1971), with right posterior parietal lobe damage caused by a surgery due to a tumor.

Five left-handed control subjects (Mean Laterality Quotient: -76; *SD* 16.2), as assessed by the Edinburgh Handedness Inventory (Oldfield, 1971), also took part in this study (Age range: 42-56; Mean age 49; *SD* 4.81; 4 female). They all had normal, or corrected to normal, vision. The subjects had no history of musculoskeletal or neurological disorders. This study was carried out in accordance with the recommendations of Bioethical Committee of the University of Bologna and in accordance with the Declaration of Helsinki. All participants gave written informed consent.

5.3.2 Case history and neuropsychological assessment

C.O. is a 61 years old left handed woman with eight years of education. Fifteen months before the testing session she was admitted to the hospital and a MRI scan revealed the presence of an intracranial lesion surrounded by peripheral edema in the right parietal-occipital cortex. She was diagnosed with cerebral abscess and was subjected to removal of right parietal-occipital abscess. Lesion extent can be seen in the MRI images in Fig. 5-1. Subsequently C.O., nine months before the testing session, was subjected to a neuropsychological examination to evaluate specific cognitive functions such as attention (Computerized test of the Italian version of the Test of Attentional Performance: Zimmerman and Fimm, 1992; Zoccolotti et al., 1994; Attentive Matrices test: Spinnler and Tognoni, 1987; Stroop test: Golden, 1978; Venturini e coll., 1983; Caffarra et al., 2002) executive functions (Tower of London: Culbertson and Zillmer, 2005; Phonemic and Semantic Verbal Fluency Test: Spinnler and Tognoni, 1987), long term and short term verbal memory (Buschke and Fuld Test: Buschke and Fuld, 1974; Spinnler and Tognoni, 1987, Digit Span: Orsini et al., 1987; Prose memory test: Spinnler and Tognoni, 1987), spatial memory (Rey and Osterrieth Complex Figure Test: Caffarra, Vezzadini, Dieci, Zonato, and Venneri, 2014; Osterrieth, 1944; Corsi-Block tapping test: Spinnler and Tognoni, 1987) working memory (computerized sub-test “Working Memory” of the Italian version of the Test of Attentional Performance: Zimmerman and Fimm, 1992; Zoccolotti et al., 1994), logical and reasoning abilities (Raven's Progressive Matrices: Spinnler and Tognoni, 1987), spatial visual attention (Line cancellation test: Albert 1973; The Single Letter Cancellation Test (SLCT): Diller et al., 1974; The bells test: Gauthier et al., 1989; Line bisection test: Milner et al., 1993). Attention analysis highlighted split attention skills and selective focus; the memory tests showed good performance in all the components investigated. The evaluation of executive functions documented good skills in planning strategies for complex problem solving. Logical-deductive reasoning abilities were comparable to the performance of healthy subjects. There was no evidence of constructional apraxia. The visual space spatial evaluation showed standard performance in all tests administered. Overall the neuropsychological examination documented a general normal cognitive framework showing standard performance in all test administered. In addition, no visual extinction or even tactile extinction was found (Visual Extinction Test and Tactile Extinction Test).

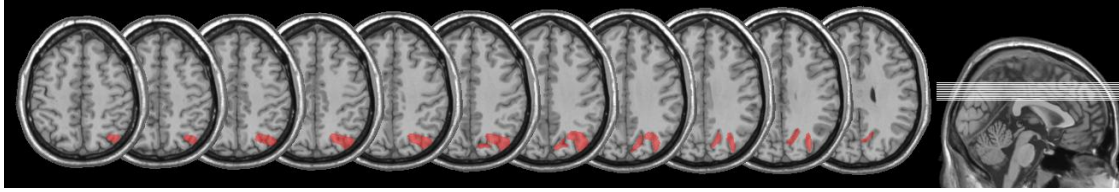


Figure 5-1. Site of the lesion of the patient in the right parietal-occipital cortex. Lesion reconstruction images from MRI scans, projected onto the normalized MRI template for patients with left hemisphere lesions and right hemisphere lesions. Mapping of brain lesion was performed using MRICron (Rorden et al., 2007; Rorden and Brett, 2000). Lesions documented by the most recent clinical MRI were traced onto the T1-weighted MRI template from the Montreal Neurological Institute provided with MRICron software (Rorden et al., 2007; Rorden and Brett, 2000).

5.3.3 Apparatus and Stimuli

The starting position of the hand (dominant left hand) was on a board placed adjacent to the touch screen at the level of the sternum, as sketched in Figs. 5-2A and B. Reaching movements were performed in a darkened room. The head of the participants was supported on a chin rest in order to prevent head movements. The stimuli were green (diameter 0.3 cm) and red dots (diameter 1.2 cm) presented at different depths and in different directions with respect to subject's midline. The stimuli presented a luminance of ~ 17 cd/m². Stimuli were presented on 19-in touchscreen laid horizontally on a desk located at waist level (ELO IntelliTouch 1939L) with a visible display size of 37.5 x 30 cm and 15,500 touch points/cm². The display had a resolution of 1152 x 864 pixels and a frame rate of 60 Hz.

The reaching movements were recorded using a motion tracking system (VICON[®]) by sampling the position of two markers at a frequency of 100 Hz; markers were attached to the wrist (on the scaphoid bone) and on the tip (nail of the index finger (reaching finger)). Participants were asked to reach and to point with the index finger toward one of the nine targets presented and to execute reaching movements as accurate as possible at a fast but comfortable speed. Endpoints were recorded through the touch screen.

During the task, fixation was monitored on-line by a second experimenter on all trials. In addition eye position was recorded using a Pan/Tilt optic eye-tracker (Eye-

Track ASL-6000) recording real- time gaze position at 60 Hz. The subject's dominant eye was illuminated by invisible infrared light, and the reflections were recorded by a video camera positioned 64 cm from the eye. The elevation distance between the eyes of subjects and the touchscreen was 27 cm. Before collecting data from each subject, the equipment was calibrated using a nine-point grid. Subjects were asked to fixate successively on each of a series of small dots arranged on three lines in the form of a square (23x23 cm).

5.3.4 Behavioral Paradigm

Participants performed reaching movements on a desk where the touch screen was positioned (see "Apparatus and Stimuli" Section and Fig. 5-2A) using their left (dominant) hand. Fig. 5-2A shows the target positions located comfortably with respect to subject's body. As depicted in Fig. 5-2B, there were 9 possible locations in which targets could appear: three placed at near distance (18.5 cm from the chest), three at intermediate distance (30 cm from the chest), and three at far distance (41.5 cm from the chest). The targets were arranged in a square of 23x23 cm, and were located 11.5 cm apart each, either on the left or the right side, the central targets were placed along the sagittal midline. All of the targets were located at comfortable reaching distance.

We tested the subjects in a visually guided reaching task as it is reported in Fig. 5-2D. The task was composed of three possible configurations: the constant gaze configuration, sketched in Fig. 5-2C, in which the eye fixated a central fixation target and the hand reached to one of the peripheral reaching targets (thus the reaching target was on the fovea only when presented at the same central location of the fixating target and on the periphery of the retina for the other eight possible locations); the constant reach configuration in which the eyes fixated one of the peripheral targets and the hand reached always the central target; and foveal reach configuration in which the fixation target and the reaching target were coincident. The constant reach and the constant gaze configuration were extrafoveal configurations in which the position of the fixation point was dissociated from the position of the reaching targets. The foveal reach configuration instead was a configuration in which the position of the fixation point coincided with the position of the reaching target. These three configurations, where eye and hand were coupled (foveal reach configuration) or decoupled (constant gaze and constant reach configurations), enabled us to define the contribution of depth and direction during

reaching in 3D space, as done in neurophysiological (Bosco et al., 2016) and in psychophysical experiments (Bosco et al., 2017).

The time sequence of the task was as follows: a fixation point (green LED, diameter 0.3 cm) appeared. The fixation target stayed on for 1.5 s and then the reaching target (red LED, diameter 1.2 cm) was turned on. As soon as the reaching target appeared, an acoustic cue indicated to the subject to reach with the hand the position of the red-reaching target while maintaining fixation on the green-fixation target. The fixation target and the reaching target lasted until the subject completed the movement (Fig. 5-2D). The task was composed of 5 blocks, each block with 27 trials. Within each block, trials of the three configurations were randomized. For stimuli presentation and data analysis, we used MATLAB with the Psychophysics toolbox extension (Brainard, 1997).

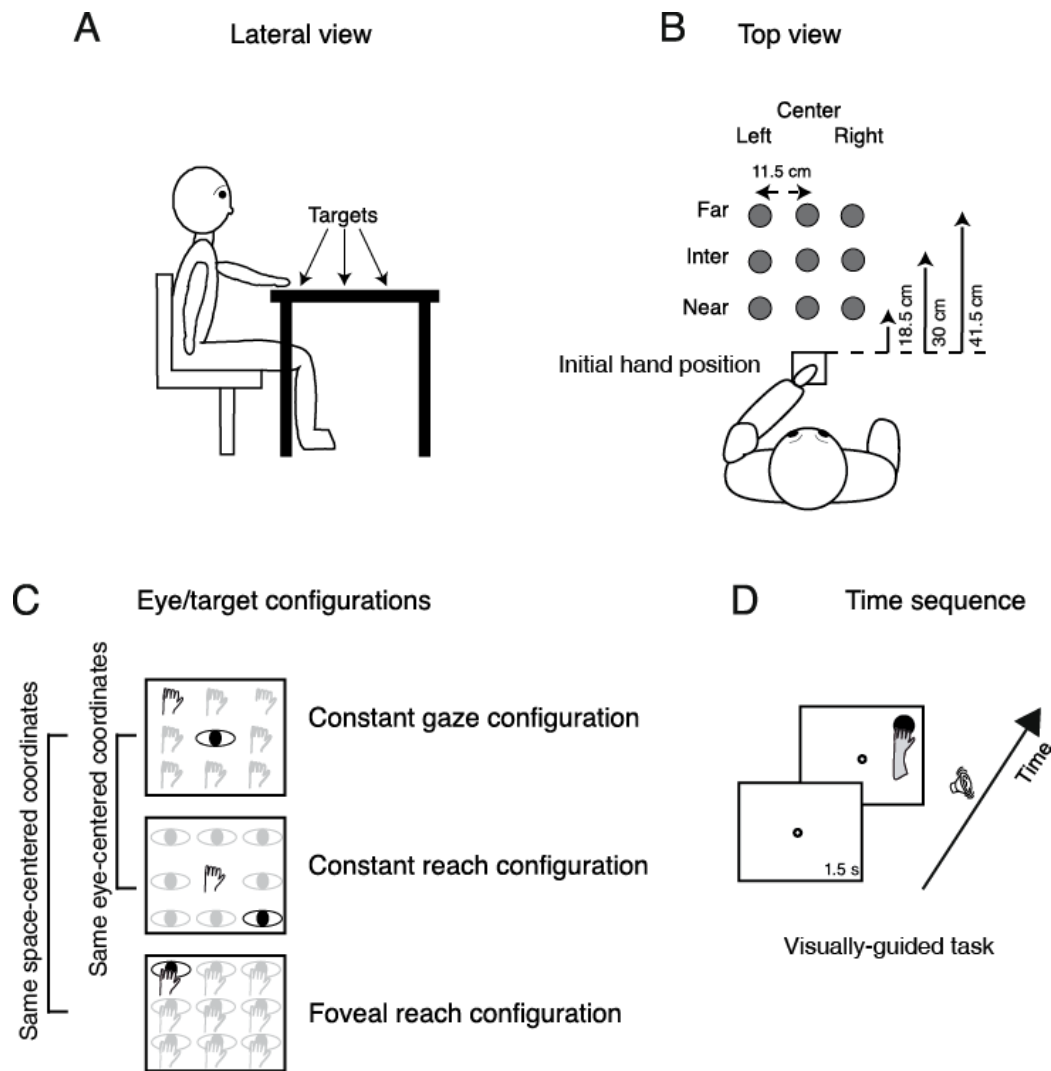


Figure 5-2. Experimental setup. A) Lateral view of the target arrangement with respect to subject's body. B) Top view of the target arrangement in the peripersonal space. The subjects performed reaching movements with their right hand towards one of the nine LEDs targets located at different depths (far, intermediate and near) and in different directions (left, center and right), grey dots. Reaching movements were performed in a darkened room from an initial hand position located next to the body. C) Top view of the three task configurations: the constant gaze configuration in which the eye fixated a central fixation target and the hand reached to one of the peripheral reaching targets (thus the reaching target was on the fovea only when presented at the same central location of the fixating target and on the periphery of the retina for the other eight possible locations); the constant reach configuration in which the eyes fixated one of the peripheral targets and the hand reached always the central target; and foveal reach configuration in which the fixation target and the reaching target were coincident. D) Example of the time sequence of the reaching task in the constant gaze configuration. The small white dot represents the fixation target; the filled black dot represents the reaching target. The fixation target (a green LED) stayed on for 1.5 sec and then the reaching target (a red LED) was

turned on in one of the nine locations. As soon as the reaching target appeared, a sound indicated to the subject to reach with his/her left hand the position of the target while maintaining fixation on the fixation target. The fixation and reaching targets lasted until the subject completed the movement.

5.3.5 Data Analysis

After recordings, data positions were interpolated at 1000 Hz and were run through a fifth-order Butterworth low-pass filter (cutoff frequency, 30 Hz, (Bosco et al., 2015b)). For data processing and analysis, we wrote custom software in Matlab (The Mathworks) to compute velocity profiles of markers. Onset of movement was detected from wrist velocity when it remained above 5 mm/s for 200 ms; offset was calculated when wrist velocity remained below 5 mm/s for 200 ms.

To study the accuracy of movements at the beginning and at the end of the trial, we measured two-dimensional reach endpoints and analyzed the horizontal (direction) and vertical (depth) dimensions of reach errors calculated by subtracting the respective horizontal and vertical coordinates of physical target location from the reach endpoint in that trial. The spatial parameters of the reaching movements (x and y coordinates) were obtained by averaging the coordinates of the index marker position for each trial.

To study the trajectories of movements during the first half and last half of the trajectory and to quantify how motor responses of participants were stereotyped we calculated the distance of the first half and last half of the trajectory with an ideal (virtual) straight trajectory. The virtual straight trajectory was defined as the line connecting the starting position of the hand and the reaching target position (similar approach in: Kasuga et al., 2015).

The smaller was the distance of the real trajectory of movement from the ideal straight trajectory and the more stereotyped and with smaller corrections was the movement execution. We compared the mean deviations of the first half and the last half of the trajectory of the patient with those of the controls by a Two-sample t-test in the three configurations (constant gaze, constant reach and foveal reach configurations).

Additionally, to obtain a global and statistical assessment of the accuracy of movements we performed a linear regression analysis among the reach errors, in depth and in

direction, of the patient with those of the controls and tested the significant linear fitting by the R-squared value (R^2).

The patient's performance (hand trajectories and reach errors) was compared to the controls' with a Two-sample t-test. For all statistical analyses, the significance criterion was set to $p < 0.05$. To check whether the trajectories were influenced by an interaction of depth and direction dimensions we performed two separate two-way ANOVAs for the patient and for the controls: as main factors the different depths (far, intermediate and near) and the different directions (right, left); to test when the interaction was significant we employed a Bonferroni *post hoc* test.

To have a representation of the correlation of the reach errors and the deviations of the first part and last part of the trajectory of the patient and the controls we plotted the reach errors against the deviation and we computed confidence ellipses (for the patient and for the controls) whose area describe the smallest ellipse that covers 95% of the data.

We excluded from the statistical analyses the central position of constant gaze, constant reach and foveal reach configurations given that it is the same in the three configurations.

5.4 Results

We employed a visually guided reaching task with nine target locations that subjects had to reach for, with different combinations of eye and hand position (Fig. 5-2C), for a total of 27 types of trials. Reaching targets were located on a table arranged at a comfortable distance from the subjects' body that allowed a natural interaction with targets.

5.4.1 Analysis of the trajectories

In Figure 5-3 it is plotted the top view of the trajectories of the patient C.O. and of an exemplary control subject (C.N.) in the three configurations. The qualitative analysis of the trajectories showed that the patient executed the movement in a more disordered and less precise manner with respect to the control. Messier and Kalaska (1999) showed that in healthy subjects the hand trajectories for movements aimed at targets placed in five different directions and distances exhibited straight movement pattern.

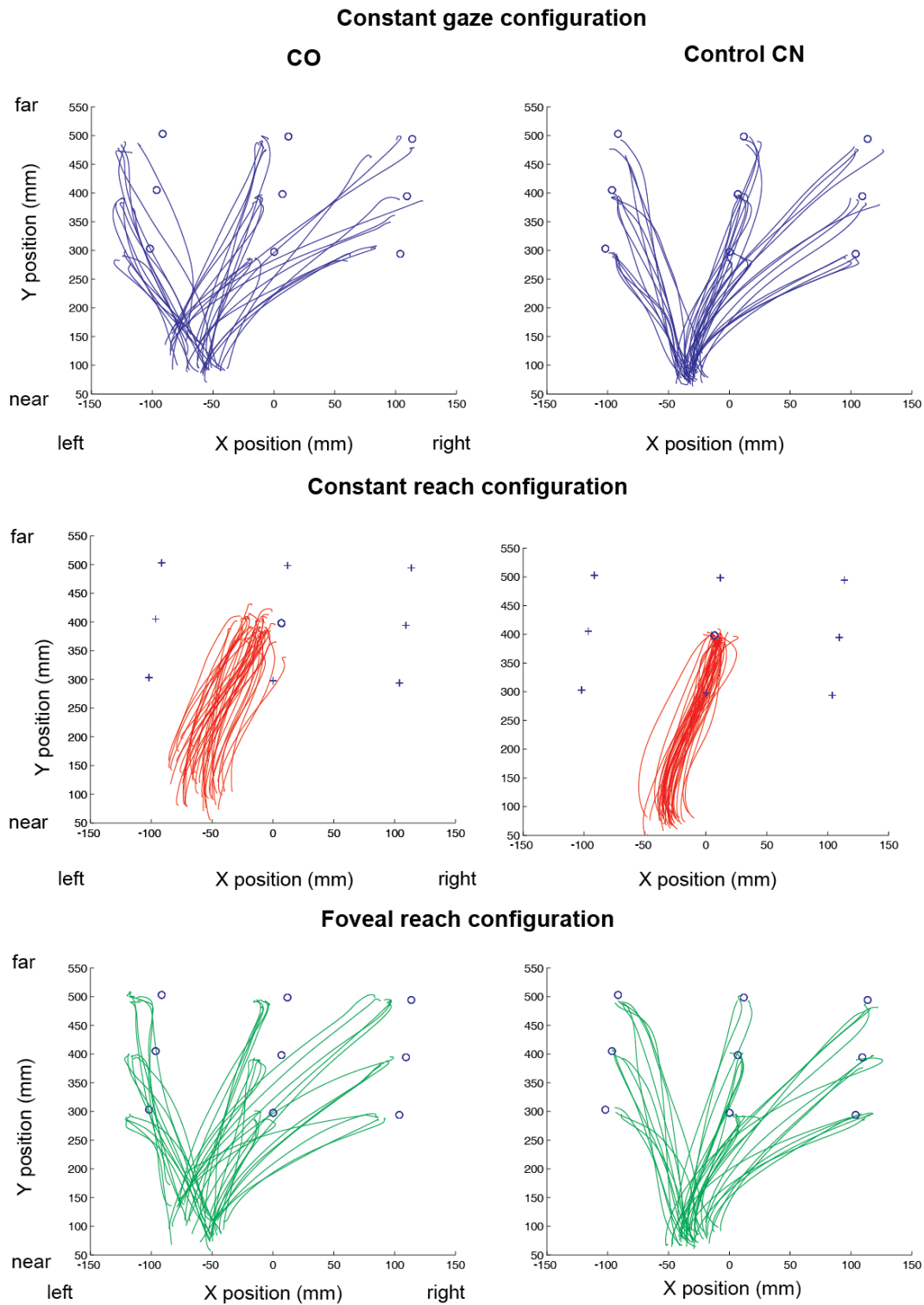


Figure 5-3. Example of hand trajectories. The panels on the left represent the top view of the trajectories of the patient (C.O.) using the left hand, in the constant gaze configuration (above panel), in the constant reach configuration (middle panel) and in the foveal reach configuration (bottom panel). The panels on the right represent the top view of the trajectories of the exemplary control (C.N.) using the left hand, in the constant gaze configuration (above panel), in the constant reach configuration (middle panel) and in the foveal reach configuration (bottom

panel). The empty dots in each diagram represent the reaching targets; the crosses depicted in the middle left and right panels represent the fixations targets; the lines depict single trajectories in all trials. On the x axis (direction) negative values represent the left side, positive values the right side; on the y axis (depth) 50 is near to the participant and 550 is far.

Therefore, to quantify the differences among the trajectories of the patient and those of the controls and to quantify how motor responses of participants were stereotyped, we calculated the deviation of the trajectories executed in each configuration from the straight-ideal trajectory. We calculated the distance of the first half and last half of the trajectory with an ideal (virtual) straight trajectory (Fig. 5-4). The virtual straight trajectory was defined as the line connecting the starting position of the hand to the position of the target (similar approach in: Kasuga et al., 2015).

We found that the deviations (mean of the deviations towards all targets) of the patient C.O. were higher than those of the controls in the constant reach (mean deviation C.O. - 11.07 mm; SE 1.6; mean deviation controls -9.03 mm; SE: 1.77) and foveal reach configuration (mean deviation C.O. -7.91 mm; SE: 5.37; mean deviation controls -6.07 mm; SE: 5.3) and smaller in the constant gaze (mean deviation C.O. -7.23 mm; SE: 3.34; mean deviation controls -9.23 mm; SE: 7.95). The patient's hand trajectories were compared to the controls' with a Two-sample t-test. In the first half of the trajectory (see left panels of Fig. 5-4 and Table 5-1) there were no significant differences ($p > 0.05$) in the mean deviation of the trajectories from the ideal straight trajectory in the constant gaze, constant reach and foveal reach configuration. Both the patient and the controls in the first half of the trajectory exhibit a deviation from the ideal trajectory on the left of it. In the last half of the trajectory (see right panels of Fig. 5-4 and Table 5-1), in the constant gaze configuration, the mean deviation of the patient C.O. (mean deviation: 6.7 mm; SE: 16.01) was significantly different from that of the controls (mean deviation: 4.42 mm; SE: 7.98), ($p < 0.001$); in the constant reach the mean deviation of the patient (mean deviation: -8.29 mm; SE: 6.8) was significantly different from that of the controls mean (deviation controls: 2.92 mm; SE: 3.73) ($p < 0.001$); and in the foveal reach configuration the mean deviation of the patient (mean deviation: 1.37 mm; SE: 5.69) was significantly different from that of the controls (mean deviation: 9.26 mm; SE: 8.24) ($p = 0.01$). In the constant gaze and constant reach configuration the patient continued to deviate on the left of the ideal trajectory while the controls corrected their

initial trajectory and deviated on the right of the ideal one. In the foveal reach configuration instead also the patient deviated on the right of the ideal trajectory. This might be due to the fact that in the configurations where eye and hand were decoupled (constant gaze and constant reach) the patient continued to deviate her trajectory without being able to adjust the initial movement, in the configuration where the target was foveated she was able to correct her behavior in the same direction of healthy participants although significantly less.

Deviation of the first and last half of the trajectories
(mean of all targets) with respect to the ideal trajectory

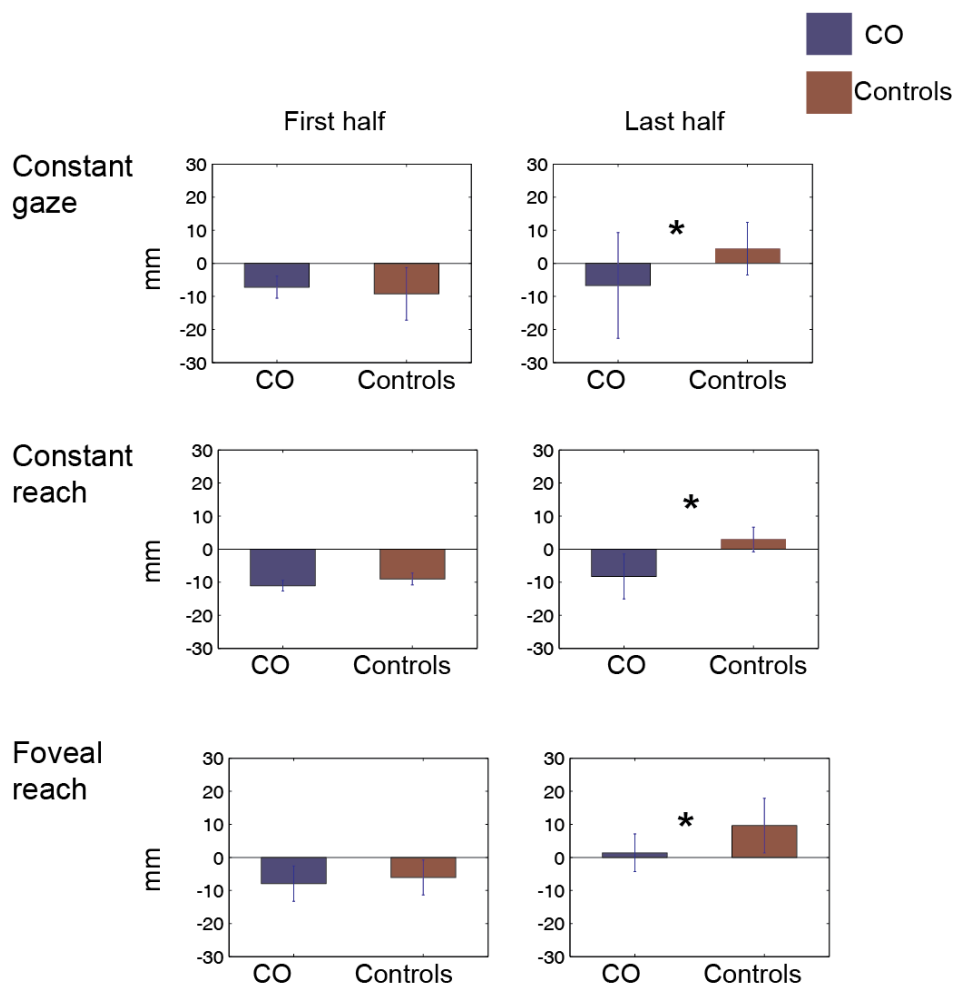


Figure 5-4. Deviation of the first and last half of the trajectories with respect to the ideal trajectory in the constant gaze (above panels), constant reach (middle panels) and foveal reach (bottom panels) configurations. Each bar represent the mean value of the deviations of the trajectories towards all the targets. Negative values mean that the deviation of the trajectory was

on the left with respect to the ideal trajectory, positive values mean that the deviation of the trajectory was on the right with respect to the ideal trajectory. The asterisks represent the comparison which reached significance ($p < 0.05$).

| Table 5-1 | Deviation (mm) of the first half of the trajectory (<i>SE</i>) | | Deviation (mm) of the last half of the trajectory (<i>SE</i>) | |
|------------------|--|--------------|---|-------------|
| | C.O. | Controls | C.O. | Controls |
| Constant gaze | -7.23 (3.34) | -9.23 (7.95) | -6.7 (16.01) | 4.42 (7.98) |
| Constant reach | -11.07 (1.6) | -9.03 (1.77) | -8.29 (6.8) | 2.92 (3.73) |
| Foveal reach | -7.91 (5.37) | -6.07 (5.3) | 1.37 (5.69) | 9.26 (8.24) |

Table 5-1. Mean values (mm) and *SE* of the deviations of the trajectories with respect to the ideal one, towards all the targets in the constant gaze, constant reach and foveal reach configurations. Negative values mean that the deviation of the trajectory was on the left with respect to the ideal trajectory, positive values mean that the deviation of the trajectory was on the right with respect to the ideal trajectory.

To better analyze how this behavior could be influenced by depth and direction dimensions, we plotted the same deviations dividing the data in deviations from the ideal trajectory to targets at near, intermediate and far distance (depth) (Fig. 5-5) and deviations from the ideal trajectory to targets on the left and on the right (direction) (Fig. 5-6).

As far as the analysis of the deviations from the ideal trajectory of the trajectories towards targets placed at different depths is concerned, we found that in each configuration (constant gaze, constant reach and foveal reach) in the first half of the trajectories there were no significant differences ($p > 0.05$) in the mean deviation of the trajectories from the ideal straight trajectory of the patient with respect to the controls both for targets placed at near, intermediate and far distance (see left panels of Fig. 5-5 and Table 5-2). In the first half of the trajectory both the patient and the controls deviated always on the left from the ideal trajectory. In the last half of the trajectory instead, in the constant gaze configuration for targets placed near, the mean deviation of the patient (mean deviation: -12.1 mm; *SE*: 6.8) was significantly different from that of the controls (mean deviation: 7.09 mm; *SE*: 5.5) ($p = 0.002$) and for targets placed at far

distance the mean deviation of the patient (mean deviation: -5.07 mm; *SE*: 16.2) was significantly different from that of the controls (mean deviation: 3.45 mm; *SE*: 7.2) ($p=0.02$); in the constant reach configuration for targets placed near the mean deviation of the patient (mean deviation: -10.08 mm; *SE*: 6.23) was significantly different from that of the controls (mean deviation: 5.16 mm; *SE*: 2.09) ($p<0.001$) and for targets placed at far distance the mean deviation of the patient (mean deviation: -7.39 mm; *SE*: 4.95) was significantly different from that of the controls (mean deviation: 2.2 mm; *SE*: 2.43) ($p=0.007$); in the foveal reach configuration for targets placed near the mean deviation of the patient (mean deviation: -2.09 mm; *SE*: 8.99) was significantly different from that of the controls (mean deviation: 11.49 mm; *SE*: 7.48) ($p=0.02$) and for targets placed at far distance the mean deviation of the patient (mean deviation: -6.12 mm; *SE*: 5.71) was significantly different from that of the controls (mean deviation: 8.77 mm; *SE*: 4.51) ($p=0.002$). No significant differences ($p>0.05$) were found among the patient and the controls in the deviations of the trajectories to targets placed at intermediate distance, in the three configurations. In the constant gaze, constant reach and foveal reach configuration the patient deviated always on the left of the ideal trajectory while the controls corrected their initial trajectory and deviated on the right of the ideal one. This might be due to the fact that the patient continued to deviate her trajectory without being able to correct the initial movement plan.

Deviation of the first and last half of the trajectories (to targets placed at different depths) with respect to the ideal trajectory

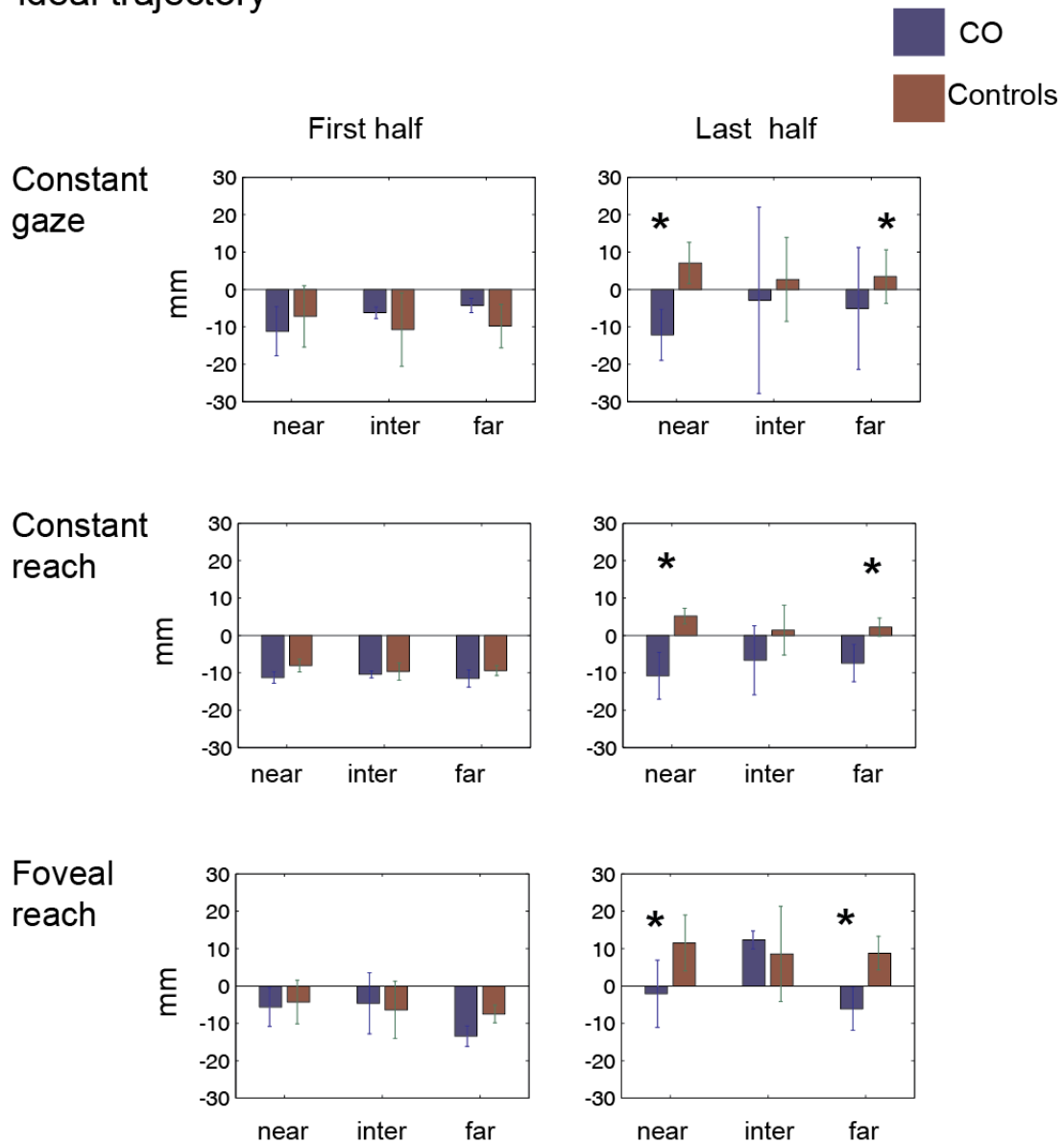


Figure 5-5. Mean deviations (mm) of the first and last half of the trajectories, towards targets placed at different depths (far, intermediate, near), with respect to the ideal trajectory in the constant gaze (above panels), constant reach (middle panels) and foveal reach (bottom panels) configurations. Each bar represent the mean value of the deviations of the trajectories towards targets placed at different depths (far, intermediate, near). Negative values mean that the deviation of the trajectory was on the left with respect to the ideal trajectory, positive values mean that the deviation of the trajectory was on the right with respect to the ideal trajectory. The asterisks represent the comparison which reached significance ($p < 0.05$).

| Table 5-2 | Deviation (mm) | | Deviation (mm) | | Deviation (mm) | | Deviation (mm) | | Deviation (mm) | | Deviation (mm) | |
|----------------|----------------------------|-----------------|----------------------------|-----------------|----------------------------|-----------------|---------------------------|-----------------|---------------------------|----------------|---------------------------|----------------|
| | First half trajectory (SE) | | First half trajectory (SE) | | First half trajectory (SE) | | Last half trajectory (SE) | | Last half trajectory (SE) | | Last half trajectory (SE) | |
| | near | | inter | | far | | near | | inter | | far | |
| | C.O. | Controls | C.O. | Controls | C.O. | Controls | C.O. | Controls | C.O. | Controls | C.O. | Controls |
| Constant gaze | -11.2 (6.5) | -7.19 (8.2) | -6.24 (1.5) | -10.72 (9.8) | -4.26 (1.9) | -9.79 (5.8) | -12.1 (6.8) | 7.09 (5.5) | -2.9 (24.9) | 2.71 (11.2) | -5.07 (16.2) | 3.45 (7.2) |
| Constant reach | -11.2 (1.5) | -8.05 (1.69) | -10.4 (0.95) | -9.64 (2.28) | -11.5 (2.29) | -9.39 (1.35) | -10.8 (6.23) | 5.16 (2.09) | -6.67 (9.22) | 1.39 (6.66) | -7.39 (4.95) | 2.2 (2.43) |
| Foveal reach | -5.65 (5.1) | -4.3 (5.85) | -4.66 (8.17) | -6.4 (7.65) | -13.4 (2.74) | -7.5 (2.39) | -2.09 (8.99) | 11.49 (7.48) | 12.34 (2.38) | 8.55 (12.7) | -6.12 (5.71) | 8.77 (4.51) |

Table 5-2. Mean values of the deviations (mm) and *SE* of the trajectories with respect to the ideal one, towards targets placed at different depths (near, intermediate and far) in the constant gaze, constant reach and foveal reach configurations. Negative values mean that the deviation of the trajectory was on the left with respect to the ideal trajectory, positive values mean that the deviation of the trajectory was on the right with respect to the ideal trajectory.

As far as the analysis of the deviations from the ideal trajectory of the trajectories towards targets placed at different directions is concerned, (see left panels of Fig. 5-6 and Table 5-3) in the first half of the trajectory we found that in the constant gaze configuration the deviation of trajectory of the patient (mean deviation: -11.2 mm; *SE*: 6.1) was significantly different from that of the controls (mean deviation: -22.3 mm; *SE*: 0.46) ($p=0.03$) for targets placed on the left, instead no significant differences ($p>0.05$) were found among the patient and the controls in the deviations of the trajectories to targets placed on the right; in the first half of the trajectories in the constant reach and foveal reach there were no significant differences ($p>0.05$) in the mean deviation of the trajectories from the ideal straight trajectory of the patient with respect to the controls both for targets placed on the left and on the right (see left panels of Fig. 5-7 and Table 5-4). In the last half of the trajectory, in the constant gaze configuration for targets placed on the right, the mean deviation of the patient (mean deviation: -28.9 mm; *SE*: 2.6) was significantly different from that of the controls (mean deviation: -8.5 mm; *SE*: 2.29) ($p<0.001$), no significant differences ($p>0.05$) were found among the patient and the controls in the deviations of the trajectories to targets placed on the left; in the constant reach configuration for targets placed on the right the mean deviation of the

patient (mean deviation: -20.3 mm; *SE*: 1.51) was significantly different from that of the controls (mean deviation: -2.46 mm; *SE*: 2.3) ($p < 0.001$), no significant differences ($p > 0.05$) were found among the patient and the controls in the deviations of the trajectories to targets placed on the left; in the foveal reach configuration for targets placed on the left the mean deviation of the patient (mean deviation: 12.7 mm; *SE*: 1.24) was significantly different from that of the controls (mean deviation: 24.4 mm; *SE*: 0.34) ($p = 0.002$), no significant differences ($p > 0.05$) were found among the patient and the controls in the deviations of the trajectories to targets placed on the right.

Deviation of the first and last half of the trajectories
(to targets placed at different directions) with respect to
the ideal trajectory

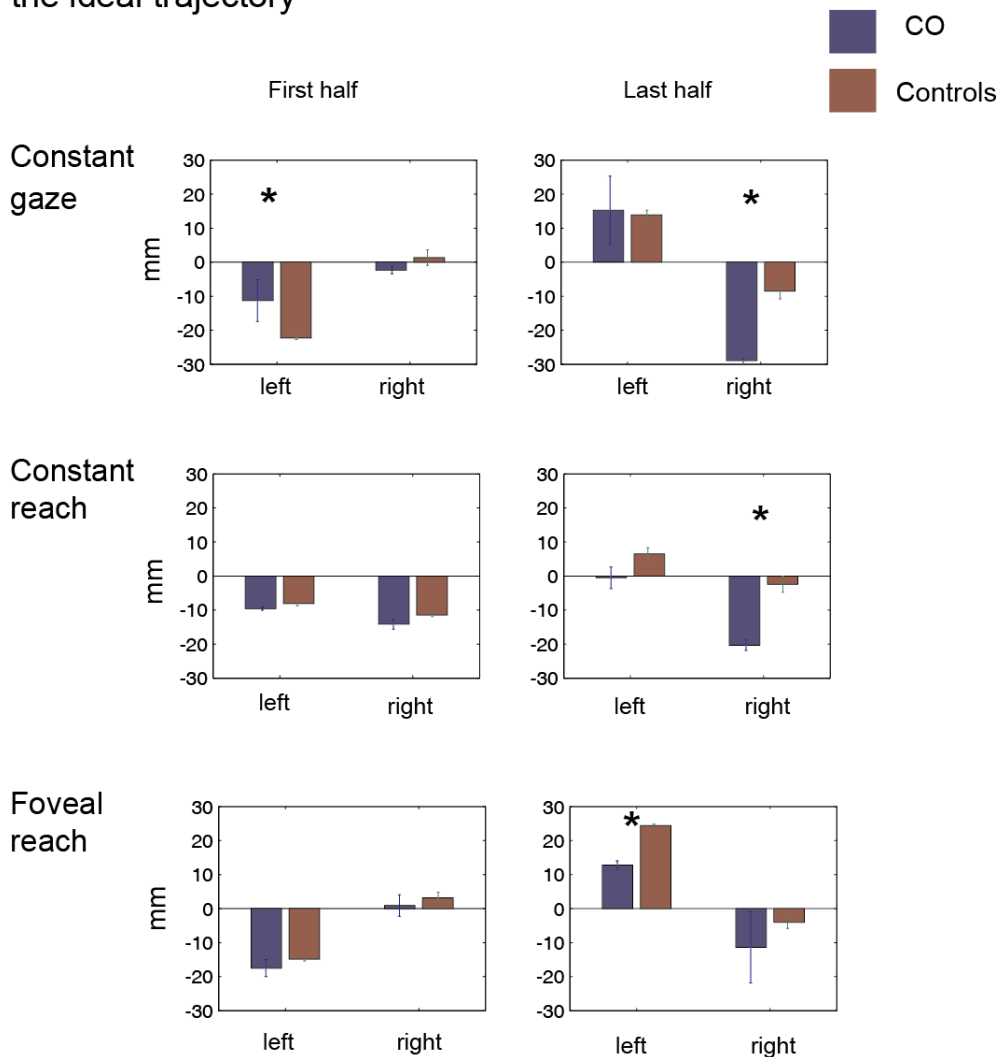


Figure 5-6. Mean deviations (mm) of the first and last half of the trajectories, towards targets placed at different directions (left, right), with respect to the ideal trajectory in the constant gaze

(above panels), constant reach (middle panels) and foveal reach (bottom panels) configurations. Each bar represent the mean value of the deviations of the trajectories towards targets placed at different directions (left, right). Negative values mean that the deviation of the trajectory is on the left with respect to the ideal trajectory, positive values mean that the deviation of the trajectory is on the right with respect to the ideal trajectory. The asterisks represent the comparison which reached significance ($p < 0.05$).

| Table 5-3 | Deviation (mm) First half trajectory (SE) | | Deviation (mm) First half trajectory (SE) | | Deviation (mm) Last half trajectory (SE) | | Deviation (mm) Last half trajectory (SE) | |
|----------------|---|-----------------|---|-----------------|--|----------------|--|----------------|
| | left | | right | | left | | right | |
| | C.O. | Controls | C.O. | Controls | C.O. | Controls | C.O. | Controls |
| Constant gaze | -11.2 (6.1) | -22.3 (0.46) | -2.34 (1.09) | 1.31 (2.31) | 15.2 (10.03) | 13,8 (1,34) | -28.9 (2.6) | -8.5 (2.29) |
| Constant reach | -9.75 (0.5) | -8.09 (0.63) | -14.1 (1.45) | -11.45 (0.5) | -0.48 (3.14) | 6,53 (1,75) | -20.3 (1.51) | -2.46 (2.3) |
| Foveal reach | -17.4 (2.5) | -14.8 (0.48) | 0.9 (3.16) | 3.17 (1.6) | 12.7 (1.24) | 24,4 (0,34) | -11.35 (10.4) | 4.02 (1.83) |

Table 5-3. Mean values of the deviations (mm) and *SE* of the trajectories with respect to the ideal one, towards targets placed at different directions (left and right) in the constant gaze, constant reach and foveal reach configurations. Negative values mean that the deviation of the trajectory is on the left with respect to the ideal trajectory, positive values mean that the deviation of the trajectory is on the right with respect to the ideal trajectory.

In addition, to evaluate the influence of depth and direction on the deviation of the first and last part of the trajectories, we conducted two separate two-way ANOVAs for the patient and for the controls, one for the first part of the trajectory and the other one for the last part: as factor 1, the different depths (far, intermediate and near, 3 levels); as factor 2, the different directions (left, right, 2 levels). For conciseness here we report only significant results.

For the patient we found a significant interaction between depth and direction in the constant gaze configuration both in the first ($F(4,29)=3.21$; $p=0.02$) and last part ($F(4,29)=5.47$; $p=0.002$) of the trajectories. Bonferroni post hoc test confirmed that in the first part of the trajectory there was a significant difference in the deviation of the

trajectory toward near targets on the left compared to the deviation of the trajectory toward near targets on the right (Bonferroni *post hoc test*, $p=0.003$). Bonferroni *post hoc test* confirmed that in the last part of the trajectory there was a significant difference in the deviation of the trajectory toward far targets on the right compared to the deviation of far targets in the center (Bonferroni *post hoc test*, $p=0.001$) and the deviation of the trajectory toward far targets on the right compared to the deviation of far targets on the left (Bonferroni *post hoc test*, $p<0.001$); there was a significant difference in the deviation of the trajectory toward intermediate targets on the right compared to the deviation of intermediate targets in the center (Bonferroni *post hoc test*, $p=0.001$) and on the left (Bonferroni *post hoc test*, $p<0.000$); there was a significant difference in the deviation of the trajectory toward intermediate targets on the left compared to the deviation of intermediate targets in the center (Bonferroni *post hoc test*, $p=0.005$); there was a significant difference in the deviation of the trajectory toward intermediate targets on the left compared to the deviation of near targets on the left (Bonferroni *post hoc test*, $p=0.001$). There was a significant difference in the deviation of the trajectory towards near targets on the left compared to far targets on the left (Bonferroni *post hoc test*, $p=0.03$); there was a significant difference in the deviation of the trajectory towards near targets on the left compared to intermediate targets on the left (Bonferroni *post hoc test*, $p=0.001$). No significant interactions were found in the other configuration for the patient, and no significant interactions were found in all configurations for the controls.

To obtain a global and statistical assessment of the deviations of the trajectories from the ideal one we performed a linear regression analysis to relate the deviations of the trajectories of the controls as a function of the deviations of the trajectories of the patient and tested the significant linear fitting by the R-squared value (R^2) (Fig. 5-7). These results showed that both in the first part and the last part of the trajectory, the mean of the deviations of the patient C.O. from the ideal trajectory and those of the controls were significantly explained by a linear model: in the first part of the trajectory the slope is 0.79 and R^2 value is 0.47 and it is significant; in the last part of the trajectory the slope is 0.49 and the R^2 value is 0.62 and it is significant. Even though both in the first part and the last part of the trajectory of the patient and the controls there was a significant linear relation, the slope of the regression line was different. This could be explained by the fact that whereas in the first part of the trajectory the variability of the deviations of the patient ($SD: 6.60$) was similar to the variability of the deviations of the controls ($SD: 7.64$), in the last part of the trajectory the variability of

the deviations of the patient ($SD: 15.88$) was higher than the variability of the deviations of the controls ($SD: 9.90$). The different slope of the regression line in the first part (0.79) and last part (0.49) of the deviations of the trajectories can be due to the higher variability that the patient exhibited in the last part of the mean deviations. Overall, in the first part of the trajectory the patient and controls managed the movement with the same variability, in the last part of the trajectory the patient was more uncertain and her deviations were more variable ($SD: 15.5$).

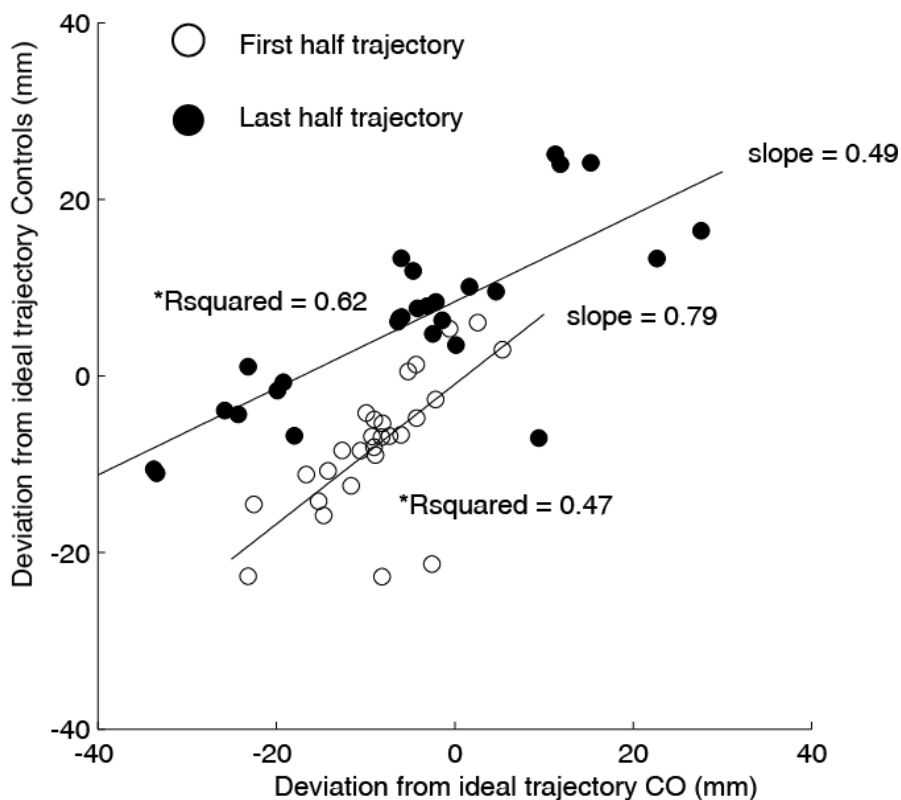


Figure 5-7. Correlation of deviations from the ideal trajectory. On the x axis the mean deviations from the ideal trajectory of the patient (C.O.) are plotted and on the y axis those of the controls. Empty circles represent the mean deviations towards each target in each configuration (constant gaze, constant reach and foveal reach) in the first half of the trajectory; filled black circles represent the mean deviations towards each target in each configuration (constant gaze, constant reach and foveal reach) in the last half of the trajectory. In the first half of the trajectory the slope is 0.79 (R-squared value is 0.47 , significant) and in the last half of the trajectory is 0.49 (R-squared value is 0.62 , significant).

5.4.2 Analysis of reach errors

To analyze the accuracy of the patient with respect to the controls in executing reaching movements, we estimated the reach errors in depth (y coordinate) and in direction (x coordinate), calculated by subtracting the respective vertical and horizontal coordinates of the physical target location from the reach endpoint in each trial of the three configurations. If the reach error (y coordinate) is positive it means that the subject is overshooting the target; if the reach error (y coordinate) is negative it means that the subject is undershooting the target. If the reach error (x coordinate) was positive it meant that the subject was deviating to the right with respect to the target and if it was negative it meant that the subject was deviating to the left with respect to the target.

Figure 5-8 shows the averaged reach errors of the patient (blue bar) and the controls (red bars) in depth (left panels) for targets placed at near, intermediate and far distance, and in direction (right panels) for targets placed on the left and right in the three configurations.

In the constant gaze configuration for targets placed at different depths, to see if there was a difference in the errors of the patient with respect to the controls (Table 5-4), we performed a Two-sample t-test. We found that the mean reach errors of the patient (mean near targets: -9.62 mm; *SE*: 5.4) were significantly different from those of the controls (mean near targets: 2.33 mm; *SE*: 4.5) for near targets ($p=0.01$); the mean reach errors of the patient (mean intermediate targets: -23.56 mm; *SE*: 0.31) were significantly different from those of the controls (mean intermediate targets: 6.19 mm; *SE*: 0.4) for intermediate targets ($p=0.01$); the mean reach errors of the patient (mean far targets: -18.2 mm; *SE*: 2.3) were significantly different from those of the controls (mean far targets: -8.18 mm; *SE*: 1.6) for far targets ($p<0.001$). The patient always undershooting targets located at different depths. This observation is not uncommon: these reach patterns have been reported both in a case of parietal occipital damage where the subject systematically undershoot the target in depth (Khan et al., 2005) and also in healthy subjects using a task design similar to our set up (Van Pelt and Medendorp, 2008).

In the constant gaze configuration for targets placed at different directions, to see if there was a difference in the reach errors of the patient with respect to the controls we performed a Two-sample t-test (Table 5-5). We found that the mean reach errors of the patient (mean right targets: -4.53 mm; *SE*: 20.4) were significantly different from those

of the controls (mean right targets: 16.82 mm; *SE*: 18) only for targets placed on the right ($p=0.03$). The patient showed reaching errors deviated on the left for targets located on the right. This result is in agreement with the literature where the deviation of the hand towards the fixation point has been shown by several authors (Khan et al, 2005; Carey et al., 1997; Jackson et al., 2005). This, so called, “magnetic misreaching” (Carey et al., 1997; Jackson et al., 2005) suggested that patients programmed their movements in oculocentric coordinates.

In the constant reach configuration for targets placed at different depths (Table 5-4), the patient overshooted the central reaching target when fixating near targets, while undershooted it when fixating intermediate and far targets. To see if there was a difference in the errors of the patient with respect to the controls we performed a Two-sample t-test. We found that the mean reach errors of the patient (mean near targets: 8.55 mm; *SE*: 4.48) were significantly different from those of the controls (mean near targets: 2.3 mm; *SE*: 1.5) for near targets ($p=0.03$); the mean reach errors of the patient (mean intermediate targets: -24.4 mm; *SE*: 0.48) were significantly different from those of the controls (mean intermediate targets: -3.4 mm; *SE*: 1.62) for intermediate targets ($p<0,001$); the mean reach errors of the patient (mean far targets: -18.1 mm; *SE*: 4.1) were significantly different from those of the controls (mean far targets: -1.57 mm; *SE*: 4.2) for far targets ($p<0.001$).

In the constant reach configuration while fixating targets placed at different directions (when fixating on the left and on the right of the reaching target) (Table 5-5) the patient made reaching errors always on the left of the central target.

To see if there was a difference in the errors of the patient with respect to the controls we performed a Two-sample t-test. We found that the reach errors of the patient while fixating on the left (mean reach error: -13.06 mm; *SE*: 2.85) were significantly different from those of the controls (mean reach error: -3.36 mm; *SE*: 1.35) when the fixation point was on the left ($p=0.02$); the reach errors of the patient while fixating on the right (mean reach error: -30.42 mm; *SE*: 1.8) were significantly different from those of the controls (mean reach error: -10.02 mm; *SE*: 1.6) when the fixation point was on the right ($p<0.001$).

In the foveal reach configuration for targets placed at different depths (Table 5-4) the patient undershooted the targets both when they were at near distance and far distance while she slightly overshooted intermediate targets. To see if there was a difference in the errors of the patient with respect to the controls we performed a Two-

sample t-test. We found that the mean reach errors of the patient (mean near targets: -8.65 mm; *SE*: 2.33) were significantly different from those of the controls (mean near targets 1.63 mm; *SE*: 2.7) for near targets ($p < 0.001$); the mean reach errors of the patient (mean far targets: -6.07 mm; *SE*: 2.7) were significantly different from those of the controls (mean far targets: 0.76 mm; *SE*: 2.4) for far targets ($p = 0.02$). No significant difference was found for intermediate targets.

In the foveal configuration for targets placed at different directions the patient made errors always on the left with respect to targets located both on the left and on the right. To see if there was a difference in the errors of the patient with respect to the controls (Table 5-5) we performed a Two-sample t-test. We found that the mean reach errors of the patient (mean left targets: -18.94 mm; *SE*: 2.28) were significantly different from those of the controls (mean left targets: -2.23 mm; *SE*: 2.38) only for targets placed on the left ($p < 0.001$); no significant difference was found for targets on the right.

Overall, in the majority of the configurations (constant reach and foveal reach) the patient showed the classic 'field effect' such that she tended to make more errors in left visual field, contralateral to that of the lesion, especially in the configurations where eye and hand are dissociated. She often executed the reaching undershooting the targets in depth and deviating the hand towards the fixation target in direction for targets on the right in the decoupled eye/hand configuration.

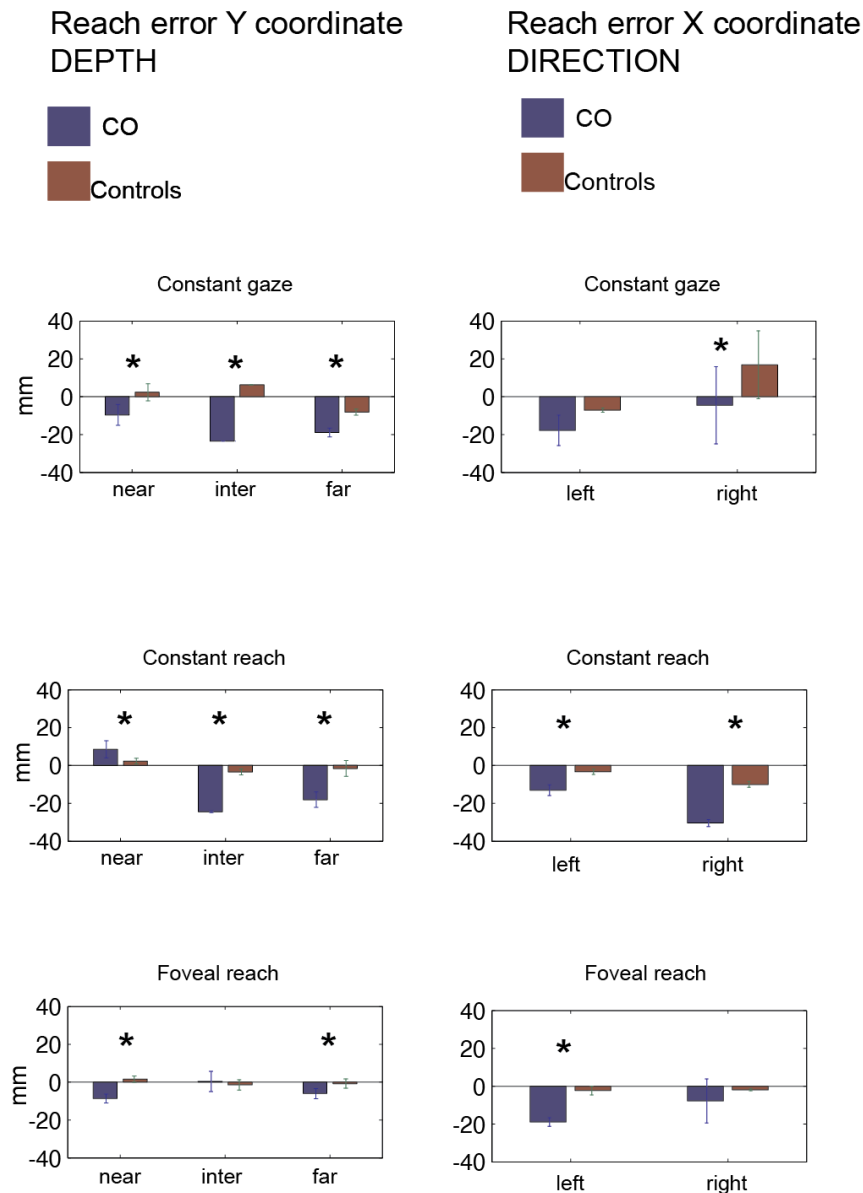


Figure 5-8. Reach errors: bar histograms representing mean reach errors (mm) of the patient (blue bars) and the controls (red bars) in depth (near, intermediate and far targets) and in directions (left and right targets) in the constant gaze, constant reach and foveal reach configuration. If the reach error (y coordinate) was positive it meant that the subject was overshooting the target and if it was negative it meant that the subject was undershooting the target (panels on the left). If the reach error (x coordinate) was positive it meant that the subject was deviating to the right with respect to the target and if it was negative it meant that the subject was deviating to the left with respect to the target (panels on the right). The error bars are standard errors (*SE*). The asterisks represent the comparison which reached significance ($p < 0.05$).

| Table 5-4 | Mean reach errors (mm) | | Mean reach errors (mm) | | Mean reach errors (mm) | |
|------------------|----------------------------|------------|------------------------------------|-------------|---------------------------|-------------|
| | near targets (<i>SE</i>) | | Intermediate targets (<i>SE</i>) | | Far targets (<i>SE</i>) | |
| | C.O. | Controls | C.O. | Controls | C.O. | Controls |
| Constant gaze | -9.62 (5.4) | 2.33 (4.5) | -23.56 (0.3) | 6.19 (0.4) | -18.2 (2.3) | -8.18 (1.6) |
| Constant reach | 8.55 (4.48) | 2.3 (1.5) | -24.4 (0.48) | -3.4 (1.62) | -18.1 (4.1) | -1.57 (4.2) |
| Foveal reach | -8.65 (2.33) | 1.63 (2.7) | 0.38 (5.35) | -1.4 (2.79) | -6.07 (2.7) | 0.76 (2.4) |

Table 5-4. Mean reach errors (mm) and *SE* of the patient (C.O.) and controls for targets placed at different depths (near, intermediate and far) in the constant gaze, constant reach and foveal reach configuration.

| Table 5-5 | Mean reach errors (mm) | | Mean reach errors (mm) | |
|------------------|----------------------------|-------------|-----------------------------|-------------|
| | Left targets (<i>SE</i>) | | Right targets (<i>SE</i>) | |
| | C.O. | Controls | C.O. | Controls |
| Constant gaze | -17.83(8.04) | -7.13(1.14) | -4.53 (20.4) | 16.82 (18) |
| Constant reach | -13.06(2.85) | -3.36(1.35) | -30.42 (1.8) | -10.02(1.6) |
| Foveal reach | -18.94(2.28) | -2.23(2.38) | -7.78 (11.6) | -1.91 (0.5) |

Table 5-5. Mean reach errors (mm) and *SE* of the patient (C.O.) and controls for targets placed at different directions (left and right) in the constant gaze, constant reach and foveal reach configuration.

To relate the reach errors of the controls as a function of the reach errors of the patient we performed a linear regression analysis and we calculated the slope and tested the significant linear fitting by the R-squared (R^2) value as depicted in Figure 5-9. To check whether the correlation among the reach errors of the patient and the controls was linearly represented we calculated the slope: in direction we found that the slope is 0.63 and in depth is 0.17. To statistically compare the performance of the patient and the controls we calculated the R^2 value: in direction the R^2 was significant (0.60), while in depth it was not significant (0.13). To summarize, in direction the reach errors of the

patients and those of the controls were significantly linearly correlated and this suggests that the patient and the controls used a similar strategy in their reaching behavior; in depth, the reach errors of the patients and those of the controls were not significantly defined by a linear equation and this could suggest that the patient and the controls used a different strategy in their reaching behavior.

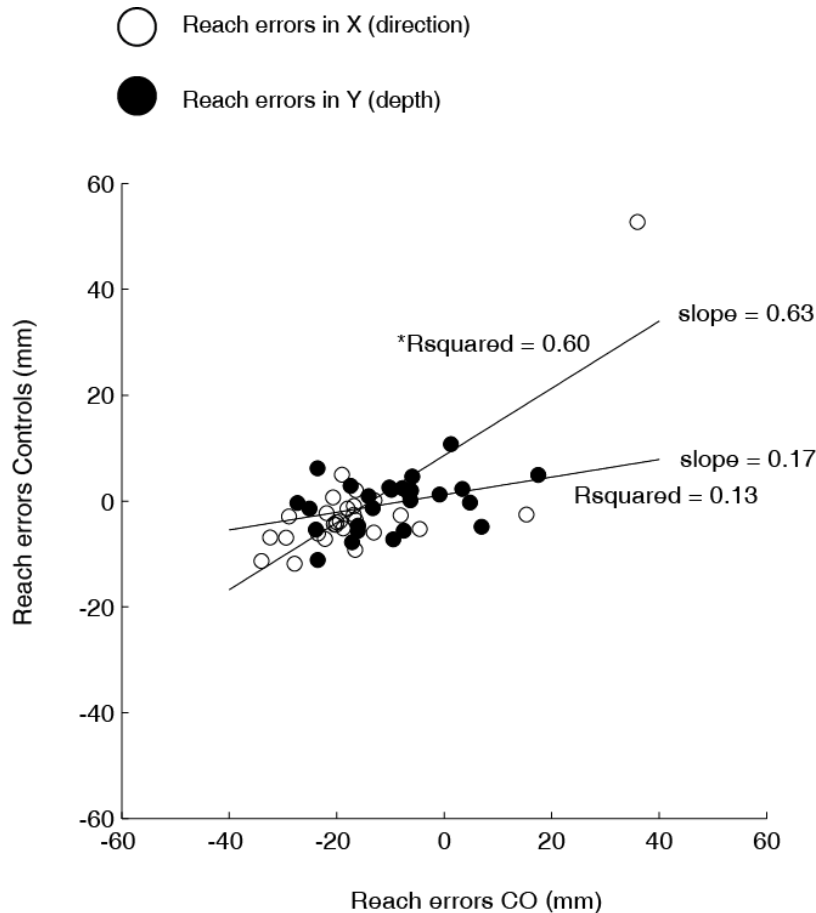


Figure 5-9. Linear regression of reach errors. On the x axis the reach errors of the patient (C.O.) are plotted and on the y axis those of the controls are plotted. Empty circles represent mean reach errors, towards each target in each configuration, in direction (x axis) and filled black circles represent mean reach errors, towards each target in each configuration, in depth (y axis). In direction the slope is 0.63 (R-squared value is 0.60) and in depth is 0.17 (R-squared value is 0.13).

To have a representation of the correlation of the reach errors and the deviations of the first part (Fig. 5-10, left panels) and last part (Fig. 5-10, right panels) of the trajectories of the patient and of the controls we plotted the reach errors against the deviations and

we computed confidence ellipses for the patient (depicted in pink in Fig. 5-10) and for the controls (depicted in blue in Fig. 5-10) whose area describe the smallest ellipse that covers 95% of the data (Fig. 5-10). We analyzed the correlation in depth (Fig. 5-10, top panels) and in direction (Fig. 5-10, bottom panels). While the correlation of reach errors and deviations of the first part of the trajectories shows that both in depth (Fig. 5-10, top left panel) and direction (Fig. 5-10, bottom left panel) the variability of the data of the patient is superimposed to that of the controls (the ellipses are almost coincident), the correlation of reach errors and deviations of the last part of the trajectories both in depth (Fig. 5-10, top right panel) and direction (Fig. 5-10, bottom right panel) shows the variability of the data of the patient was higher than that of the controls.

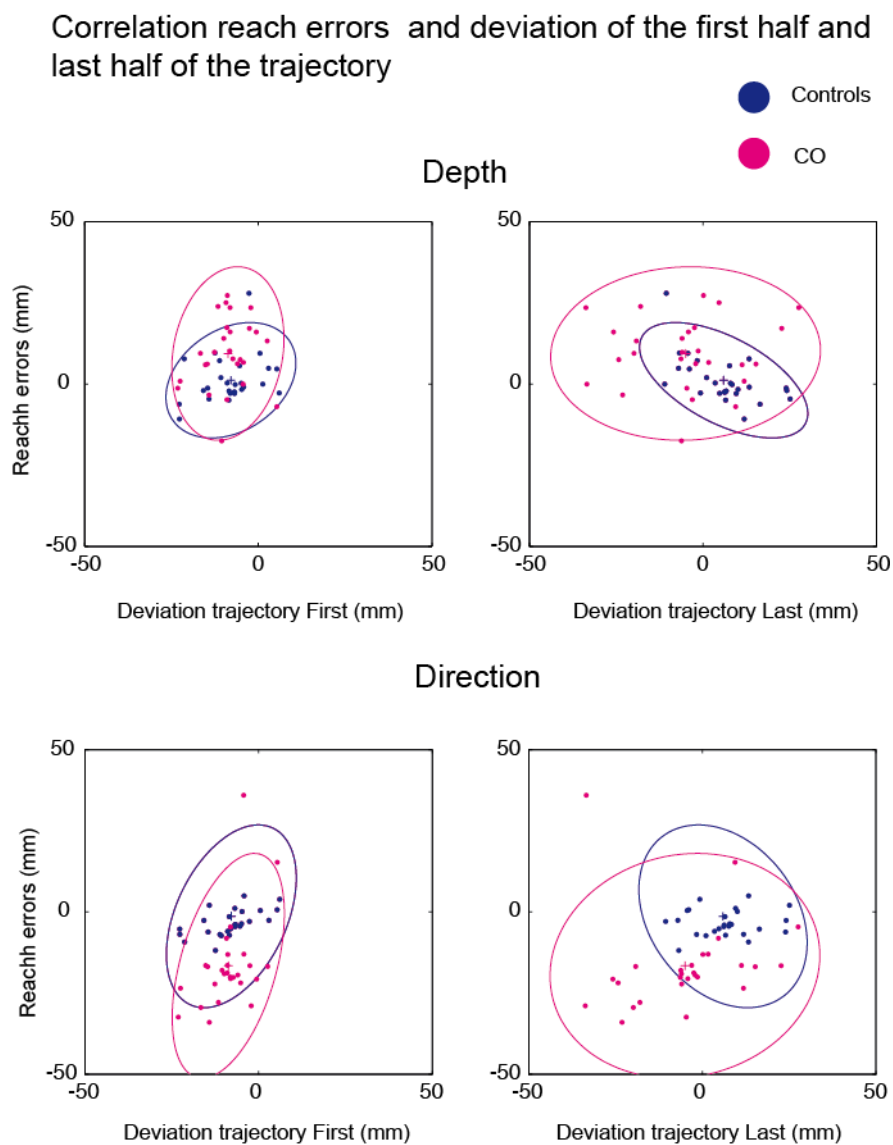


Figure 5-10. Representation of the correlation of the reach errors and the deviations of the first and last half of the trajectory. The pink dots are the values of the mean reach errors and

deviations of the patient for every target, in the constant gaze, constant reach and foveal reach configuration; the pink ellipse describes 95% of the variability of the data of the patient. The blue dots are the values of the mean reach errors and deviations of the controls for every target in the constant gaze, constant reach and foveal reach configuration and the blue ellipse describes 95% of the variability of the data of the controls.

5.5 Discussion

In the current study, we presented data obtained from a patient, C.O., with unilateral optic ataxia. After a lesion on the right side of the parietal-occipital cortex, the patient showed impairments in reaching a target that was not foveated. We wanted to explore what were the conditions in which a subject with OA makes more reach errors with respect to healthy controls. The novelty of our approach resides on having three types of task configuration (Bosco et al., 2016; Bosco et al., 2017): we employed different configurations of gaze and hand relative positions, in depth and direction, so to test all possible conditions of dissociation of visual target and reaching target. In the constant gaze configuration and the constant reach configuration eye and hand were decoupled and the participants always had to reach a target that was not foveated (peripheral viewing reaching); in the foveal reach configuration eye and hand were coupled and participants had to reach a foveated target. The decoupled conditions, which imply the ability to control hand location without central vision, gave us the opportunity to analyze the proprioceptive updating of the patient. Indeed it has been found that patients with OA had impaired proprioceptive updating during reaches in the dark (Blangero et al., 2007).

5.5.1 Trajectory impairments

Firstly, we have studied the trajectories and, to this end, we have analyzed the first and last part of the trajectories. We have found that the initial part of the trajectories of the patient followed the same path of that of the controls, and this suggests that they both have a similar planning of the movement. The last part of the trajectories is where the differences among the patient and controls emerged; in the last part of the trajectory, the controls were able to correct the initial planned trajectory, whereas in the last part of the trajectory of the subject with OA prevailed the initial planning and in fact her reaching

errors were significantly higher than those of the controls in each configuration and in particular for targets placed in depth more than for those placed in direction. The patient failed to make adjustments of the trajectory contrary to the controls, especially in the configurations where eye and hand were dissociated (constant gaze and constant reach configuration). In the foveal reach configuration, in which the eye is fixating the target, the patient was able to correct more the deviation of the trajectory, instead. These results could be explained by the fact that when the reaching was in peripheral vision, the processing of hand location and target location was impaired more than when the reaching was foveated: in this case, the central vision of the target helped the patient to mildly reduce the error and to integrate better hand and target location.

5.5.2 Reaching errors

Trough the evaluation of reach errors in depth (y coordinate) we have found that the performance of the patient was significantly different from that of the controls in the configuration where eye and hand were decoupled (constant gaze and constant reach), for targets placed at near, intermediate and far distance; in the foveal reach configuration there was a significant difference only for targets placed at near and far distance. When reaching targets were placed at different depths the patient undershooting them in all configurations. This observation is in line with the literature which showed that, in a case of parietal lesion, the subject systematically undershooting the target in depth (Khan et al., 2005). Similarly, also healthy subjects undershooting targets placed in depth (Van Pelt and Medendorp, 2008).

Trough the evaluation of reach errors in direction (x coordinate) we have found that the performance of the patient was significantly different from that of the controls in the constant gaze configuration for targets placed on the right, in the constant reach configuration when fixating both on the left and on the right of the reaching target and in the foveal reach configuration when reaching targets were placed on the right; in addition, for any target location and in any configuration, the patient tended to reach on the left showing the classical field effect, such that she exhibited impairments in reaching targets placed in the contralesional left visual field (Blangero et al., 2008; Danckert et al., 2009).

Pointing errors are not typically observed in central vision in OA patients (Perenin and Vighetto, 1998), our results though showed that, in the foveal reach configuration, the

patient exhibited reaching errors, even though reduced compared to the configurations of peripheral vision. This could be due to the fact that in our set up the room was darkened and the visual feedback of the hand was poor. Without a proper vision of the reaching hand, the visuo-manual transformation relies more on its proprioceptive localization (Blangero et al., 2007). The inaccuracy of the patient in reaching also in central vision could be the result of impaired proprioception. In addition, the patient is using her left hand which is the hand contralesional/ataxic hand.

In the light of our knowledge about OA, overall we suggest that the reaching inaccuracies observed in the patient, in particular in the configurations where the direction of gaze and reach direction differ, can be explained by the lack of the “automatic pilot” which is able to adjust in healthy subjects the predefined motor plan (Goodale et al., 1986; Pisella et al., 2000; Blangero et al., 2009).

Several studies have shown that reach errors in OA are due to a disruption of the online correction mechanism (Rossetti et al., 2003, 2005; Blangero et al., 2008; Gaveau et al., 2014) and that PPC is involved in automatic corrections (Pisella et al., 2000; Rossetti and Pisella, 2003). Blangero and colleagues (2008) proposed that the lack of automatic corrections observed in OA could suggest a specific “disruption of the visuo-propriceptive comparison of target and hand locations or an impaired forward modeling of the hand trajectory used for on-line comparison to visual target location” (Desmurget and Grafton, 2000). Hand location information can be provided by vision and proprioception and it was shown that OA subjects make both visual and proprioceptive reaching errors, when the target it is not foveated (Jackson et al., 2009).

In our data, since the initial part of the trajectories (first half) of the patient do not show differences from those of the healthy subjects, it seems that the planning of the movement is the same across patient and healthy subjects. The differences arise later in the movement, in the last part of the trajectory (last half), indicating an on-line control deficit of the action, which is based on visual and proprioceptive feedbacks (Glover, 2003, 2004; Rossetti, Pisella, and Vighetto, 2003). We are aware of the limitations of our single case study especially because each patient shows different patterns of errors according to the site and extension of the lesion, future works with additional patients are required to understand the underpinnings of the visuo-motor transformation deficits occurring after parietal lesions.

6. General conclusions

The aim of the presented thesis was to investigate how reaching for visual targets placed in 3D space influences the coordinate frames and the kinematics in non-human and human primates. To this end, I conducted three studies which provided new insights in this topic. Here I will briefly summarize the main results, which were discussed in more detail in the previous chapters.

In the first study, I aimed to examine the coordinate system displayed by cells of the macaque medial posterior parietal area PEc, during reaching movements in the 3D space. The PPC plays an important role in the coding of three-dimensional space, in particular related to the depth and direction dimension.

Several physiological studies showed that the PPC encodes the direction and depth of reaching movements. Each area of the PPC of non-human primates encodes the distance in a specific coordinate system: PRR/MIP, located in the medial bank of the intraparietal sulcus, encodes the location of reach targets in an eye-centered reference frame (Batista et al., 1999; Bhattacharyya et al., 2009); area PE, located in the rostral part of the SPL, in hand-centered frame (Ferraina et al., 2009); area V6A, located in the caudal part of the superior parietal lobule (Galletti et al., 1999) in a body-centered and mixed-centered frame of reference (Hadjidimitrakis et al., 2014a). We used the same experimental paradigm employed by Hadjidimitrakis and colleagues (2014a) in nearby area V6A and tested whether PEc reaching cells displayed hand-centered and/or body-centered coding of reach targets. We found that the majority of PEc neurons encodes targets in a mixed body/hand-centered reference frame. Our findings highlight a role for area PEc as intermediate node between the visually dominated area V6A and the somatosensory dominated area PE.

On the basis of this result, using a psychophysical approach we have conducted a further study on healthy human subjects. The aim of this second study was to find the reference frames used while reaching towards targets placed at different depths and directions. We examined different aspects of the encoding of memory-guided reaching movements to targets placed at different depths and different directions.

Our results revealed reach error patterns based on both eye- and space-centered coordinate systems: in depth more biased towards a space-centered representation and in direction mixed between space- and eye-centered representation.

My laboratory has recently investigated the encoding of reaching target located at different depths and directions in a parietal area of the macaque (Bosco et al., 2016) and the results showed both eye- and space-centered representations differently balanced across neurons, similarly to present behavioral results and similar to mixed coordinate systems that have been found in the PPC regions (Stricanne et al., 1996; Buneo et al., 2002; Cohen and Andersen, 2002; Battaglia-Mayer et al., 2003; Avillac et al., 2005; Mulette-Gillman et al., 2005, 2009b; Chang and Snyder, 2010; McGuire and Sabes, 2011; Hadjidimitrakis et al., 2014a; Bosco et al., 2015a, 2016; Piserchia et al., 2017); therefore it can be suggested that what we have found here is the outcome, at behavioral level, of the neural discharges investigated in those previous works. Overall our results indicate that the brain needs the conjunct contribution of multiple coordinate system to retain a coherent representation of a position of an object and efficiently execute reaching movements in 3D space.

Based on this result, we have conducted a third study on a human subject with OA, employing a similar experimental paradigm used in the previous study on healthy human subjects (Bosco et al., 2017). With this study, I aimed to verify which component of visuo-motor control was impaired in a patient with OA, given that these patients experience deficits in visuo-manual guidance especially when reaching occurs to targets located in the periphery of the visual field. By manipulating gaze position and hand position of visual reaching targets, placed at different depth and directions, we investigated how reaching in peripheral and central viewing conditions influenced the trajectories and reach errors of the patient and control subjects. The novelty of our approach resides on having three types of task configuration (Bosco et al., 2016; Bosco et al., 2017) so to test all possible conditions of dissociation of visual target and reaching target. We have found that the initial part of the trajectories of the patient followed the same path of that of the controls and this suggests that both the patient and the controls have a similar planning of the movement. In the last part of the trajectory instead while the controls were able to correct the initial planned trajectory, the patient failed to make adjustments of the trajectory especially in the configurations where eye and hand were dissociated. In fact, the reaching errors of the patient were significantly higher than those of the controls in each configuration and in particular for targets placed in depth more than in direction. Taken together, we suggest that the reaching inaccuracies observed in particular in the configurations where the direction of gaze and reach direction differ are due to a disruption of the online correction mechanism

(Rossetti et al., 2003, 2005; Blangero et al., 2008; Gaveau et al., 2014) which is able to adjust in healthy subjects the predefined motor plan (Goodale et al., 1986; Pisella et al., 2000; Blangero et al., 2009), and that PPC is involved in these automatic corrections (Pisella et al., 2000; Rossetti and Pisella, 2003).

In conclusion, the findings that I have described in this thesis aim for a deeper understanding of how the brain represents objects in 3D space and how action related regions of the dorso-medial visual stream are involved in higher level cognitive functions related to actions such that of coordinate frame transformations. The presence of mixed reference frames that we observed in area PEc is in line with the idea that the brain's strategy is that of converting signals into a specific, clear reference frame later in the motor pathway, that is to say only when the motor command begins to prepare and direct the effector on a specific location in space; this specifically occurs in the PPC (Stricanne et al., 1996; Avillac et al., 2005; Mullette-Gillman et al., 2005, 2009; Chang and Snyder, 2010; McGuire and Sabes, 2011; Hadjidimitrakis et al., 2014a) which, situated between visual and somatosensory cortex, receives sensory signals and sends those to the motor cortex. Visually guided reaching of a target takes place thanks to a series of reference frame transformations, from eye-centered first to body- and then hand-centered representation (Flanders et al., 1992). The advantage of a flexible coordinate system, that we have found in the results of our reaching in 3D task, both in human and non-human primates, it is due to the fact that the motor response is complicated by the necessity to integrate signals in retinal, proprioceptive and motor reference frames (Buneo et al., 2002). In the network of parietal regions, the adoption of such a flexible, mixed coordinate system, which takes into account different landmarks, is a strategy the system use to face movement corrections. Our findings on area PEc not only confirm the view that reference frame transformations occurs in the PPC but also support the idea that different areas along the dorsal stream represent different stages of these transformations (Hadjidimitrakis et al., 2014a; Bosco et al., 2015a). In addition, the results obtained from our case study of a PPC lesion support the view that impaired function of visuomotor transformation of the retinal input of target position into body-centered coordinates, causes the deficits in visually guided reaching that we observed in our study of an OA patient (Ogawa et al., 2011).

Currently neuroscience is a useful mean to improve robots control, interaction and design. There is a lot of present research on coordinate transformations in robotics. Understanding the neural mechanisms of reference frame transformation and the

behavioral aspects of movement control can be helpful in developing neural prosthetics to decode movement goals through cell recordings in non-human (Mulliken et al., 2008) and human primate studies (Hochberg et al., 2012; Aflalo et al., 2015). The control of robotic limbs is challenging also because these structures demand sophisticated sensory-motor control. With this thesis, we have established a new paradigm for reaching in 3D space that could be used in future research and we have provided new insights on an area of the PPC, PEc that could potentially be used to decode cognitive control signals for neural prosthetics that assist paralyzed patients who have impaired sensorimotor functions. The PPC is a useful candidate to be used for prosthetic control since in these areas the intended movement activity can be carried on by just thinking about a movement, without actually having to initiate it (Cohen and Andersen, 2002; Aflalo et al., 2015).

7. References

- Aflalo T *et al.* (2015). Neurophysiology. Decoding motor imagery from the posterior parietal cortex of a tetraplegic human. *Science*, 348, 906–910.
- Alemayehu B, Pavlovsky N, Chiou J, Tyler-Kabara E, Hatsopoulos N, Chase S, Batista A (2015). Eye-centered tuning is weak in dorsal premotor cortex when monkeys are not trained to fixate. *SFN Meeting planner*, 46705.
- Andersen RA, Snyder LH, Li CS, Stricanne B (1993). Coordinate transformations in the representation of spatial information. *Curr Opin Neurobiol*, 3:171-176.
- Andersen RA, Buneo CA, (2002). Intentional maps in posterior parietal cortex. *Annu Rev Neurosci*, 25:189 –220.
- Andersen RA, Andersen KN, Hwang EJ and Hauschild M, (2014). Optic ataxia: from Balint's syndrome to the parietal reach region. *Neuron*, 81:967–983.
- Avillac M, Denève S, Olivier E, Pouget A, Duhamel JR (2005). Reference frames for representing visual and tactile locations in parietal cortex. *Nat Neurosci*, 8:941-949.
- Badde S, Heed T, and Röder B (2014). Processing load impairs coordinate integration for the localization of touch. *Atten Percept Psychophys*, 76:1136–50.
- Badde S, Röder B, and Heed T (2015). Flexibly weighted integration of tactile reference frames. *Neuropsychologia*, 70:367–374.
- Bagesteiro LB, Sarlegna FR, and Sainburg RL (2006). Differential influence of vision and proprioception on control of movement distance. *Exp Brain Res*, 171:358–370.
- Bakola S, Gamberini M, Passarelli L, Fattori P, Galletti C (2010). Cortical connections of parietal field PEc in the macaque: linking vision and somatic sensation for the control of limb action. *Cereb Cortex*, 20:2592-2604.
- Bakola S, Passarelli L, Gamberini M, Fattori P, Galletti C (2013). Cortical connectivity suggests a role in limb coordination for macaque area PE of the superior parietal cortex. *J Neurosci*, 33:6648-6658.
- Bálint R (1909). "Seelenlähmung des "Schauens", optische Ataxie, räumliche Störung der Aufmerksamkeit". *Europ Neurol*, 25: 51–66, 67–81.
- Batista AP, Buneo CA, Snyder LH, Andersen RA (1999). Reach plans in eye-centered coordinates. *Science* 285:257-260.
- Batista AP, Santhanam G, Yu BM, Ryu SI, Afshar A, Shenoy KV (2007). Reference frames for reach planning in macaque dorsal premotor cortex. *J Neurophysiol*, 98:966-983.
- Battaglia-Mayer A, Ferraina S, Genovesio A, Marconi B, Squatrito S, Molinari M, Lacquaniti F, Caminiti R (2001). Eye-hand coordination during reaching. II. An

analysis of the relationships between visuomanual signals in parietal cortex and parieto-frontal association projections. *Cereb Cortex*, 11:528-544.

Battaglia-Mayer A, Caminiti R, Lacquaniti F, and Zago M (2003). Multiple levels of representation of reaching in the parieto-frontal network. *Cereb Cortex* 13, 1009-1022.

Battaglia-Mayer A, Archambault PS, Caminiti R (2006). The cortical network for eye-hand coordination and its relevance to understanding motor disorders of parietal patients. *Neuropsychologia*, 44:2607–2620.

Baylis GC and Baylis LL (2001). Visually misguided reaching in Balint's syndrome. *Neuropsychologia*, 39:865-875

Bernier PM, Grafton ST (2010). Human posterior parietal cortex flexibly determines reference frames for reaching based on sensory context. *Neuron*, 68:776-788.

Beurze SM, Van Pelt S, and Medendorp W.P (2006). Behavioral reference frames for planning human reaching movements. *J Neurophysiol*, 96:352–362.

Beurze SM, Toni I, Pisella L, Medendorp WP (2010). Reference frames for reach planning in human parietofrontal cortex. *J Neurophysiol*, 104:1736-1745.

Bhattacharyya R, Musallam S, Andersen RA (2009). Parietal reach region encodes reach depth using retinal disparity and vergence angle signals. *J Neurophysiol*, 102:805-816.

Binkofskia F, and Buxbaum LJ, (2013). Two action systems in the human brain. *Brain Lang*, 127: 222–229.

Blangero A, Gaveau V, Luauté J, Rode G, Salemme R, Guinard M et al., (2008). A hand and field effect in on-line motor control in unilateral optic ataxia. *Cortex*, 44:560-568.

Blohm G, Crawford JD (2009). Fields of gain in the brain. *Neuron*, 64:598-600.

Blohm G, Keith GP, Crawford JD (2009). Decoding the cortical transformations for visually guided reaching in 3D space. *Cereb Cortex*, 19:1372-1393.

Blohm G (2012). Simulating the cortical 3D visuomotor transformation of reach depth. *PLoS One*, 7:e41241.

Bock O (1986). Contribution of retinal versus extraretinal signals towards visual localization in goal-directed movements. *Exp Brain Res*, 64:476–82.

Bosco A, Breveglieri R, Reser D., Galletti C, and Fattori P (2015a). Multiple representation of reaching space in the medial posterior parietal area V6A. *Cereb Cortex*, 25:1654-1667.

Bosco A, Lappe M, and Fattori P (2015b). Adaptation of saccades and perceived size after trans-saccadic changes of object size. *J Neurosci*, 35:14448-14456.

Bosco A, Breveglieri R, Hadjidimitrakis K, Galletti C, and Fattori P (2016). Reference frames for reaching when decoupling eye and target position in depth and direction. *Sci Rep*, 6, 21646.

Bosco A, Piserchia V and Fattori P (2017). Multiple coordinate systems and motor strategies for reaching movements when eye and hand are dissociated in depth and direction. *Front Hum Neurosci*, 11:323.

Brain WR, (1941). Visual disorientation with special reference to lesions of the right hemisphere. *Brain*, 64:224–272.

Brainard, DH (1997). The Psychophysics Toolbox. *Spat Vis*, 10:433-436.

Bremner LR, Andersen RA (2012). Coding of the reach vector in parietal area 5d. *Neuron* 75:342-351.

Bremner LR, and Andersen RA (2014). Temporal analysis of reference frames in parietal cortex area 5d during reach planning. *J Neurosci*, 34:5273-5284.

Breviglieri R, Galletti C, Gamberini M, Passarelli L, Fattori P (2006). Somatosensory cells in area PEc of macaque posterior parietal cortex. *J Neurosci*, 26:3679-3684.

Breviglieri R, Galletti C, Monaco S, Fattori P (2008). Visual, somatosensory, and bimodal activities in the macaque parietal area PEc. *Cereb Cortex*, 18:806-816.

Breviglieri R, Galletti C, Monaco S, Fattori P (2008). Visual, somatosensory, and bimodal activities in the macaque parietal area PEc. *Cereb Cortex*, 18:806-816.

Breviglieri R, Kutz DF, Fattori P, Gamberini M, Galletti C (2002). Somatosensory cells in the parieto-occipital area V6A of the macaque. *Neuroreport*, 13:2113-2116.

Breviglieri R, Galletti C, Gamberini M, Passarelli L, Fattori P (2006). Somatosensory cells in area PEc of macaque posterior parietal cortex. *J Neurosci*, 26:3679-3684.

Brodman K (1909). *Vergleichende Lokalisationslehre der Grosshirnrinde in ihren Prinzipien dargestellt auf Grund des Zellenbaues*.

Buneo CA, Jarvis MR, Batista AP, Andersen RA (2002). Direct visuomotor transformations for reaching. *Nature*, 416:632-636.

Buneo CA (2011). Analyzing neural responses with vector fields. *J Neurosci Methods*, 197:109-117.

Buneo CA, Andersen RA (2012). Integration of target and hand position signals in the posterior parietal cortex: effects of workspace and hand vision. *J Neurophysiol*, 108:187-199.

Buneo CA, Batista AP, Jarvis MR, and Andersen RA. (2008). Time-invariant reference frames for parietal reach activity. *Exp Brain Res*, 188:77-89.

- Buchholz VN, Jensen O, and Medendorp WP (2013). Parietal oscillations code nonvisual reach targets relative to gaze and body. *J Neurosci*, 33:3492-3499.
- Buschke H, and Fuld PA (1974). Evaluating storage, retention, and retrieval in disordered memory and learning. *Neurology*, 24: 1019-1025.
- Buxbaum LJ and Coslett HB (1997). Subtypes of optic ataxia: Reframing the disconnection account. *Neurocase*, 3:159-166.
- Caffarra P, Vezzadini G, Dieci F, Zonato F, and Venneri A (2014). Rey-osterrieth complex figure: Normative values in an Italian population sample. *Neurological Sciences*, 22:443-447.
- Carey DP, Hargreaves EL, and Goodale MA (1996). Reaching to ipsilateral or contralateral targets: within-hemisphere visuomotor processing cannot explain hemispacial differences in motor control. *Exp Brain Res*, 112:496-504.
- Carlton LG (1992). Visual processing time and the control of movement. In *Vision and Motor Control*, 3–31, eds L. Proteau and D. Elliot (Amsterdam: Elsevier).
- Cavina-Pratesi C, Ietswaart M, Humphreys GW, Lestou V, and Milner AD (2010). Impaired grasping in a patient with optic ataxia: primary visuomotor deficit or secondary consequence of misreaching. *Neuropsychologia*, 48:226–234.
- Chang SW, Dickinson AR, Snyder LH (2008). Limb-specific representation for reaching in the posterior parietal cortex. *J Neurosci*, 28:6128-6140.
- Chang SW, Papadimitriou C, Snyder LH (2009). Using a compound gain field to compute a reach plan. *Neuron*, 64:744-755.
- Chang SW, Snyder LH (2010). Idiosyncratic and systematic aspects of spatial representations in the macaque parietal cortex. *Proc Natl Acad Sci U S A*, 107:7951-7956.
- Cisek P, Grossberg S, and Bullock D (1998). A cortico-spinal model of reaching and proprioception under multiple task constraints. *J Cogn Neurosci*, 10:425-444.
- Cohen YE, and Andersen RA (2002). A common reference frame for movement plans in the posterior parietal cortex. *Nat Rev Neurosci*, 3:553-62.
- Colby CL and Duhamel JR (1991). Heterogeneity of extrastriate visual areas and multiple parietal areas in the macaque monkey. *Neuropsychologia*, 29:517-37.
- Colby CL, (1998). Action-oriented spatial reference frames in cortex. *Neuron*, 20:15-24.
- Crawford JD and Guitton D (1997). Visual-motor transformations required for accurate and kinematically correct saccades. *J Neurophysiol*, 78:1447-1467.
- Crawford JD, Henriques DY, Medendorp WP (2011). Three-dimensional transformations for goal-directed action. *Annu Rev Neurosci*, 34:309-331.

- Culbertson WC, and Zillmer EA (2005). Tower of London-Drexel University (TOL-DX): technical manual. New York: MHS
- Danckert J, Goldberg L, Broderick C, (2009). Damage to superior parietal cortex impairs pointing in the sagittal plane. *Exp Brain Res*, 195:183–191.
- Davare M, Zénon A, Desmurget M, and Olivier E (2015). Dissociable contribution of the parietal and frontal cortex to coding movement direction and amplitude. *Front Hum Neurosci*, 9:241.
- Day BL and Lyon IN (2000). Voluntary modification of automatic arm movements evoked by motion of a visual target. *Exp Brain Res*, 130:159-168.
- Deneve S, Latham PE, Pouget A (2001). Efficient computation and cue integration with noisy population codes. *Nat Neurosci*, 4:826-831.
- Dessing JC, Crawford JD, and Medendorp WP (2011). Spatial updating across saccades during manual interception. *J Vis*, 11:1-18.
- Elliott D, Binsted G, and Heath M (1999). The control of goal-directed limb movements: Correcting errors in the trajectory. *Hum Mov Sci*, 18:121–136.
- Enright JT (1995). The non-visual impact of eye orientation on eye-hand coordination. *Vision Res*, 35:1611-1618.
- Fattori P, Gamberini M, Kutz DF, and Galletti C, (2001). ‘Arm-reaching’ neurons in the parietal area V6A of the macaque monkey. *Eur J Neurosci*, 13:2309-2313.
- Fattori P, Kutz DF, Breveglieri R, Marzocchi N, Galletti C (2005). Spatial tuning of reaching activity in the medial parieto-occipital cortex (area V6A) of macaque monkey. *Eur J Neurosci*, 22:956-972.
- Fattori P, Breveglieri R, Raos V, Bosco A, and Galletti C, (2012). Vision for action in the macaque medial posterior parietal cortex. *J Neurosci*, 32:3221-3234.
- Ferraina S, Garasto MR, Battaglia-Mayer A, Ferraresi P, Johnson PB, Laquaniti F, Caminiti R (1997). Visual control of hand-reaching movement: activity in parietal area 7m. *Eur J Neurosci*, 9:1090-1095.
- Ferraina S, Battaglia-Mayer A, Genovesio A, Marconi B, Onorati P, Caminiti R (2001). Early coding of visuomanual coordination during reaching in parietal area PEc. *J Neurophysiol*, 85: 462–467.
- Ferraina S, Brunamonti E, Giusti MA, Costa S, Genovesio A, Caminiti R (2009). Reaching in depth: hand position dominates over binocular eye position in the rostral superior parietal lobule. *J Neurosci*, 29:11461-11470.
- Fielher K, Schütz I, and Henriques D (2011). Gaze-centered spatial updating of reach targets across different memory delays. *Vision Res*. 51:890–897.

Filimon F (2015). Are all spatial reference frames egocentric? Reinterpreting evidence for allocentric, object-centered, or world-centered reference frames. *Front Hum Neurosci*, 9:648.

Flanders M, Tillery SIH, and Soechting JF (1992). Early stages in a sensorimotor transformation. *Behav Brain Sci*, 15:309-320.

Franklin DW, and Wolpert DM (2008). Specificity of reflex adaptation for task-relevant variability. *J Neurosci*, 28:14165-14175.

Frassinetti F, Bonifazi S and Làdavvas E (2007). The influence of spatial coordinates in a case of an optic ataxia-like syndrome following cerebellar and thalamic lesion. *Cogn Neuropsychol*, 24:3, 324-337.

Fu QG, Flament D, Coltz JD, and Ebner TJ (1995). Temporal encoding of movement kinematics in the discharge of primate primary motor and premotor neurons. *J Neurophysiol*, 73:836–854.

Gail A and Andersen RA (2006). Neural dynamics in monkey parietal reach region reflect context-specific sensorimotor transformations. *The Journal of Neuroscience: The Official Journal of the Society for Neuroscience*, 26:9376–84.

Galletti C, Battaglini PP, and Fattori P (1991). Functional properties of neurons in the anterior bank of the parieto-occipital sulcus of the macaque monkey. *Eur J Neurosci*, 3:452–461.

Galletti C, Battaglini PP, Fattori P (1995). Eye position influence on the parieto-occipital area PO (V6) of the macaque monkey. *Eur J Neurosci*, 7:2486-2501.

Galletti C, Fattori P, Battaglini PP, Shipp S, Zeki S (1996). Functional demarcation of a border between areas V6 and V6A in the superior parietal gyrus of the macaque monkey. *Eur J Neurosci*, 8:30-52.

Galletti C, Fattori P, Kutz DF, Gamberini M (1999). Brain location and visual topography of cortical area V6A in the macaque monkey. *Eur J Neurosci*, 11:575-582.

Galletti C, Kutz DF, Gamberini M, Breveglieri R, Fattori P (2003a). Role of the medial parieto-occipital cortex in the control of reaching and grasping movements. *Exp Brain Res*, 153:158-170.

Galletti C and Fattori P (2003b). Neuronal mechanisms for detection of motion in the field of view. *Neuropsychologia*, 41:1717–27.

Galletti C and Fattori P (2017). The dorsal visual stream revisited: stable circuits or dynamic pathways? *Cortex*, 203-217.

Gamberini M, Passarelli L, Fattori P, Zucchelli M, Bakola S, Luppino G, Galletti C. (2009). Cortical connections of the visuomotor parietooccipital area V6Ad of the macaque monkey. *J Comp Neurol*, 513:622-42.

- Gamberini M, Galletti C, Bosco A, Breveglieri R, Fattori P (2011). Is the medial posterior parietal area V6A a single functional area? *J Neurosci*, 31:5145-5157.
- Gentilucci M, Benuzzi F, Gangitano M, and Grimaldi S. (2001). Grasp with hand and mouth: a kinematic study on healthy subjects. *J Neurophysiol*, 86:1685–1699.
- Goodale MA, Milner AD, Jakobson LS and Carey DP (1991). A neurological dissociation between perceiving objects and grasping them. *Nature*, 349:154-156.
- Goodale MA, Milner AD (1992). Separate visual pathways for perception and action. *Trends Neurosci*, 15:20-25.
- Gordon J, Ghilardi MF, Ghez C (1994a). Accuracy of planar reaching movements. I. Independence of direction and extent variability. *Exp Brain Res*, 99:97-111.
- Gordon J, Ghilardi MF, Cooper SE, and Ghez C (1994b). Accuracy of planar reaching movements - II. Systematic extent errors resulting from inertial anisotropy. *Exp Brain Res*, 99:112–130.
- Graziano MS, Gross CG (1998). Spatial maps for the control of movement. *Curr Opin Neurobiol*, 8:195-201.
- Graziano MS (1999). Where is my arm? The relative role of vision and proprioception in the neuronal representation of limb position. *Proc Natl Acad Sci U S A*, 96:10418-10421.
- Graziano MS (2001a). Is reaching eye-centered, body-centered, hand-centered, or a combination? *Rev Neurosci*, 12:175-185.
- Graziano MS (2001b). A system of multimodal areas in the primate brain. *Neuron*, 29:4-6.
- Hadjidimitrakis K, Bertozzi F, Breveglieri R, Fattori P, Galletti C (2014a). Body-centered, mixed, but not hand-centered coding of visual targets in the medial posterior parietal cortex during reaches in 3D space. *Cereb Cortex*, 24:3209-3220.
- Hadjidimitrakis K, Bertozzi F, Breveglieri R, Bosco A, Galletti C, Fattori P, (2014b). Common neural substrate for processing depth and direction signals for reaching in the monkey medial posterior parietal cortex. *Cereb Cortex*, 24:1645-1657.
- Hadjidimitrakis K, Dal Bo' G, Breveglieri R, Galletti C, Fattori P (2015). Overlapping representations for reach depth and direction in caudal superior parietal lobule of macaques. *J Neurophysiol*, 114:2340-2352.
- Heed T, Beurze SM, Toni I, Röder B, Medendorp WP (2011) Functional rather than effector-specific organization of human posterior parietal cortex. *J Neurosci*, 31:3066-3076.
- Henriques DY, Klier EM, Smith MA, Lowy D, Crawford JD (1998). Gaze-centered remapping of remembered visual space in an open-loop pointing task. *J Neurosci*, 18:1583-1594.

- Himmelbach M and Karnath HO (2005). Dorsal and ventral stream interaction: Contributions from optic ataxia. *Journal of Cognitive Neuroscience*, 17:632–640.
- Hochberg LR *et al.* (2012). Reach and grasp by people with tetraplegia using a neurally controlled robotic arm. *Nature*, 485:372–375.
- Holmes G (1918). Disturbances of visual orientation. *Brit J Ophthalmol*, 2:449-468.
- Holmes G, and Horrax G, (1919). Disturbances of spatial orientation and visual attention with loss of stereoscopic vision. *Arch Neurol Psychiatry*, 1: 385–407.
- Hwang EJ, Hauschild M, Wilke M, and Andersen RA (2014). Spatial and temporal eye-hand coordination relies on the parietal reach region. *The Journal of Neuroscience: The Official Journal of the Society for Neuroscience*, 34:12884–92.
- Jax SA, Buxbaum LJ, Lie E, Coslett HB (2009). More than (where the target) meets the eyes: disrupted visuomotor transformations in optic ataxia. *Neuropsychologia*, 47:230-238.
- Karnath HO, Perenin MT (2005). Cortical control of visually guided reaching: evidence from patients with optic ataxia. *Cereb Cortex*, 15:1561–1569.
- Kasuga S, Telgen S, Ushiba J, Nozaki D, and Diedrichsen J (2015). Learning feedback and feedforward control in a mirror-reversed visual environment. *J Neurophysiol*, 114:2187-2193.
- Khan MA, Elliott D, Coull J, Chua R, and Lyons J (2002). Optimal control strategies under different feedback schedules: Kinematic evidence. *J. Mot. Behav*, 34: 45–57.
- Khan MA, Lawrence G, Fourkas A, Franks IM, Elliott D, and Pembroke S (2003). Online versus offline processing of visual feedback in the control of movement amplitude. *Acta Psychol. (Amst)*, 113:83–97.
- Khan AZ, Pisella L, Rossetti Y, Vighetto A, and Crawford JD, (2005). Impairment of gaze-centered updating of reach targets in bilateral parietal-occipital damaged patients. *Cereb Cortex*, 15:1547–1560.
- Khan AZ, Crawford JD, Blohm G, Urquizar C, Rossetti Y, and Pisella L, (2007). Influence of initial hand and target position on reach errors in optic ataxic and normal subjects. *J Vision*, 7:8, 1–16.
- Khan AZ, Pisella L, Blangero A, Rossetti Y, and Crawford JD (2008). Sensorimotor aspects of reach deficits in optic ataxia. In *Cortical Mechanisms of Vision*, 4: 53-80, Cambridge University Press.
- Khan AZ, Pisella L, and Blohm G (2013). Causal evidence for posterior parietal cortex involvement in visual-to-motor transformations of reach targets. *Cortex*, 49: 2439-2448.
- Klier EM, Wang H, Crawford JD (2001). The superior colliculus encodes gaze commands in retinal coordinates. *Nat Neurosci*, 4:627-632.

- Krakauer JW, Pine ZM, Ghilardi MF, and Ghez C (2000). Learning of visuomotor transformations for vectorial planning of reaching trajectories. *J Neurosci*, 20:8916–8924.
- Kutz DF, Marzocchi N, Fattori P, Cavalcanti S, Galletti C (2005). Real-time supervisor system based on trinary logic to control experiments with behaving animals and humans. *J Neurophysiol*, 93:3674-3686.
- Lacquaniti F, Guigon E, Bianchi L, Johnson PB, Ferraina S, Caminiti R (1995). Representing spatial information for limb movement: the role of area 5 in the monkey. *Cereb Cortex*, 5:391–409.
- Lee J, Groh JM (2012). Auditory signals evolve from hybrid- to eye-centered coordinates in the primate superior colliculus. *J Neurophysiol*, 108:227-242.
- Lewald J and Ehrenstein WH (2000). Visual and proprioceptive shifts in perceived egocentric direction induced by eye-position. *Vision Res*, 40:539-547.
- Luppino G, Ben Hamed S, Gamberini M, Matelli M, Galletti C (2005). Occipital (V6) and parietal (V6A) areas in the anterior wall of the parieto-occipital sulcus of the macaque: a cytoarchitectonic study. *Eur J Neurosci*, 21:3056-3076.
- Martin JA, Karnath HO and Himmelbach M (2015). Revisiting the cortical system for peripheral reaching at the parietal-occipital junction. *Cortex*, 64:363-379.
- Marzocchi N, Breveglieri R, Galletti C, Fattori P (2008). Reaching activity in parietal area V6A of macaque: eye influence on arm activity or retinocentric coding of reaching movements? *Eur J Neurosci*, 27:775-789.
- McGuire LM, Sabes PN (2009). Sensory transformations and the use of multiple reference frames for reach planning. *Nat Neurosci*, 12:1056-1061.
- McGuire LM, Sabes PN (2011). Heterogeneous representations in the superior parietal lobule are common across reaches to visual and proprioceptive targets. *J Neurosci*, 31:6661-6673.
- Medendorp WP and Crawford JD (2002). Visuospatial updating of reaching targets in near and far space. *Neuroreport*, 13:633–636.
- Medendorp WP, Goltz HC, Vilis T, Crawford JD (2003). Gaze-centered updating of visual space in human parietal cortex. *J Neurosci*, 23:6209-6214.
- Medendorp WP, Goltz HC, Vilis T (2005a). Remapping the remembered target location for anti-saccades in human posterior parietal cortex. *J Neurophysiol*, 94:734-740.
- Medendorp WP, Goltz HC, Crawford JD, Vilis T (2005b). Integration of target and effector information in human posterior parietal cortex for the planning of action. *J Neurophysiol*, 93:954-962.

- Messier J and Kalaska JF (2000). Covariation of primate dorsal premotor cell activity with direction and amplitude during a memorized reaching task. *J Neurophysiol*, 84:152–65.
- Milner AD, Goodale MA (1995). *The visual brain in action*. Oxford: Oxford University Press, 87-119.
- Milner AD, Perrett DI, Johnston RS, Benson PJ, Jordan TR, Heeley DW, Bettucci D, Mortara F, Mutani R and Terrazzi E (1991). Perception and action in “visual form agnosia”. *Brain*, 114:405-428
- Milner AD, Dijkerman HC, Pisella L, McIntosh RD, Tilikete, C, Vighetto A, et al. (2001). Grasping the past: Delay can improve visuomotor performance. *Curr Biol*, 11:1896–1901.
- Milner AD, Dijkerman HC, McIntosh RD, Pisella L and Rossetti Y (2003). Delayed reaching and grasping in patients with optic ataxia. *Prog Brain Res*, 142: 225–242.
- Mountcastle VB, Lynch JC, Georgopoulos A, Sakata H, Acuna C (1975). Posterior parietal association cortex of the monkey: command functions for operations within extrapersonal space. *J Neurophysiol*, 38:871-908.
- Mueller S and Fiehler K (2016). Mixed body- and gaze-centered coding of proprioceptive reach targets after effector movement. *Neuropsychologia*, 87:63–73.
- Mullette-Gillman OA, Cohen YE, Groh JM (2005). Eye-centered, head-centered, and complex coding of visual and auditory targets in the intraparietal sulcus. *J Neurophysiol* 94:2331-2352.
- Mullette-Gillman OA, Cohen YE, Groh JM (2009). Motor-related signals in the intraparietal cortex encode locations in a hybrid, rather than eye-centered reference frame. *Cereb Cortex*, 19:1761-1775.
- Mulliken GH, Musallam S, Andersen RA (2008). Decoding trajectories from posterior parietal cortex ensembles. *J Neurosci*, 28:12913-12926.
- Naka KI, Rushton WA (1966a). S-potentials from luminosity units in the retina of fish (Cyprinidae). *J Physiol*, 185:587-599.
- Naka KI, Rushton WA (1966b). S-potentials from colour units in the retina of fish (Cyprinidae). *J Physiol*, 185:536-555.
- Naka KI, Rushton WA (1966c). An attempt to analyse colour reception by electrophysiology. *J Physiol*, 185:556-586.
- Ogawa K and Inui T (2011). Reference frame of human medial intraparietal cortex in visually guided movements. *J Cogn Neurosci*, 24:171-182.
- Oldfield RC (1971). The assessment and analysis of handedness: The Edinburgh inventory. *Neuropsychologia*, 9:97–113.

- Osterrieth P (1944). Le test de copie d'une figure complexe; contribution à l'étude de la perception et de la mémoire. [Test of copying a complex figure; contribution to the study of perception and memory.]. *Archives de Psychologie*, 30: 206-356.
- Pandya DN, Seltzer B (1982). Intrinsic connections and architectonics of posterior parietal cortex in the rhesus monkey. *J Comp Neurol*, 204:196-210.
- Pelisson D, Prablanc C, Goodale M, and Jeannerod M (1986). Visual control of reaching movements without vision of the limb. *Exp Brain Res*, 62:303-311.
- Peña JL, Konishi M (2001). Auditory spatial receptive fields created by multiplication. *Science*, 292:249-252.
- Perenin MT, and Vighetto A, (1988). Optic ataxia: a specific disruption in visuomotor mechanisms. I. Different aspects of the deficit in reaching for objects. *Brain*, 111:643-674.
- Pesaran B, Nelson MJ, Andersen RA (2006). Dorsal premotor neurons encode the relative position of the hand, eye, and goal during reach planning. *Neuron*, 51:125-134.
- Pesaran B, Nelson MJ, and Andersen RA (2010). A relative position code for saccades in dorsal premotor cortex. *J Neurosci*, 30:6527-37.
- Pisella L, Grea H, Tilikete C, Vighetto A, Desmurget M, Rode G, Boisson D, and Rossetti Y, (2000). An 'automatic pilot' for the hand in human posterior parietal cortex: toward reinterpreting optic ataxia. *Nat Neurosci*, 3:729-736.
- Pisella L, Michel C, Grea H, Tilikete C, Vighetto A and Rossetti Y (2004). Preserved prism adaptation in bilateral optic ataxia: strategic versus adaptive reaction to prisms. *Exp Brain Res*, 156:399-408.
- Piserchia V, Breveglieri R, Hadjidimitrakis K, Bertozzi F, Galletti C, and Fattori P (2017). Mixed body/hand reference frame for reaching in 3D space in macaque parietal area PEc. *Cereb Cortex*, 27:1976-1990.
- Pouget A, Snyder LH (2000). Computational approaches to sensorimotor transformations. *Nat Neurosci*, 3 Suppl: 1192-1198.
- Previc FH (1998). The neuropsychology of 3-D space. *Psychol. Bull*, 124:123-164.
- Proteau L and Isabelle G (2002). On the role of visual afferent information for the control of aiming movements towards targets of different sizes. *J Mot. Behav*, 34:367-384.
- Reichenbach A, Franklin DW, Zatska-Haas P, and Diedrichsen J (2014). A dedicated binding mechanism for the visual control of movement. *Curr Biol*, 24:780-785.
- Reuschel J, Rosler F, Henriques D, and Fiehler K (2012). Spatial updating depends on gaze direction even after loss of vision. *J Neurosci*, 32:2422-2429.

- Rorden C, and Brett M (2000). Stereotaxic display of brain lesions. *Behav Neurol*, 12:191-200.
- Rorden C, Karnath HO, and Bonilha L (2007). Improving lesion-symptom mapping. *J Cogn Neurosci*, 19:1081-1088.
- Rossetti Y, Pisella L and Vighetto A (2003). Optic ataxia revisited: visually guided action versus immediate visuomotor control. *Exp Brain Res*, 153: 171-179.
- Rossetti Y, Revol P, McIntosh R, Pisella L, Rode G, Danckert J, Tilikete C, Dijkerman HC, Boisson D, Vighetto A, Michel F, Milner AD, (2005). Visually guided reaching: bilateral posterior parietal lesions cause a switch from fast visuomotor to slow cognitive control. *Neuropsychologia*, 43:162–177.
- Roy AC, Paulignan Y, Farnè A, Joffrais C, and Boussaoud D (2000). Hand kinematics during reaching and grasping in the macaque monkey. *Behav. Brain Res*, 117:75–82.
- Sainburg RL, Lateiner JE, Latash ML, and Bagesteiro LB (2003). Effects of altering initial position on movement direction and extent. *J Neurophysiol*, 89:401–415.
- Sakata H, Takaoka Y, Kawarasaki A, Shibutani H (1973). Somatosensory properties of neurons in the superior parietal cortex (area 5) of the rhesus monkey. *Brain Res* 64:85-102.
- Scherberger H, Goodale M, and Andersen R (2003). Target selection for reaching and saccades share a similar behavioral reference frame in the macaque. *J Neurophysiol*, 89:1456-1466.
- Sereno MI, Pitzalis S, Martinez A (2001). Mapping of contralateral space in retinotopic coordinates by a parietal cortical area in humans. *Science*, 294:1350-1354.
- Snyder LH, Batista AP, Andersen RA (1997). Coding of intention in the posterior parietal cortex. *Nature*, 386:167-170.
- Sober SJ, Sabes PN (2005). Flexible strategies for sensory integration during motor planning. *Nat Neurosci*, 8:490-497.
- Soechting JF, Flanders M, (1992). Moving in three-dimensional space: frames of reference, vectors, and coordinate systems. *Ann Rev Neurosci*, 15: 167-191.
- Spinnler H and Tognoni G (1987) “Standardizzazione e Taratura Italiana di Test Neuropsicologici,” *The Italian Journal of Neurological Sciences*, 8: 44-46.
- Squatrito S, Raffi M, Maioli MG and Battaglia-Mayer A (2001). Visual motion responses of neurons in the caudal area PE of macaque monkeys. *J Neurosci*, 21:1-5.
- Stricanne B, Andersen RA, Mazzone P (1996). Eye-centered, head-centered, and intermediate coding of remembered sound locations in area LIP. *J Neurophysiol*, 76:2071-2076.

Szczepanski SM and Saalman YB (2013). Human fronto-parietal and parietal-hippocampal pathways represent behavioral properties in multiple spatial reference frames. *Bio-Architecture*, 3:5, 147-152.

Tramper JJ and Medendorp WP (2015). Parallel updating and weighting of multiple spatial maps for visual stability during whole-body motion. *J Neurophysiol*, 114:3211-3219.

Ungerleider LG, Mishkin M (1982). Two cortical visual systems. In: *Analysis of visual behavior* (Ingle DJ, Goodale MA, Mansfield RJW, eds), pp 549-586. Cambridge: MIT Press.

Van Pelt S and Medendorp WP (2008). Updating target distance across eye movements in depth. *J Neurophysiol*, 99:2281-2290.

Vindras, P, Desmurget M, and Viviani P (2005). Error parsing in visuomotor pointing reveals independent processing of amplitude and direction. *J Neurophysiol*, 94:1212-1224.

Zar J (1999). *Biostatistical analysis*. Pearson Prentice-Hall, Upper Saddle River, NJ.

Zimmerman P and Fimm B (1992). Testbatterie zur Aufmerksamkeitsprüfung (TAP). In Wurselen: psytest.

Zoccolotti P, Pizzamiglio L, Pittau P, and Galati G (1994). Batteria di Test per l'esame dell'Attenzione.